ΕΘΝΙΚΟ ΜΕΤΣΟΒΙΟ
ΠΟΛΥΤΕΧΝΕΙΟ
ΣΧΟΛΗ ΜΗΧΑΝΟΛΟΓΩΝ ΜΗΧΑΝΙΚΩΝ
ΤΟΜΕΑΣ ΘΕΡΜΟΤΗΤΑΣ
Καθηγητής Δρ. ΕΜΜ. ΚΑΚΑΡΑΣ

ΔΙΠΛΩΜΑΤΙΚΗ ΕΡΓΑΣΙΑ

“Προσδιορισμός των Χαρακτηριστικών Παραμέτρων Λειτουργίας Εγκαταστάσεων Δέσμευσης CO_2 από Καυσαέρια με Χρήση CaO”

Του Φοιτητή

Κοπανάκη Γεώργιου

Επιβλέποντες Καθηγητές

Καθηγητής Δρ. Κακαράς Εμμανουήλ, Εθνικό Μετσόβιο Πολυτεχνείο
Prof. Dr. techn. G. Scheffknecht, University of Stuttgart

Acknowledgements

My most grateful thank for my diploma thesis is dedicated to Prof. Emmanouil Kakaras, who offered me the opportunity to carry out my diploma thesis at University of Stuttgart.
The support of Prof. Dr. Techn. G. Scheffknecht was also important during my research period at the Institute of Combustion and Power Plant Technology (IFK).
I would also like to thank the supervisor of my work, Dipl.- Ing. Alexander Charitos and Dr. Karellas Sotirios, who helped me to accomplish my diploma thesis and who showed great tolerance towards my questions.
Finally a special thank to my parents, my brother and my friends who suported me all these years and through this experience.

Περίληψη της Διπλωματικής Εργασίας στα Ελληνικά

Είναι γενικά αποδεκτό ότι η συγκέντρωση του CO_2 στην ατμόσφαιρα αυξάνεται ραγδαία τις τελευταίες δεκαετίες και είναι ο κύριος παράγοντας που οδηγεί στην κλιματική αλλαγή. Οι απαιτήσεις της παγκόσμιας ενέργειας αυξάνονται συνεχώς, για παράδειγμα η κατανάλωση ηλεκτρικού ρεύματος για 7 από τις 10 μεγαλύτερες πόλεις του κόσμου βρίσκεται μεταξύ 4.5-7 MWh/cap [1]. Επιπρόσθετα, η αύξηση της κατανάλωσης ορυκτών καυσίμων υπολογίζεται να προκαλέσει αύξηση των εκπομπών CO_2 από 29 Gt/a το 2007 σε πάνω από 40 Gt/a το 2030 [2].
Οι ανανεώσιμες πηγές ενέργειας μπορεί να είναι ένα μέρος της λύσης στο πρόβλημα αυτό. Μελλοντικές τεχνολογίες φωτοβολταϊκών δείχνουν πως μπορούν να πετύχουν ανταγωνιστικό κόστος παραγώμενης ηλεκτρικής ενέργειας [3]. Εξελιγμένες ιδέες για ρευστοποιημένες κλίνες με φωτο-αντιδραστήρες μπορούν να αποτελέσουν μια λύση με μεγάλους βαθμούς απόδοσης, αλλά η χρήση τους αυτή τη στιγμή σε σχέση με την ηλιακή ακτινοβολία είναι περιορισμένη [4].
Μία άλλη προσέγγιση στο πρόβλημα είναι η δέσμευση του CO_2 μετά την καύση με διάφορες τεχνολογίες όπως οι μεμβράνες αμίνης [5, 6, 7]. Η πιο εφαρμόσιμη από όλες είναι η δέσμευση του CO_2 που προέρχεται από τα καυσαέρια, από το ασβέστιο (CaO) με χρήση συζυγών ρευστοποιημένων κλινών (DFB). Η διαδικασία περιλαμβάνει δύο ρευστοποιημένες κλίνες , οι οποίες συνδέονται με ένα σύστημα σωληνώσεων για την μεταφορά στερεών σωματιδίων και είναι γνωστη σαν Calcium Looping Process (CaL). Το ασβέστιο χρησιμοποιείται ως μεταφορέας του CO_2 μεταξύ των δύο αντιδραστήρων. Τα καυσαέρια, τα οποία αποτελούνται από 15 % CO_2 κατ' όγκο εισέρχονται στην κλίνη που δεσμεύει το διοξείδιο του άνθρακα. Το ασβέστιο που βρίσκεται μέσα αντιδρά με το CO_2 και δημιουργείται ανθρακικό ασβέστιο ($CaCO_3$). Μετά από αυτήν την διαδικασία τα καυσαέρια ελεύθερα από το CO_2 οδηγούνται στην ατμόσφαιρα. Το σχηματισμένο $CaCO_3$ μεταφέρεται στην δεύτερη κλίνη, όπου η αντίθετη αντίδραση λαμβάνει χώρα για να σχηματιστεί και πάλι ασβέστιο και διοξείδιο του άνθρακα. Από αυτήν την κλίνη τώρα το ασβέστιο μεταφέρεται πίσω στην πρώτη για περεταίρω δέσμευση του CO_2, ενώ το CO_2 που απελευθερώθηκε, συμπιέζεται και αποθηκεύεται.
Η τεχνική αυτή έχει εφαρμοστεί σε πολλές εγκαταστάσεις ανα τον κόσμο σε μικρής κλίμακας συστημάτων με συζυγείς ρευστοποιημένες κλίνες [9, 10, 11, 12, 13, 14] για να αποδείξουν την σπουδαιότητα της. Ο βαθμός απόδοσης που έχουν επιτύχει είναι πάνω από 90 %, παρ' όλα αυτά περισσότερες πειραματικές διαδικασίες είναι απαραίτητες για την σωστή αξιολόγηση των αποτελεσμάτων και την εφαρμογή της διαδικασίας σε μεγάλης κλίμακας εγκαταστάσεις. Στο πανεπιστήμιο της Στουτγκάρδης (IFK) η πειραματική μελέτη της διαδικασίας γίνεται σε μια συζυγή ρευστοποιημένη κλίνη, με συνεχή ανακυκλοφορία ασβεστίου.

Αποτελείται από μία αναδεύουσα ρευστοποιημένη κλίνη για την αναγένηση του $CaCO_3$ (BFB) και μία ανακυκλοφορούσα ρευστοποιημένη κλίνη (CFB) για την δέσμευση του CO_2. Η θεωρητική γνώση έχει ήδη καθιερωθεί από προηγούμενες πειραματικές μελέτες στο πανεπιστήμιο σε μικρής κλίμακας κρύα μοντέλα [15, 16]. Η συγκεκρινένη πειραματική εκστρατεία έχει σκοπό τον χαρακτηρισμό της λειτουργείας του CFB, λειτουργώντας στην γρήγορη περιοχή ρευστοποίησης και τον χαρακτηρισμό λειτουργείας του BFB.

Χρησιμοποιώντας διαφορετικούς τύπους ασβεστίου και διαφορετικά μεγέθη σωματιδίων, ο βαθμός απόδοσης σε όλες τις περιπτώσεις ξεπέρασε το 85 %. Επιπλέον, ο βαθμός απόδοσης του BFB όπου γίνεται η αναγένηση του $CaCO_3$ ξεπέρασε το 90 %. Η λειτουργεία της εγκατάστασης επιβεβαίωσε αρχικά πλήρως όλα τα αποτελέσματα και τις υποθέσεις του κρύου μοντέλου ενώ απέδειξε πως η διεργασία μπορεί να αποτελέσει μία σημαντική τεχνική δέσμευσης του CO_2, ώστε να εφαρμοστεί σε εγκαταστάσεις μεγάλης κλίμακας.

Institute of Combustion and Power Plant Technology

University of Stuttgart
Germany

ifk

Director: Prof. Dr. techn. G. Scheffknecht
Pfaffenwaldring 23 • 70569 Stuttgart • Germany
Phone +49 (0) 711-685 63487 • Fax +49 (0) 711-685 63491

Diplom Thesis Nr. 2981
Giorgos Kopanakis
cand. mach.

Characterization of the Carbonator and Regenerator for the Calcium Looping CO_2 capture Process

Anschrift:	Allmandring I
	70569 Stuttgart
Ausgabe:	01.10.2009
Abgabe:	04.05.2010
Betreuer:	Dipl.-Ing. Alexander Charitos
	Dipl.-Ing. Zieba

Institute of Combustion and Power Plant Technology

University of Stuttgart
Germany

Director: Prof. Dr. techn. G. Scheffknecht
Pfaffenwaldring 23 • 70569 Stuttgart • Germany
Phone +49 (0) 711-685 63487 • Fax +49 (0) 711-685 63491

Stuttgart, 01.10.2009
Prof. Sch./Char.

Diploma Thesis No.: 2981
for Mr. Giorgos Kopanakis (ERASMUS Student)
Matr.-No. 2647445

Characterization of the carbonator and regenerator for the Calcium Looping CO_2 capture process

Motivation: A lot of methods to separate CO_2 from combustion flue gases exist. The Calcium Looping post-combustion process utilizes established equipment (fluidized beds) and an easily available sorbent (CaO). These advantages motivate process development. At IFK a 10 kW_{th} Dual Fluidized Bed (DFB) is used for process characterization, and is shown in Fig. 1, in combination with a 200 kW_{th} unit which is currently undergoing commissioning.

Process description: Flue gases (15% CO_2 vol.) enter the carbonator at 650 °C. There, CaO will react with CO_2 to $CaCO_3$. The $CaCO_3$ will be circulated to a regenerator, where a pure CO_2 stream is produced. The CaO than will be transported to the carbonator for further CO_2 capture.

Status of IFK research: Initial campaigns demonstrated the process technical feasibility. Characterization reactor operation is needed.

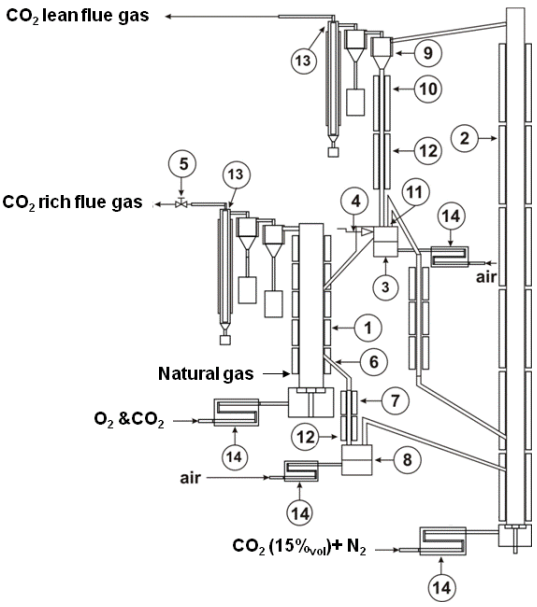

Fig. 1: Scheme of IFK Calcium Looping DFB facility: (1) BFB regenerator, (2) riser carbonator, (3) double exit loop seal, (4) cone valve, (5) pressure control valve, (6) BFB overflow, (7) lower standpipe, (8) lower loop seal, (9) cyclone, (10) upper standpipe, (11) loop seal weir, (12) quartz standpipe segments (13) candle filter (14) preheaters

Institute of Combustion and Power Plant Technology

University of Stuttgart
Germany

ifk

Director: Prof. Dr. techn. G. Scheffknecht
Pfaffenwaldring 23 • 70569 Stuttgart • Germany
Phone +49 (0) 711-685 63487 • Fax +49 (0) 711-685 63491

Goal of the thesis:

- To characterize carbonator operation through definition of: (i) carbonator hydrodynamics (ii) the effect of the calcium looping rate between reactors on the CO_2 capture efficiency (iii) the decay of sorbent carbonation capacity (iv) a factor determining the carbonator performance and (v) the carbonator CO_2 concentration profiles
- To characterize regenerator operation through definition of: (i) a factor determining the calcination extent in the regenerator and (ii) show its impact on the DFB system.

The Diploma Thesis is supervised by Mr. Dipl.-Ing. Charitos and Mr. Dipl.-Ing. Zieba.

Start of the Diploma Thesis: 01.10.2009
Submission date: 04.05.2010

- (Prof. Dr. techn. G. Scheffknecht) (Dipl.-Ing. M. Zieba)

Adresse/Kontaktdaten Student:
Herr
Giorgos Kopanakis
Lamprou Katsoni 12
15121 Athens

Abstract

Calcium looping (CaL) is an option for post-combustion separation of CO_2 by carbonation of lime. It is carried out in a dual fluidized bed facility. A continuous loop of limestone is established between these two. CO_2 is separated at temperatures of 600–700 °C in the Carbonator and released at over 900 °C in the regenerator, hence, a very pure stream of CO_2 is emitted. The present experimental campaign has been conducted in order to characterize the operation of the CFB carbonator, operating within the fast fluidization regime, and the regenerator, in order to aid modeling, design and scale-up. Steady states were established under various realistic conditions and CO_2 capture efficiencies of over 90 % were achieved.

Contents

List of Figures

Notation

Symbols	Significance	Unit
C_{CO2}	Molar Concentration of CO_2	[mol/m³]
$C_{CO2, eq}$	Chemical Equilibrium Molar Concentration of CO_2	[mol/m³]
E_{CO2}	CO_2 Capture Efficiency	[-]
$E_{CO2, eq}$	Chemical Equilibrium CO_2 Capture Efficiency	[-]
F_0	Make-Up Flow	[kg/h]
f_a	Free Active Part of Sorbent Particle/Bed	[-]
F_{Ca}	Calcium Looping Rate	[kg/h]
F_{CO2}	Carbonator Inlet CO_2 Stream	[m³/h]
F_{CO2}	Carbonator Outlet CO_2 Stream	[m³/h]
$F_{ges, out}$	Total Gas Flow leaving the Carbonator	[m³/h]
$F_{Luft, in}$	Carbonator Inlet Air Stream	[m³/h]
$F_{Luft, out}$	Carbonator Outlet Air Stream	[m³/h]
F_{Ca}/F_{CO2}	Calcium Looping Ratio	[-]
k_S	Rate Constant for Surface Carbonation	[m^4 mol/s]
$Gs_{entrainment}$	Entrainment of Carbonator	[kg/ m^2s]
P_{eq}	Equilibrium Partial Pressure of CO_2	[Pa]
P_{Total}	Total Pressure	[Pa]
S_O	Initial Surface Area of the Particle	[m^2/ cm^3]
e_o	Particle Porosity Constant	[-]
T_{Carb}	Temperature in Carbonator	[°C]
X_{Carb}	Average Carbonation of the Particles in the Carbonator	[-]
X_{Calc}	Average Carbonation of the Particles in the Regenerator	[-]
X_{max}	Maximum Possible Carbonation Conversion	[-]
X_N	Maximum Carbonation Conversion after N cycles	[-]
X_R	Lower Limit of the Maximum Capacity for Rapid Integration of CO_2	[-]
$y_{CO2, in}$	CO_2-Inlet Concentration	[-]

$y_{CO2,\ out}$	CO_2-Outlet Concentration	[-]
$y_{O2,\ in}$	O_2-Inlet Concentration	[-]
ε_s	Solid Fraction	[-]
τ	Space Time	[h]
τ_α	Active Space Time	[h]
r_i	Sorbent Flow Residence Time	[min]
r_{reg}	Regenerator Residence Time	[min]
r_{carb}	Carbonator Residence Time	[min]
$L(t)_{CO2}$	Comulative Sorbent CO_2 Loading	[-]
n_{reg}	Regenerator Efficiency	[%]
$n_{ca,total}$	Total Inventory	[kg]
ε_{sd}	Solid Fraction in Bed Region	[-]
ε_{slean}	Solid Fraction in Core Annulus Region	[-]

1.Introduction

It is generally accepted that the concentration of CO_2 in the atmosphere has been increasing within the last decades and that it is the primary contributor leading to climate change phenomena. Global energy requirements are rising continuously, e.g. the electricity consumption for seven of the ten biggest cities in the world is within a range of 4.5-7 MWh/cap [1]. In addition, the increasing rising global fossil fuel consumption is expected to cause an increment in energy related CO_2 emissions from 29 Gt/a in 2007 to over 40 Gt in 2030 [2].

Renewable energy sources might be part of the solution to this problem. Future photovoltaic technologies seem to be promising as relevant results suggest a high likelihood that this technology will achieve a competitive electricity production cost [3]. Advanced concepts as fluidized/fixed bed photo-reactors may represent an optimal method with extremely high quantum efficiencies but their current use with solar radiation is limited [4]. Another approach in order to achieve deep cuts in emissions from fossil fuels and meet the challenges of growing energy demand and consumption is the capture and sequestration of CO_2 with use of pre-combustion (IGCC cycles), advanced combustion (oxy-fuel, Chemical Looping Combustion) and post-combustion technologies. For the post-combustion CO_2 capture route various techniques are available such as amine/scrubbing systems, membranes and a range of adsorption/desorption techniques [5, 6, 7], while one of the most feasible is the use of calcium-based sorbents to capture CO_2 from gases with use of a Dual Fluidized Bed system (DFB). The process consists of two fluidized bed reactors connected by solid transportation pipes and is known as the Calcium Looping (CaL) process. Calcium oxide (CaO) is used as a CO_2 carrier between a Fluidized Bed (FB) carbonator and a FB regenerator. The incoming power plant flue gas stream consists typically of 15 % CO_2 by volume and enters the carbonator. The CaO in the carbonator reacts with the CO_2 to form $CaCO_3$. Therefore, a CO_2 lean gas exits the carbonator and is released to the atmosphere. The produced $CaCO_3$ is transported to the regenerator where the reverse chemical reaction takes place in order to generate CaO and a pure CO_2 stream. The produced CaO is transported back to the carbonator to further capture flue gas CO_2, while the CO_2 released from the regenerator can be directed to compression and then be storage.

Although the technique was patented in 1867 by Du Motay and Marechal [8], who used limestone to support gasification, experimental tests in regard to the CaL process are limited. Practical tests have been conducted so far only on a few small scale DFB facilities [9, 10, 11, 12, 13, 14] in order to demonstrate the overall feasibility of the procedure. The authors of the

above works managed to achieve CO_2 capture efficiencies of above 90 % during various steady states. The results of the work above are promising but still a lot of further experimental tests are needed. Moreover, these tests need to be conducted at more realistic conditions (e.g. carbonator operation at fast-fluidized bed conditions, presence of sulphur in the system, oxy-fuel conditions in the regenerator, etc.) and at bigger scale. In addition, small scale DFB facilities have to be used in order to characterize limestones for their suitability in regard to the CaL process, as results may differ to previous Thermo-Gravimetric Analysis (TGA) testing.

1.1 Goal of Thesis

At IFK the Calcium Looping (CaL) process is carried out in the 10 kW_{th} Dual Fluidized Bed facility, with continuous looping of CaO, which consists of a Bubbling Fluidized Bed (BFB) regenerator and a Circulating Fluidized Bed (CFB) carbonator. The theoretical background has already been established in previous experimental campaigns in a scaled cold model of IFK [15, 16], while successful experimental campaigns have been carried out in the DFB facility using the BFB as carbonator and the riser as regenerator [17]. The present experimental campaign has been conducted in order to characterize the operation of the CFB carbonator, operating within the fast fluidization regime, and the regenerator. Characterization of the regenerator involves the definition of a characteristic factor that defines the extent of calcination for a sorbent particle (i.e. the regenerator efficiency). Similar factors have been identified in previous studies [9, 12] for the carbonator in order to draw correlations to the CO_2 capture efficiency. This work aims in checking the correctness of previous approaches and to make corrections-additions where necessary. For further characterization of the carbonator the experimental determination of the pressure drop profiles and the CO_2 capture profiles in the carbonator is necessary. In addition, the impact of operating with different limestones and Particle Size Distributions (PSDs) are still undefined issues. Moreover, the experimental assessment of the calcium looping rate to achieve high CO_2 capture is important since this key variable is related to oxygen consumption in the regenerator of an industrial system and therefore to operational cost.

2. State of the Art Regarding the Calcium Looping Process

In this chapter the Calcium Looping Process is going to be analyzed concerning the process itself and the impact on the industry nowadays. Furthermore, the most important DFB facilities will be analyzed meticullusly.

2.1 The Calcium Looping Process and Related Solid Looping Technologies

The Calcium Looping process falls into the broader category of Dual Fluidized Bed processes (DFB) aiming at mitigation of CO_2 emissions. Although, these processes exhibit a different chemical background they utilize similar, although design specific, DFB settings. Therefore, progress and development of one DFB technology often influences the other positively. The most popular of them, besides Calcium Looping, include O_2 looping cycles (known as chemical looping combustion), and gasification of coal or biomass with or without CO_2 adsorption. The Calcium Looping process is presented in detail below, as perhaps the most feasible of these technologies due to its unmatched process advantages (e.g. utilization of natural sorbents, additional energy production to that of the original power plant, coupling with the cement industry etc.).

2.1.1 The Calcium Looping Process

Calcium looping (CaL) is a post-combustion route for power generation with CO_2 capture. The procedure is based on the carbonation reaction of CaO. The CO_2 is adsorbed from CaO as shown by Eq.2.1:

$$CaO + CO_2 \rightarrow CaCO_3 \tag{2.1}$$

The process was initially proposed by Shimizu et al. [18]. The technology comprises of a Dual Fluidized Bed (DFB) system with continuous looping of CaO. The principle of calcium looping process is shown in Fig. 2.1 below.

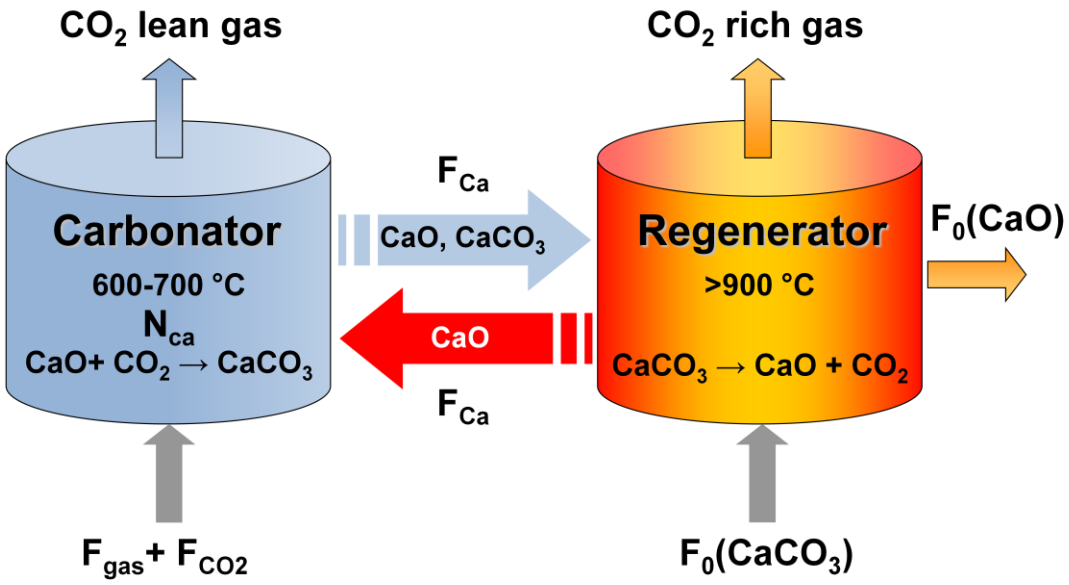

FIG 2.1: CALCIUM LOOPING PROCESS SCHEMATIC

A certain flue gas flow enters in the carbonator containing diluted CO_2 (approx. 15 % vol.) where CO_2 is adsorbed at temperatures of 600-700 °C. Therefore, a lean flue gas is produced and released to the atmosphere. The partially carbonated sorbent is transferred to the regenerator and the reverse calcination reaction takes place to regenerate the sorbent at temperatures above 900 °C, as shown by Eq. 2.2:

$$CaCO_3 \rightarrow CaO + CO_2 \tag{2.2}$$

In the regenerator, the oxy-combustion of a carbonaceous fuel provides the necessary energy to raise the particle temperature to the temperature level of the regenerator (> 900 °C) and in order to drive the endothermic calcination. The incoming O_2 is usually diluted with recycled CO_2 in order to control the reactor temperature. Therefore, the regenerator off gas consists mainly of CO_2 and steam. After condensation, a pure stream of CO_2 is produced which can be compressed and then be sequestered. Due to the decay in the maximum conversion of limestone with increasing carbonation/calcination cycles, a make-up flow of fresh $CaCO_3$ is necessary [19, 20]. Recently, experimental work has been successful in demonstrating CO_2 capture efficiencies of above 90 % with use of 10-50 kW_{th} facilities [9, 10, 11]. In addition, certain aspects of the CaL process, such as the utilization of spent sorbent for cement production and the ability to drive a high efficiency steam cycle with the heat provided in the DFB system lead to the fact that the CaL process is one of the most feasible CCS technologies to date, also from an economic sense.

2.1.1.1 Coupling with Steam Cycle and Process Economics

The distinctive characteristic of this process is that that energy spent in the regenerator (at 900 °C) is recovered as carbonation heat in the carbonator (at 650 °C) in order to drive a high-efficiency steam cycle. Therefore, evaporator heat surfaces can be installed within the carbonator while re-heat and super-heat surfaces can be installed in the convective back-pass of the carbonator and the regenerator. Thereby, supercritical steam can be produced. Hawthorne et al. [21] modeled such as a steam cycle which was chosen to be independent of the steam cycle of the initial power plant. They concluded that the net output of the initial power plant can be increased by almost 50 % with application of the Calcium Looping process, while the efficiency penalty would be lower than 6 %. A separate study [22], has shown that the capture system, utilizing a superctrical steam cycle can produce power with an efficiency of 27 %, while the original power plant retains its 45 % efficiemcy. The overall efficiency penalty has been shown to be around 4.5 % only. In regard to process economics, different studies, taking into account the CaL configuration of Fig. 2.1., result in modest CO_2 avoidance and electricity production costs. The CO_2 avoidance cost is predicted to be below 20 €/t_{CO2} from three studies, namely 19 €/t_{CO2} [23], 16 €/t_{CO2} [24] and 11 €/t_{CO2} [25]. The electricity production cost is predicted to be in the range of 41 €/MWh [23]. Advanced CaL systems, such as those providing the heat for calcination with solids as a heat carrier, instead of oxy-fuel combustion, may exhibit even better economic values since the capital and operational costs related to the Air Separation Unit (ASU) are omitted [12].

2.1.1.2 Impact on the Cement Industry

Nowadays, the cement industry generates approximately 5 % of global CO_2 emissions [26]. Recent publications show that cement production grew from 594 Mt in 1970 to 2200 Mt in 2005 [27] and is predicted to increase more [28]. Due to these indications much research has been carried out concerning the reduction of CO_2 emissions from existing and new cement plants. Calcined limestone, CaO, is the main precursor to cement and is fed to the kiln for clinker production. Limestone calcination, which is the reverse reaction of Eq. 2.1, is responsible for 70 % of the power required. The energy required for calcination and the related CO_2 emmisions can be avoided by feeding calcined material to the kiln that originates from the purge flow (F_0) removed from the calciner of a CaL facility, which is capturing CO_2 from a large scale power plant, as shown in Fig. 2.1. An integration of CO_2 free power production and clinker production has been shown to be feasible leading to large economic savings[29].

2.2 Review of Calcium Looping Dual Fluidized Bed Facilities

Four Calcium Looping Dual Fluidized Bed (DFB) facilities in the range of 10-75 kW_{th} have reported successful operation. These facilities are significant instruments testing of parameters (e.g., calcium looping rate, solid inventory, effect of sulphur, etc.) and for sorbent characterization. To further demonstrate the process a 200 kW_{th} DFB facility is undergoing commissioning in the University of Stuttgart, while a 1 MW_{th} plant is expected to commence operation in 2011 in La Pereda Spain. The above plants are presented below.

2.2.1 The 30 kWth DFB Test Facility at INCAR- CSIC in Spain

The INCAR-CSIC facility is shown in Fig. 2.2 and consists of two circulating fluidized bed reactors: a carbonator and an air-fired regenerator. The height of the carbonator and the regenerator is 6.5 m and 6.0 m, respectively while both reactors have a 0.1 m internal diameter. The first 2.5 m of the risers and the loop seals are surrounded by electric ovens. The facility is also equipped with zirconia oxygen probes to measure local O_2 concentration due to the fact that aeration in the loop seal can reach 20 % of the total flow of gas entering the risers and there is uncertainty about the path of this aeration gas. In order to extract solid samples for further analysis and measure circulation rates (G_s, kg/m²s) a bypass of solids is located below the loop seals which divert solids to a dead volume for a certain period of time.

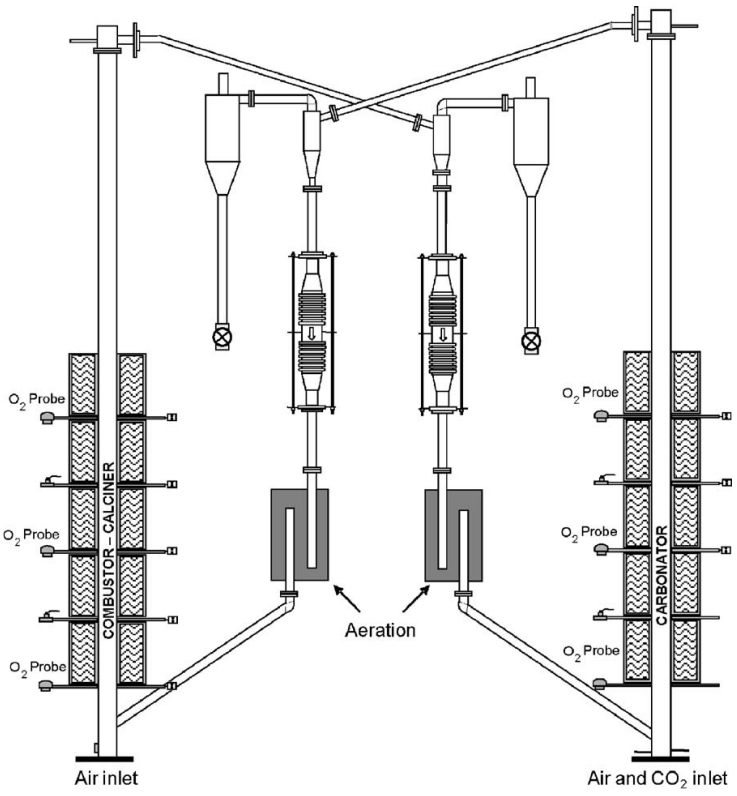

FIG 2.2: 30 kWth DFB TEST FACILITY AT INCAR- CSIC [12]

Moreover, quartz glasses are located in the inclined standpipe between the loop seals and the risers and are used for visual confirmation that the solid circulation rate remains stable. The flue gas, entering the carbonator, is synthetically pre-mixed and consists of air and carbon dioxide. The carbon dioxide reacts with active calcium oxide coming from the regenerator at temperatures between 600 and 700 °C. The formed calcium carbonate is regenerated in the CFB regenerator at temperatures between 800 and 900 °C. The mixture of gases and solids leave the risers through the primary cyclones from where the solids fall through a vertical standpipe to bubbling fluidized bed loop seals. The loop seals are aerated with air and solids flow over them towards an inclined standpipe that directs them to the other reactor. Recent experiments proved that the CFB carbonator reactor can reach high capture efficiencies between 70-90 %, during continuous operation for a range of experimental conditions [12]. All of the experimental campaigns conducted with use of the INCAR-CSIC facility [12, 30] proved that the CFB carbonator works as an effective carbon dioxide adsorber when supplied with sufficient flow of active calcium oxide while can reach high capture efficiencies.

2.2.2 The 75 kW DFB Test Facility at CANMET- Canada

The CANMET 75 kW_{th} dual fluidized bed facility [13] is illustrated in Fig. 2.3. The facility consists of a CFB regenerator and a two stage combustor-carbonator. The regenerator is a CFB combustor designed to operate in oxy-fuel conditions using recycled flue gas. The carbonator is divided into two stages which operate in bubbling-moving bed mode. The total height of the riser is 5 m while both reactors have an internal diameter of 100 mm. In order to provide supplemental heating the bottom of the riser is surrounded with three electric heaters 5 kW each.

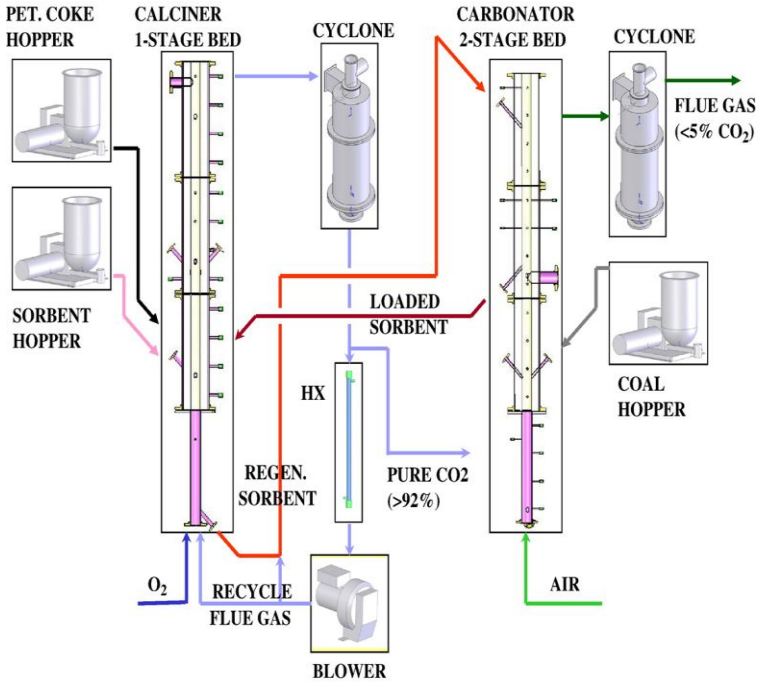

FIG 2.3: CANMET 75 kWth DUAL FLUIDIZED BED FACILITY [13]

The carbonator can be fluidized only with air or with a mixture of air and superheated steam. The first stage of the carbonator is comprised of the combustor which provides flue gas to the second stage (actual carbonator). The ability to demonstrate the process with "real" combustion flue gas is a novelty of this facility. The second stage is located two meters above the bottom of the first stage. As a result a single gas stream fluidizes both of the stages while they operate at different conditions. The carbonated sorbent is calcined in the regenerator and returns back to the carbonator to repeat the cycle trough a conveying line (red line). The calciner is fluidized with oxygen-enhanced air and/or recycle gas from a blower. This is essential for the oxy-fuel process in order to achieve high concentration of CO_2 in the exit gas from the calciner. Flue gas exits at the top of the calciner and directed to the cyclone from where it passes through a heat exchanger (HX) for fine particle removal. In order to achieve solid transportation, the solids from the distributor are collected through a 45 degree 'T'. A solenoid valve controls the solid flow by conveying air through a 6.0 m conveying line so as to lift the solids up to the carbonator. This system allows collecting solid samples from the line and calculating the sorbent cycle number based on the total amount of calcined sorbent in the system and the solid conveying line. A series of experiments conducted in the facility proved that is capable of achieving high CO_2 capture efficiencies over 95 %. A CO_2 capture efficiency up to 98 % was observed during the very first cycles and decreased to 72 % once the solids looping reached 25 cycles. Some of the decrease in CO_2 capture efficiency , with increasing loop-

ing cycles, can be attributed to the attrition, which was about 60 %. The highest CO_2 capture efficiency (98 %) was achieved in the temperature window of 580-600 °C.

2.2.3 The DFB Test Facility of the Department of Thermal Engineering, University of Tsinghua- P.R. China

This DFB reactor system [14] consists of two bubbling fluidized bed facilities and is presented in Fig. 2.4. The reactors are two bubbling fluidized beds. First, a cold model was built to provide guidance for the hot facility design. The downcomers are located on the wall side of each reactor to improve the solid flow. The novelty of this facility is the use of solid injection nozzles inside the reactors leading to immersed pipes of small diameter (risers) that convey the solids between reactors.

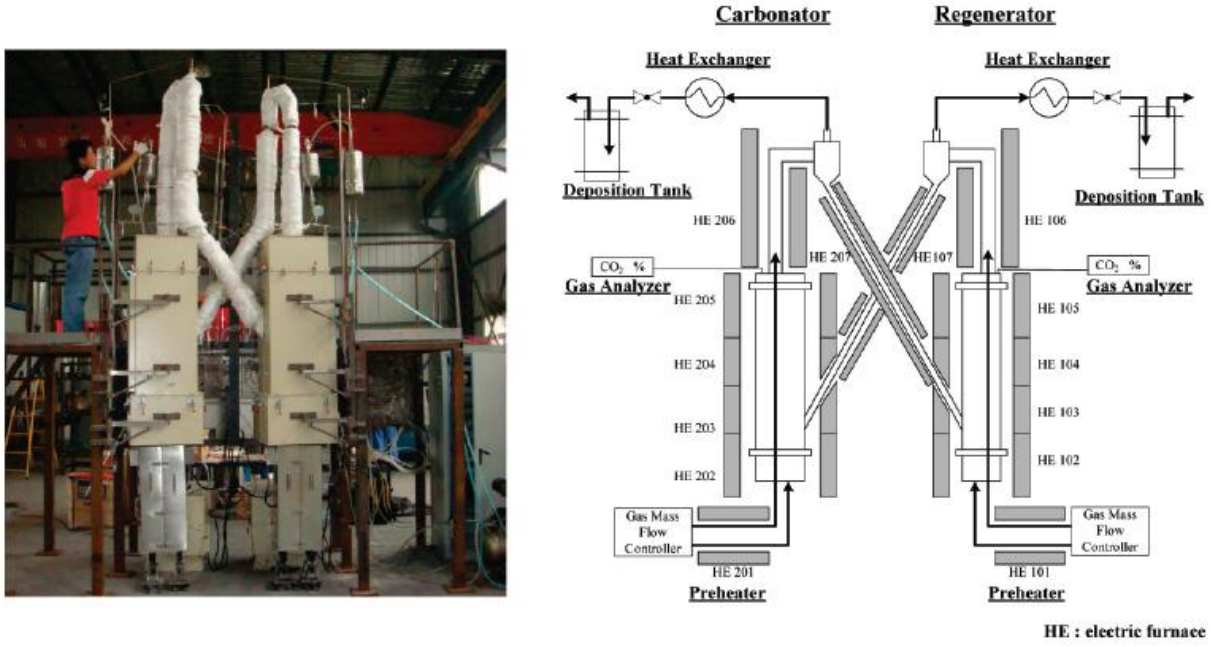

FIG 2.4: SCHEMATIC OF THE HOT MODEL DFB FACILITY [14]

The internal diameter of the carbonator is 0.15 m while that of the regenerator is 0.12 m. Each reactor is surrounded by four electrical heaters of 2.5 kW. The flue gas stream which fluidizes the carbonator consists of a mixture of air and pure CO_2 while air fluidizes the regenerator. The gas for carrying the sorbent in the solid injection nozzles is also air. Before the gases enter the reactors they are pre-heated. The solid circulation rate between the reactors has been shown to be adjustable by changing the gas velocity in the solid injection nozzles, the amount of the sorbent and the structure of the solid injection nozzles. Moreover, CO_2 capture efficiency higher than 95 % has been also recored in this facility.

2.2.4 Previous work at the 10 kW_{th} DFB Test Facility at IFK, Germany

The 10 kW_{th} DFB facility at IFK comprises of a Bubbling Fluidized Bed (BFB) with a diameter of 114 mm and a Circulating Fluidized Bed (CFB) riser with a diameter of 71 mm and height of 12.4 m. The solids exchange between the reactors is controlled with use of a cone valve, which is a novelty of this facility. A detailed description of this facility and the standard experimental procedure used by IFK is found in Chapter 4 and is therefore ommitted here. The first experimental campaigns were carried out in a scaled cold model and were focused on hydrodynamic aspects [9]. Later a parametric study was conducted with use of the 10 kW_{th} DFB facility [11]. Moreover, attrition rate was found to be below the limestone make up requirements estimated to maintain sorbent activity. Steady state CO_2 capture efficiency up to 93 % has been recorded during previous operation.

2.2.5 The 200kW$_{th}$ DFB Test Facility at IFK, Germany- commissioning in 2010

The 200 kW$_{th}$ DFB test facility at IFK comprises of a 10 m high carbonator (blue reactor) with a diameter of 0.23 m, a 10 m regenerator (red reactor) with a diameter of 0.15 m and a 6 m combustor (yellow reactor) with a diameter of 0.35 m. The facility is presented schematically in Fig. 2.5 [31] below:

The DFB facility does not require electric heating due to the fact that the oxy-fuel fired regenerator will provide the necessary heat. It is designed in such a way that the operating conditions fulfil the requirements for low specific heat loss, compact reactors and high throughput. The design case of the facility is CO_2 capture efficiency of 85 %. Parametric variation of temperature, circulation rate, make-up flow and bed mass is considered. Basic process requirements, considered for the design are good gas-solid contacting using high velocity in the CFBs for all reactors, homogeneous temperature distribution and Calcium Looping rate control through cone valves.

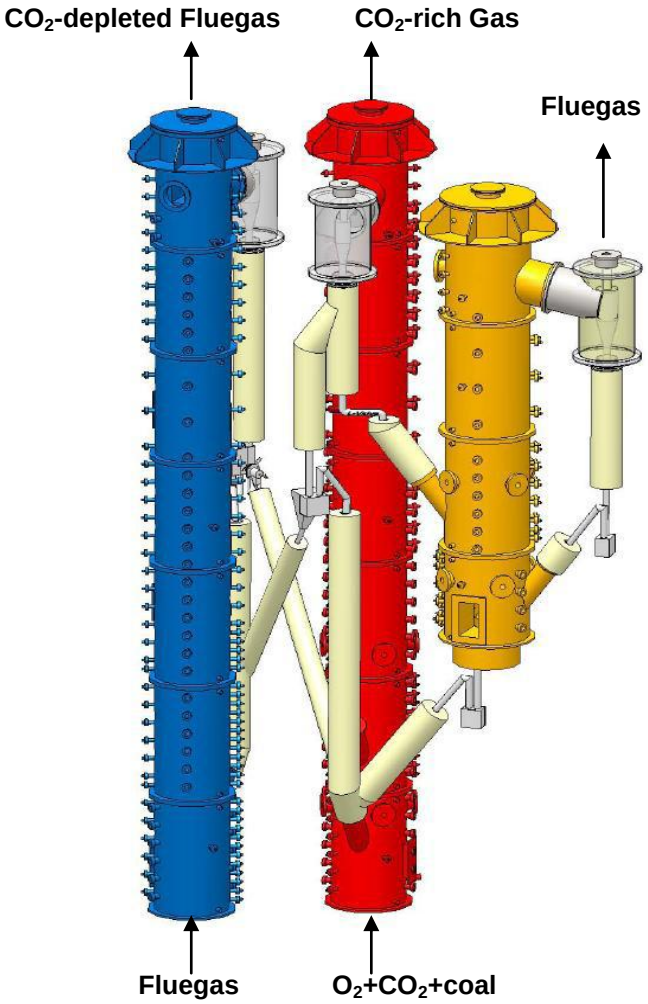

FIG 2.5: SCHEMATIC OF 200kWth TEST FACILITY IFK [31]

The aim of the facility is the experimental testing of Calcium Looping Process (CaL) under realistic conditions by using different limestones. The determination of the CO_2-capture costs and efficiency penalty through this pilot plant will contribute for the scale-up of the process to the next scale.

2.2.6 The 1 MW_{th} DFB Test Facility at La Pereda, Spain-commissionig in 2011

The 1 MW_{th} Calcium Looping pilot will be built in the Hunosa 50 MW_e CFB coal power plant of La Pereda, using a side stream of flue gases of the commercial plant [32]. The purpose is to evaluate and optimise the concept in the 1 MW_{th} facility in operating conditions equivalent to large-scale industrial units and integrated in a commercial plant by analysing the controllability and stability of the process. The research efforts will be focused in minimizing sorbent make-up flow, operational cost, measuring the effects of attrition, determining the effects of coal ash and sulphur content. New techniques of reactivation and preactivation will be tested also. The goal of the project is to generate a conceptual design for a 20-30 MW Calcium Looping demonstration plant which is the next development step of the CaL process

3. Theoretical Background

In this chapter is going to be analyzed the theoretical backround of the Calcium Looping Process (CaL) as far as the chemistry and the process itself is concerned.

3.1 Chemistry of the Sorbent Particle

The chemistry of the sorbent of the particle has been investigated in many studies the last decate and concerns important factors such as the chemical equilibrium, the decay of the maximum carbonation conversion and the reactivation of the particle, points that are being analyzed below.

3.1.1 Chemical Carbonation-Calcination Equilibrium

The equilibrium CO_2 concentration, in regard to the carbonation-calcination reaction, defines the maximum possible capture efficiency that can be achieved with the CaL process. It is a function of temperature and is given by Eq. 3.1, for the temperature interval of interest, which was established by Baker [33]:

$$C_{CO\,2,eq} = \frac{1.462 \cdot 10^{11}}{T_{Carb}} \cdot \exp\left(\frac{-19130}{T_{Carb}}\right) \tag{3.1}$$

The chemical equilibrium can be further expressed as a function of the equilibrium partial pressure of CO_2 in the flue gas and the reaction temperature [34], as shown by Eq. 3.2:

$$\log_{10} P_{CO\,2,eq}(atm) = 7.079 - \frac{8308}{T_{Carb}} \tag{3.2}$$

The equilibrium CO_2 concentration and partial pressure increases with temperature. Due to the fact that coal-fired power plant flue gas exhibits a partial pressure of CO_2 below 0.15, the temperatures to achieve a sufficient level of carbonation are between 600-750 °C. The maximum possible CO_2 capture efficiency, or in other words CO_2 conversion, through carbonation is termed as E_{eq}. It is defined through the equilibrium partial pressure of CO_2, given in Eq. 3.2, and the volumetric concentration of CO_2 in the flue gas to be treated ($y_{CO2,\,in}$). The E_{eq} is given in Eq. 3.3:

$$E_{eq} = 1 - \frac{P_{eq}(1 - y_{CO\,2,in})}{y_{CO\,2,in}(P_{total} - P_{eq})} \tag{3.3}$$

This equilibrium allows for CO_2 capture efficiencies higher than 89 % for the above mentioned parameters and at temperatures of around 650 °C [22]. Carbonator operation at 600 °C results in E_{eq} values higher than 96 %. Should a CO_2 capture efficiency of above 90 % be required in todays coal-fired power plants carbonator operation would be realized within the temperature window of 600-650 °C.

3.1.2 Fast and Slow Carbonation Reaction Regime

The carbonation reaction is a gas-solid reaction which goes through two different successive regimes, the fast and the slow reaction regime, which are depcted in Fig. 3.1:

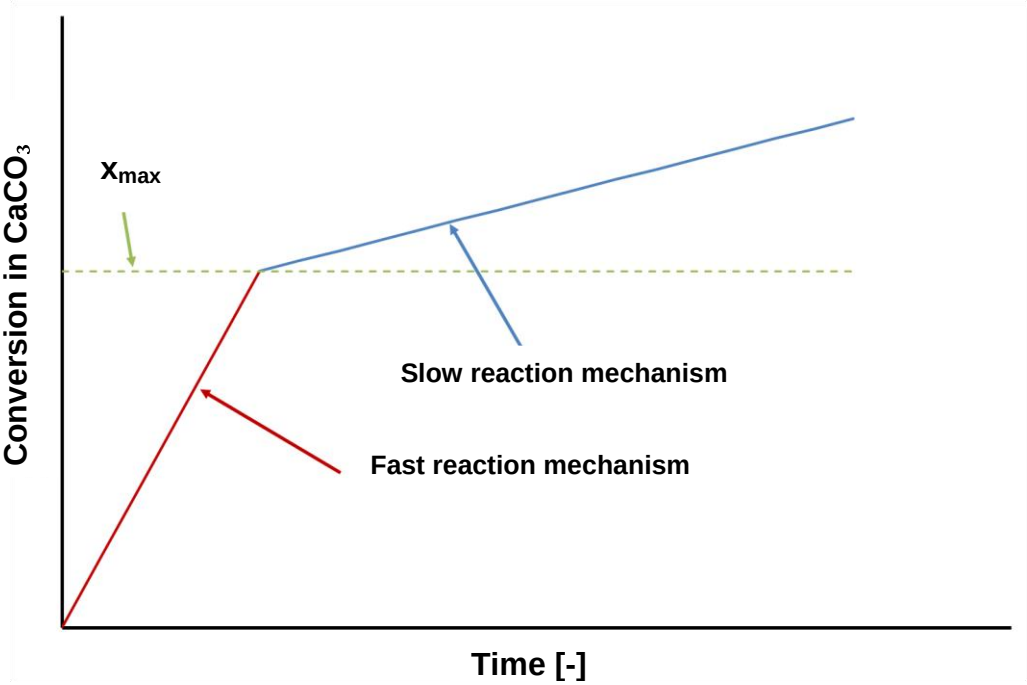

FIG 3.1: FAST AND SLOW MECHANISM OF CARBONATION REACTION

Initially the reaction proceeds quickly and is controlled through surface kinetics. At a certain point the fast reaction regime stops abruptly and the reaction becomes diffusion controlled, since the gas has no direct contact with active CaO [17]. The carbonation conversion at which the reaction regime shifts from fast to slow is termed as maximum carbonation conversion (X_{max}) or sorbent carrying capacity and is illustrated in Fig. 3.1 with the green line. The shift from fast to slow carbonation regime takes place when a product layer of $CaCO_3$ of 50 nm is formed [17]. The reaction rate of the slow reaction regime is generally so small that it is interesting for technical applications [17].

Recently, this equation has been modified to account for the limit of maximum carbonation [35], as shown in Eq. 3.4:

$$\left(\frac{dX_{Carb}}{dt}\right)_{Karbonator} = \frac{k_S S_o}{(1 - e_o)}(X_{max} - X_{Carb})^{\frac{2}{3}}(C_{CO_2} - C_{CO_2,eq}) \quad (3.4)$$

In Eq. 3.4 k_S is the rate constant for surface carbonation, S_o is the initial surface area and e_o is the particle porosity which are all constants and are dependant on the type of limestone used. The concentration of CO_2 in the flue gas, C_{CO2}, is dependent on the fuel type used and the excess of air setting, while $C_{CO2,eq}$ and X_{max} have been defined in Eq. 3.4 and Fig. 3.1, respectively. The X_{carb} is the actual conversion of the CaO particle to $CaCO_3$. To better explain the physical meaning of X_{max}, X_{carb} and their difference Fig. 3.2 is used.

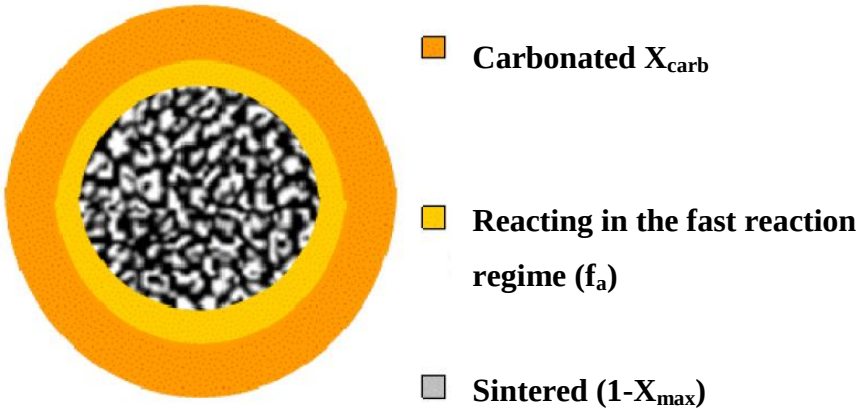

FIG 3.2: PARTICLE BALANCE AND CRITICAL THICKNESS

This part depicted by the addition of the orange and yellow regions of the particle represents the maximum possible conversion of a CaO particle to $CaCO_3$ (X_{max}), first defined in Fig. 3.2. The rest of particle ($1-X_{max}$) can not react to $CaCO_3$, in the fast reaction regime, because the diffusion resistance of the $CaCO_3$ layer formed in the outer part is too big. The part that has converted to $CaCO_3$ (X_{carb}) is depicted by the orange region and is smaller than the maximum possible conversion, X_{max}. The carbonated part of the particle, X_{carb}, is naturally located in the outer part of the particle, since it is easily accessible from CO_2. The difference between the maximum possible conversion of a CaO particle (X_{max}) and the actual conversion of a particle (X_{carb}) represents the available part for reaction with CO_2. This part is called the free active part of the paricle (f_a). It is respesented by the yellow region of the particle and is shown by Eq. 3.5:

$$f_a = X_{max} - X_{Carb} \quad (3.5)$$

3.1.3 Decay of Maximum Carbonation Conversion

The maximum carbonation conversion of calcium-based sorbents decreases with each carbonation-calcination cycle due to sintering phenomena [19, 36, 37, 38]. When the exact carbonation-calcination cycle of a sorbent particle is known the symbol X_N is used rather than X_{max} to describe the maximum possible carbonation conversion. The X_N decay as a function of the complete carbonation-calcination cycle number (N) can be calculated, for the average limestone, using the following formula [39] where k an X_r (residual CO_2 capacity) are empirically derived constants:

$$X_N = \frac{1}{\frac{1}{1 - X_R} + kN} + X_R \qquad X_R = 0.075,\ k = 0.52 \tag{3.6}$$

The values of the constants of Eq. 3.6 are representative for the average limestone and have been derived from a large limestone database. Naturally, the constants of Eq. 3.6 differ for spericific limestones. The maximum carbonation conversion has been studied by Abanades and Grasa extensively [39]. Eq. 3.6 plotted in Fig. 3.3. The decay of X_N is shown to be steep over the first 20 cycles, while it is smaller as N increases. Finally, the X_N converges to the residual activity value X_R, noted in Eq. 3.6.

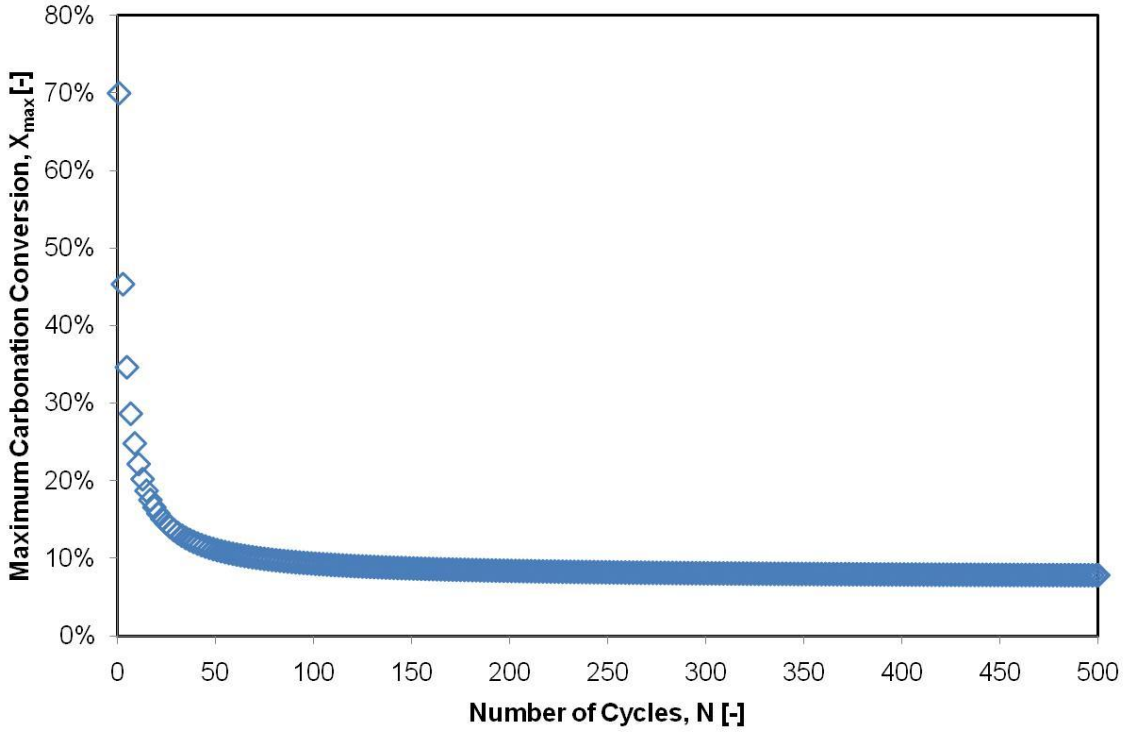

FIG 3.3: CARBONATION CAPACITY X_{MAX} DECAY OVER 500 CYCLES

The decay of X_N (or X_{max}) with increasing number of cycles (N) is a result of particle sintering. Particle sintering is a process where the small pore distribution (< 200 nm) of the sorbent particle decreases, resulting in a lower particle surface area and therefore a lower X_{max}. This is illustrated in Fig. 3.4, where sorbent samples, from the Swabian Alb limestone, exhibiting a less small pores and a smaller surface area have a smaller maximum carbonation capacity. The data of Fig 3.4 have been derived from previous experimentation in the 10 kW_{th} DFB facility of the University of Stuttgart [11].

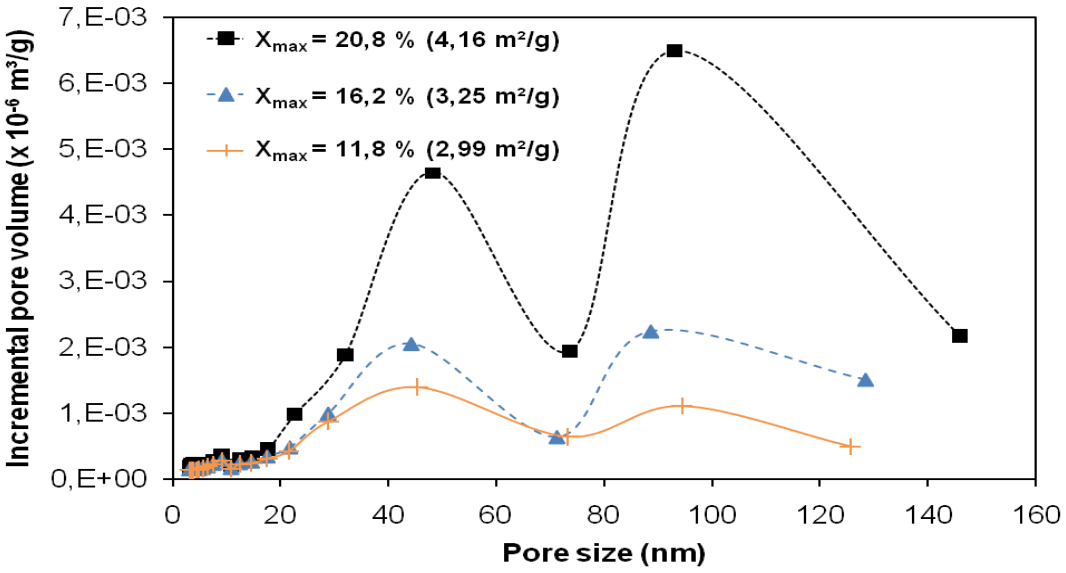

FIG 3.4: INCREMENTAL PORE VOLUME DISTRIBUTION FOR SOLID SAMPLES COLLECTED AFTER THE REGENARATOR AND WITH DIFFERENT CO_2 CARRYING CAPACITIES (X_{max}) [11]

3.1.4 Reactivation of CaO-Based Sorbents

Sorbent deactivation, as shown in Fig. 3.4, is a considerable problem for the calcium looping cycle caused by sintering. Thermal pretreatment and hydration of spent sorbent have been examined, as countermeasures hereto, in order to improve sorbent reversibility.

3.1.4.1 Thermal Pretreatment

Lysikov first studied the effects of thermal pretreatment [36]. At first, the maximum carbonation conversion (X_{max}) of the sorbent was lower than might be expected for an untreated one. Consecutively, some of them displayed an increase in $X_{max,}$ which started to decrease after a few cycles. Recently, Manovic and Anthony published a study about thermal pretreatment [40]. In the first series of experiments pretreatment was performed at different temperatures (800-1300 °C) and different durations (6-48 h) using four Canadian limestones. This study presented a method which includes activation by grinding and thermal treatment. The combi-

nation of both leads to a new behavior of the sorbent which called self- reactivation. Three types of pretreatment can be used in a thermogravimetric analysis (TGA) reactor which are carbonation, calcination and sintering under different conditions each time. The results indicated that thermal pretreatment can lead to better performance of a sorbent in a longer series of cycles, especially for powdered samples pre-heated at 1000 °C. These results were explained with a newly proposed pore-skeleton model as shown in Fig.3.5. During thermal pretreatment two activities occur. Bulk diffusion during calcinations and ion diffusion after decomposition of $CaCO_3$ which leads to a hard skeleton formation. In subsequent cycles, the external (soft) skeleton grows as a result to accelerate the carbonation rate. Simultaneously, the inward hard skeleton keeps the particle morphology stable and reduction of surface is presented. In addition, the surface area which is smooth due to thermal pretreatment may be transformed and lead to increased conversions The conversion for one sorbent after infinite cycles is the consequence of the competition between ion diffusion (hard skeleton) and bulk mass transfer (sintering) which results in the formation of the sorbent morphology with a stable skeleton that determines conversions. Contrary to these results the second series of experiments [41], investigating the behavior of La Blanca limestone, indicated that the pretreated sorbent has a lower CO_2 capture capacity, even after 30 cycles. Developing sorbents with self-reactivation performance will be very important due to economic and environmental advantages. However, it should be mentioned that as LaBlanca limestone a lot of sorbents show similar behavior by not responding to thermal pretreatment.

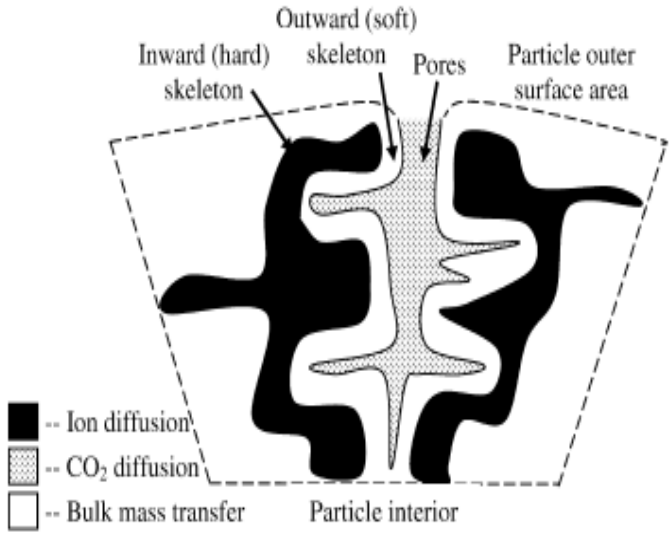

FIG 3.5: SCHEMATIC REPRESENTATION OF PORE SKELETON MODEL [36]

3.1.4.2 Reactivation of Sorbent using Hydration

The hydration of spent sorbents is a promising reactivation method [42, 43, 44]. It occurs in two stages, one fast surface controlled stage and one slow diffusion controlled stage. Two groups of researchers reported that reactivity of spent sorbent can be doubled using hydration: Manovic and Anthony who performed experiments in a pressurized reactor containing steam at 473 K [45] and Fennell et al. [42] who hydrated the sorbent at room temperature in a humid vessel. Higher capture efficiencies have also been achieved by hydrating particles whilst grinding in wet conditions but the most important drawback for industrial scale use is that wet mixtures have a tendency to solidify (cement) if not used rapidly [42]. A recent study of Manovic and Anthony examined steam reactivation of the sorbent to improve the reversibility of multiple capture cycles [41]. The types of experiments, performed in a tube furnace, were calcinations/sintering of samples under different conditions and cyclic carbonation of partially sulfated and unsulfated sorbents. The particles were hydrated in a pressure reactor and placed on filter paper in an aluminum sample dish within the vapor space of the pressurized reactor at temperature of 200 °C. When the hydration experiment finished after 30 min the samples were transferred to a vacuum oven to get dried at 50 °C for 2 h. After two repetitions of the hydration process the samples were merged. For both types of samples the carbonation of the initial cycles was higher than for the natural sorbent (35-40 %) approximately up to 70 % as shown in Fig. 3.6 and in Fig. 3.7.

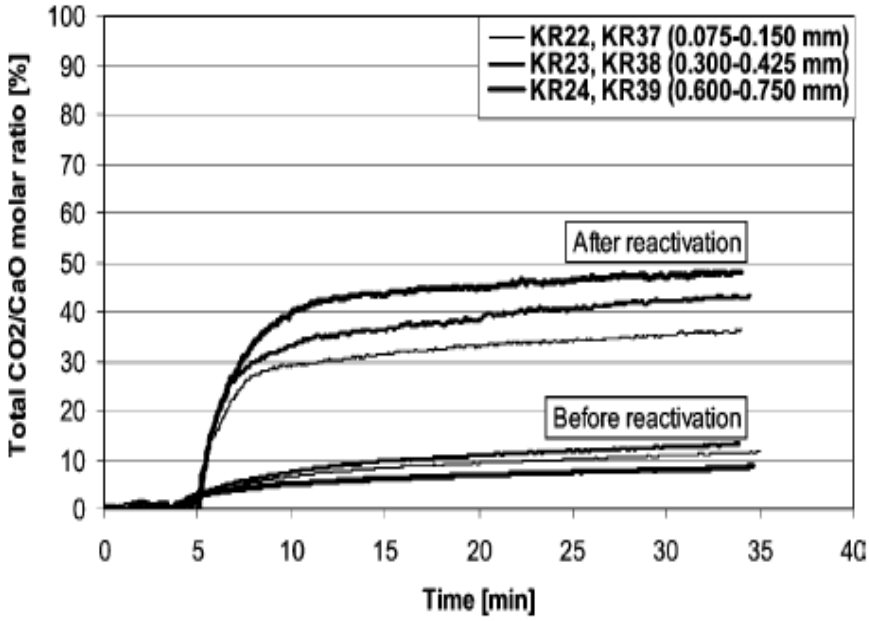

FIG 3.6: STEAM REACTIVATION EFFECT ON SORBENT ACTIVITY DURING CARBONATION IN THE TGA PARTIALLY SULFATED SORBENT [42]

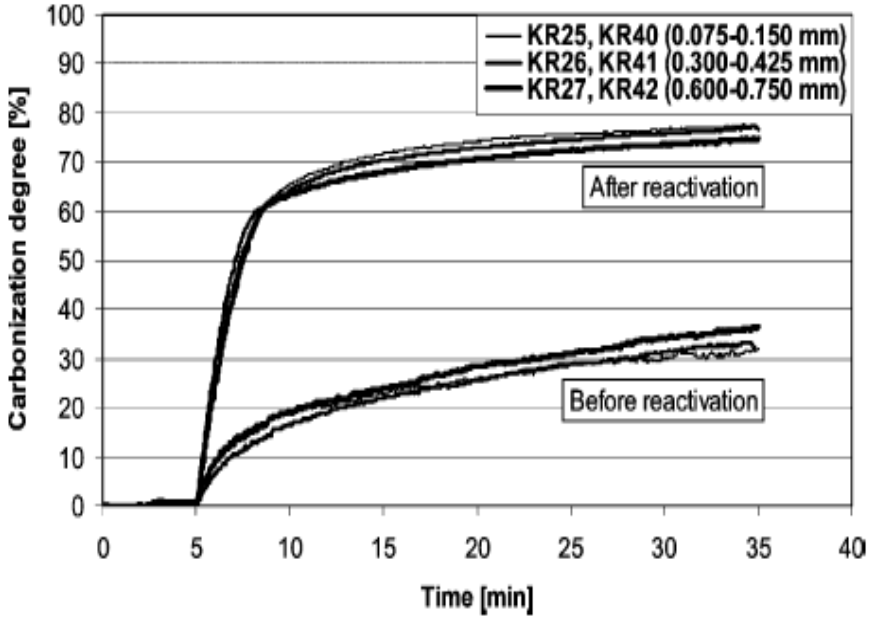

FIG 3.7: STEAM REACTIVATION EFFECT ON SORBENT ACTIVITY DURING CARBONATION IN THE TGA UNSULFATED SORBENT [42]

This analysis shows that steam reactivation actually improves sorbent characteristics in comparison to original sorbent and could contribute in the commercialization of the process of CO_2 separation by CaO-based sorbent.

3.2 Characteristic Values of the Calcium Looping Process

In order to utilize particle chemistry, i.e. the carbonation-calcination reaction, it is important to examine the CaL Dual Fluidized Bed facility as a whole. This is realized by performing a mass balance and defining, analyzing the primary and intermediate facility operational parameters. The primary parameters that can be directly influenced by the handling of the operator, such the calcium looping ratio between the carbonator and regenerator, while the intermediate parameters are mainly a result of the variation of primary parameters and particle chemistry.

3.2.1 Carbonator-Regenerator Efficiency and CO_2 Molar Balance of the CaL System

The process of the CaO-based looping cycle is presented meticullusly in the following schematic.

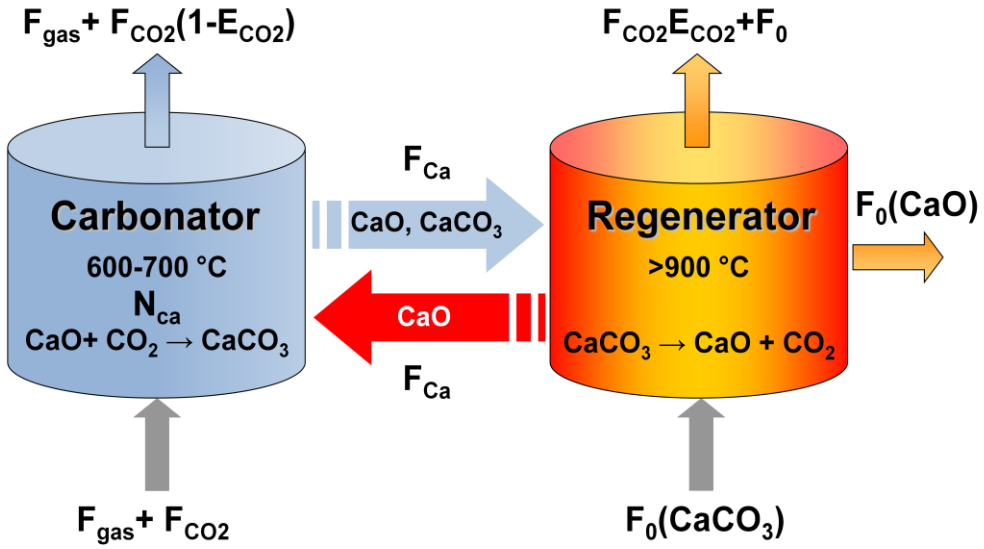

FIG 3.8: SCHEMATIC OF THE CaO-BASED CO_2 LOOPING CYCLE DENOTES PRESENCE OF CaO AND $CaCO_3$ IN STREAM

The molar balance of Calcium Looping (CaL) is demonstrated in Fig. 3.8. The CO_2 is adsorbed from CaO in the carbonator (n_{Ca}) and a CO_2-lean flue gas is produced. A fraction (X_{carb}) of the calcium looping rate (F_{Ca}) exiting the bed is carbonated. The CO_2 captured ($F_{Ca} \cdot X_{carb}$) is transferred to the regenerator with the calcium flow. A make up flow of fresh $CaCO_3$ (F_0) is necessary to compensate for the decay of the carrying capacity of the sorbent

[37]. The CO_2 capture efficiency (E_{CO2}) of the carbonator is the most important metric of its performance. It is defined as the ratio of the moles of CO_2 captured in the carbonator and is given by the Eq. 3.7:

$$E_{CO\,2} = 1 - \frac{F_{CO\,2,out}}{F_{CO\,2,in}} \tag{3.7}$$

The regenerator performance is expressed through the regenerator efficiency (η_{reg}). The regenerator efficiency is defined based on how complete the calcination reaction in the regenerator is. The η_{reg} is given in Eq. 3.8 based on the carbonation conversion of the incoming (X_{carb}) and outgoing (X_{calc}) sorbent in regard to the regenerator.

$$\eta_{reg} = 1 - \frac{X_{calc}}{X_{carb}} \tag{3.8}$$

If X_{calc}= 0, than η_{reg} would be 100 % and hence, the regenerator would calcine the sorbent fully. On the other hand if X_{calc}=X_{carb} than η_{reg} would be 0 % and hence, the regenerator would not calcine the sorbent at all.

For the carbonator mass balance to be satisfied the CO_2 removed from the gas phase is equal to that adsorbed by the bed and equal to the increase of $CaCO_3$ moles after leaving the carbonator. In mathematical terms this is expressed by Eq. 3.9 and Eq. 3.10:

$$F_{CO\,2} \cdot E_{CO\,2} = n_{Ca} \cdot \left(\frac{dX_{Carb}}{dt} \right) \tag{3.9}$$

$$F_{CO\,2} \cdot E_{CO\,2} = F_{Ca} \cdot (X_{Carb} - X_{Calc}) \tag{3.10}$$

3.2.2 Primary CaL Operational Parameters

Primary CaL operational parameters are defined as those that are directly influenced from the CaL operator or/and facility designer. These are the calcium looping ratio (F_{Ca}/F_{CO2}) between the carbonator and regenerator, the make-up flow ratio (F_0/F_{CO2}), the carbonator space time (τ) and the carbonator and regenerator residence time (r_{carb} and r_{reg}, respectively).

The calcium looping ratio F_{Ca}/F_{CO2} is defined as the molar ratio of calcium (F_{Ca}) and CO_2 flow entering the carbonator. Increasing the sorbent looping ratio imposes a significant energy penalty on the process because more fuel must be combusted in the oxyfuel regenerator in order to heat up and calcine the circulating sorbent, thereby increasing the parasitic load from the ASU. A larger oxyfuel regenerator (and associated auxiliary equipment) also increases the Calcium Looping capital cost. In order not to operate with excessive F_{Ca}/F_{CO2} values resulting to extra costs it would be optimum that the regeneration efficiency 100 %. This can be explained through Eq. 3.11 which is derived through Eq. 3.8 and Eq. 3.10.

$$E_{CO\,2} = \left(\frac{F_{Ca}}{F_{CO\,2}} \eta_{reg} \right) X_{Carb} \tag{3.11}$$

From Eq. 3.11 it is clear that any given pair of E_{CO2} and X_{carb} can be achieved through infinite combinations of F_{Ca}/F_{CO2} and η_{reg}, while their product remains constant. Naturally, the lowest value of F_{Ca}/F_{CO2} is achieved when η_{reg} is 100 %.

The make-up flow ratio F_0/F_{CO2} is defined as the molar ratio of fresh $CaCO_3$ and CO_2 flow entering the carbonator. The make-up flow of fresh limestone is added as a countermeasure to the decay of the maximum carbonation conversion [37]. However, the addition of large amounts of fresh limestone leads to a slight increase in CO_2 avoidance costs Poboß et al. [23] and may also present a disposal problem if the purged CaO-rich material does not have a market capable of handling large quantities. However, as reported by Weimer et al. [29] and noted above the purge molar flow (F_0) can be used for the production of cement clinker.

The carbonator space time (τ) is defined as the ratio of moles of CaO (n_{Ca}) present in the carbonator and the molar flow of CO_2 in the flue gas feed. The space time is given by Eq. 3.12:

$$\tau = \frac{n_{Ca}}{F_{CO\,2}} \tag{3.12}$$

The space time expresses the carbonator inventory for a given CO_2 flow. Through combination of the space time definition of Eq. 3.12 and the mass balance equation of Eq. 3.9, the re-

lation between E_{CO2} and τ is shown. The space time is related to capture efficiency, combining Eq. 3.9 and Eq. 3.12:

$$E_{CO_2} = \tau \cdot \left(\frac{dX_{Carb}}{dt} \right) \tag{3.13}$$

Increasing the space time in the carbonator has the disadvantage that it increases the carbonator pressure drop and therefore results to a higher parasitic load due to the electricity consumed through the carbonator blower.

The residence time of a sorbent particle in the carbonator and regenerator is defined as the ratio of the calcium moles existing in each respective reactor and the calcium looping ratio. The definition of the residence time is given in Eq. 3.14. The residence time of a sorbent flow in the regenerator is given by Eq. 3.14 below:

$$r_i = \frac{n_{Ca}}{F_{Ca}} \tag{3.14}$$

The residence time in the carbonator (r_{carb}) is limited to 2-5 min., as has been shown from previous TGA studies, e.g. [37]. The reason here to is that the carbonation reaction would proceed after such a residence time through the slow diffusion controlled carbonation regime, as shown in Fig. 3.1, and the CO_2 capture efficiency values would become moderate. The residence time in the carbonator is fully defined when the space time (τ) and calcium looping ratio (F_{Ca}/F_{CO2}) are given. The relationship connecting the above values is derived through the definition of space time, Eq. 3.12, and residence time, Eq. 3.14 and is given by Eq. 3.15:

$$r = \frac{\tau}{F_{Ca} / F_{CO_2}} \tag{3.15}$$

Regarding the regenerator, longer residence time (r_{reg}) would mean higher values of regenerator efficiency (η_{reg}). This true provided that temperatures in the regenerator remained below 950 °C. Otherwise increased sintering phenomena would occur to the sorbent through increasing r_{reg}. The residence time in the carbonator and regenerator are coupled with each other through the calcium looping ratio. However, the r_{carb} and r_{reg} can be set independently, taking into consideration hydrodynamic limitations, by variation of the inventory of the carbonator and the regenerator, respectively.

3.2.3 Intermediate CaL Operational Parameters

Intermediate CaL operational parameters are those that cannot be directly set from the operator, but are a result of primary parameters and particle chemistry and are directly linked to the

CO_2 capture efficiency (E_{CO2}). These are the maximum carbonation conversion (X_{max}) the actual carbonation conversion (X_{carb}), the free active Ca part of the bed (f_a) and the active space time (τ_a).

The actual carbonation conversion (X_{carb}) is shown to be mainly a function of the F_{Ca}/F_{CO2}, as is shown by the carbonator CO_2 mass balance of Eq. 3.11. Assuming that η_{reg} is 100 %, it is clear that the variation range of F_{Ca}/F_{CO2} is greater than that of E_{CO2}. For example, if during steady state operation the E_{CO2} value is 80 % and the F_{Ca}/F_{CO2} value is doubled, the only way the mass balance of Eq. 3.11 can be satisfied is by the reduction of X_{carb}. This relationship has been experimentally demonstrated in [11].

The maximum carbonation conversion (X_{max}) was initially calculated through a population balance by assuming that every physical loop between the carbonator and the regenerator corresponds to a full carbonation-calcination cycle [19]. This is, however, not the case in a real reactor, as has been shown in [21] where the carbonator bed mass will have an average maximum carbonation conversion, X_{max}, an average carbonated fraction, X_{carb}, and an average free active CaO fraction, f_a. Therefore, particles in the early carbonation-calcination cycles will have "spare" capacity which will be carried to the subsequent loop. For example, $X_{N=1}= 0.7$ from Eq. 3.6 and assuming $X_{carb} = 0.07$, the particle must be circulated 10 times between carbonator and regenerator before this capacity is consumed and $X_{N=2}$ is reached. The decay in maximum carbonation conversion as a function of X_{carb} is included in the transformation of X_N to $X_{N,pc}$ which is the maximum carrying capacity due to partial carbonation. The average carrying capacity of the system, based on the population balance, is given by Eq. 3.16:

$$X_{max} = \sum_{N=1}^{\infty} \frac{F_0}{F_{Ca}} \cdot \left(1 - \frac{F_0}{F_{Ca}}\right)^{N-1} \cdot X_{N,PC} \tag{3.16}$$

The above equation and Eq. 3.11 show that the parameters defining the X_{max} are the make-up flow (F_0/F_{CO2}), the calcium looping ratio (F_{Ca}/F_{CO2}) and the X_{carb} which is also related to the F_{Ca}/F_{CO2}, as well as the decay curve of Eq. 3.6. A recent study [85], produced a similar equation taking into account not only the effect of partial carbonation but also the effect of partial calcination in the regenerator, i.e. when $\eta_{reg} \neq 1$ and $X_{calc} \neq 0$.

However, during small scale experimentation (10-50 kW_{th}) that has been conducted to date [11, 30], no make-up flow has been used and the X_{carb}, F_{Ca}/F_{CO2} values have been intentionally varied. Therefore, equations of the sort of Eq. 3.16 cannot be used for determination of X_{max} during such experimentation. In such cases the X_{max} will decrease continuously since the average number of cycle of the particles will increase due to the exposition of the sorbent to

carbonation-calcination conditions in DFB mode. A first simplistic approach would be to correlate the X_{max} decay with the cumulative sorbent specific CO_2 loading $L(t)_{CO2}$, although parameters such as the X_{carb}, X_{calc}, the calcination conditions, residence time in the regenerator play a definite role. The cumulative sorbent specific CO_2 loading ($L(t)_{CO2}$) is defined as the total moles of CO_2 captured until a given time during experimentation per mol of sorbent in the DFB system and is given in Eq. 3.17. The $L(t)_{CO2}$ increases with time since no or minimal amount of mass is added to the system during operation.

$$L(t)_{CO_2} = \frac{\int_o^t F_{CO_2} E_{CO_2}(t)dt}{n_{Ca,total}} \tag{3.17}$$

In Eq. 3.17, $E_{CO2}(t)$ is the instantaneous CO_2 capture efficiency while $n_{Ca,total}$ is the total inventory in the DFB system. The $E_{CO2}(t)$ is calculated through gas analysis, while the total calcium moles ($n_{Ca,total}$) are known through weight measurement. A link can be established between the theoretical carbonation-calcination cycle (N), of the TGA full carbonation-calcination experiments (see Eq. 3.6), and $L(t)_{CO2}$ obtained during operation of a DFB CaL system. This is possible if the assumption is made that in both cases the decay of the maximum carbonation conversion, expressed as X_{max} for the DFB system and X_N for the TGA, is a function of the moles of CO_2 captured per mol of CaO only. Such a link is given by Eq. 3.18, which allows for the calculation of the theoretical carbonation-calcination cycle N.

$$L(t)_{CO_2} = \sum_0^N X_N \tag{3.18}$$

The free active CaO part of the average particle and of the carbonator bed (f_a) is established through the difference of X_{max} and X_{carb}, as noted in Eq. 3.5. Naturally, the f_a is dependant to the same parameters as X_{max} and X_{carb} and is a key parameter defining the average carbonation reaction rate of the bed, as shown in Eq. 3.4.Therefore, in many modeling and experimental studies considering constant space time, the CO_2 capture efficiency has been related to f_a, e.g. [37, 38].

The carbonator active space time (τ_a) is defined as the product of space time (τ_α) and the free active CaO part bed (f_a), as shown in Eq. 3.19 below:

$$\tau_a = \frac{n_{Ca} f_a}{F_{CO_2}} \tag{3.19}$$

The active space time (τ_a) is the product of τ and f_a. At a given inlet gas CO_2 concentration, molar flow, carbonator temperature and gas-solid contacting mode the active space time has shown to strongly correlate with the CO_2 capture efficiency [11]. This because space time defines the carbonator inventory and the f_a determines the average reaction rate of that inventory, as shown in Eq. 3.4. However, this parameter must be put to further test to examine possible modifications. For example questions such as a) should the τ, f_a in the active space time formula of Eq. 3.16 be both in the power of 1? b) is the reaction rate for two beds exhibiting the same active space time but different X_{max} values the same?, still remain open.

4. Experimental Setup and Methodology

In this chapter is analyzed the experimental Calcium Looping Facility of IFK which has been used for our experimental campaign and the procedure as well as the experimental strategy that has been followed.

4.1 Description of the 10 kW_{th} Calcium Looping Facility of IFK, University of Stuttgart

A DFB Calcium Looping facility consists of a 12.4 m high, 70 mm diameter riser and a 114 mm diameter Bubbling Fluidized Bed (BFB), as shown in Fig. 4.1. To assure the suitability of the facility, scaled cold model testing was performed and summarized by [9]. The riser is used as the carbonator (2) and the BFB as the regenerator (1). The novelty of this rig in comparison to other DFB systems is the control of the calcium looping rate between the beds by a cone valve. Flue gas enters the CFB carbonator, while the carbonated CaO flows from the double exit loop seal (3) through the cone valve (4) and enters the BFB regenerator where CO_2 is seperated from $CaCO_3$. The partially calcined $CaCO_3$ exits the carbonator through the overflow (6), enters the lower standpipe (7) and subsequently the lower loop seal (8) through which the sorbent flow proceeds to the carbonator. The carbonator off gas proceeds to the stack while the riser

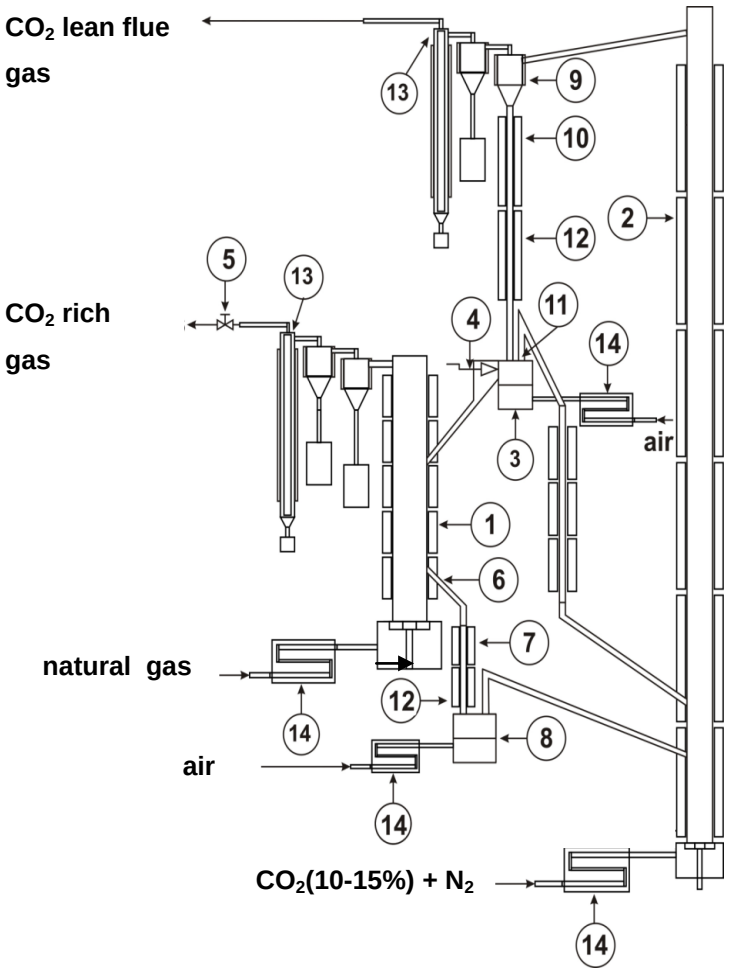

FIG 4.1: SCHEME OF 10 KW_{th} IFK CALCIUM LOOPING DFB FACILITY: (1) BFB REGENERATOR, (2) RISER CARBONATOR, (3) DOUBLE EXIT LOOP SEAL, (4) CONE VALVE, (5) PRESSURE CONTROL VALVE, (6) BFB OVERFLOW, (7) LOWER STANDPIPE, (8) LOWER LOOP SEAL, (9) CYCLONE, (10) UPPER STANDPIPE, (11) LOOP SEAL WEIR, (12) QUARTZ STANDPIPE SEGMENTS, (13) CANDLE FILTERS, (14) ELECTRICAL GAS PRE-HEATERS

entrainment is separated with a cyclone (9), proceeds to the upper standpipe (10) and reaches the double exit loop seal. A desired fraction of the riser entrainment proceeds to the BFB regenerator and the rest of the flow returns to the riser through the loop seal weir (11). The calcium looping rate is controlled by varying the cone valve opening and the BFB absolute pressure through a pressure control valve (5). The carbonator, regenerator and solid circulation system are electrically heated. Electrical pre-heaters (14) are used to heat up inlet gas flows up to a temperature of 900 °C. Flue gases exiting from riser and BFB pass eventually through candle filters (13) to remove any remaining fines.

4.2 Control Strategy of the Facility

The LabView® software program is used for control of the facility and data acquisition. Electrical heaters are controlled automatically through type N thermocouples to maintain the desired process temperature. Pressure is measured through differential and absolute pressure transducers placed so that facility pressure drop profiles can be obtained. All gas flows are controlled with Mass Flow Controllers (MFCs) except loop seal aeration which is controlled through rotameters. The carbonator is fluidized with a synthetic mixture of CO_2 and N_2, while the regenerator and loop seals are fluidized with air. The regenerator is fluidized with O_2 enriched air, where O_2 reaches a volumetric concentration of up to 40 % vol.

4.3 Gas-Solid Analysis

The carbonator flue gas was analyzed by an ABB Advance Optima 2020 continuous gas analyzer, measuring CO_2 (0-30 vol-%) and O_2 (0- 29 vol-%) while the regenerator flue gas was analyzed by an ABB EasyLine 3020 continuous gas analyzer, measuring CO_2 (0-100 vol-%) and O_2 (0-100 vol-%). The air flow stream coming from the loop seals to the CFB is calculated from the O_2 concentration measurement in the carbonator off-gas allowing for correct estimation of the CO_2 capture efficiency. At regular intervals the carbonator inlet gas volumetric CO_2 concentration was measured by the ABB analyzer to ensure that the value calculated from MFC settings was accurate. The conversion of a sorbent particle to $CaCO_3$ after the carbonator (X_{carb}) and the regenerator has been measured with a thermobalance at IFK. A large number of the samples were further analyzed with a TGA by the National Institute of Coal (INCAR) Consejo Superior de Investigaciones Cientificas (CSIC) of Spain to define the carbonation conversion (X_{carb}) and the maximum CO_2 carrying capacity (X_{max}) in order to calculate the free active fraction of CaO (f_a).

4.4 Experimental Procedure

The experimental plan is presented below as far as the facility start-up, the measurements, the evaluation of the results and the parameter variation is concerned.

4.4.1 Facility Start-Up

Before beginning with experimentation, the system was emptied in regard to solids and the material was always pre-calcined. In addition, the amount of sorbent to be introduced to the facility was weighed. The BFB was than filled up to the overflow level (6, see Fig. 4.1) and the rest of solids were filled into the upper standpipe and the lower standpipe. Than all rotameters, MFCs were checked to ensure that the corresponding valves were properly closed. Afterwards, the riser (2), the BFB (1) and the double exit loop seal (3) were supplied with air. Subsequently, the double exit loop seal (3) flow was increased till the solids in the upper standpipe (4) appeared to be in slightly bubbling condition. Solid circulation through the upper loop seal began and became steady. Thereby, the CFB loop commenced operation. Slowly the air flow was started in the lower loop seal until the solids there also reached bubbling conditions. Finally, the calcium looping rate between the riser and the BFB was set by opening and adjusting the position of the cone valve (4).

4.4.2 Measurements During Steady States and Solid Sampling

In order to assess the results obtained, it is important to not take into account data resulting from transient modi of operation. For example, if the calcium looping rate would be changed through cone valve variation, gas phase data would not stabilize immediately to a new value, but after a period of time. As a result, it is important to take into account only measurements attained during operational steady states. Steady states are defined as the time period (lasting at least 15 min) where all gas phase variables (e.g. outlet CO_2 concentration) remain unchanged. After each steady state solid samples were collected (three samples from the carbonator and one from the regenerator). Subsequently, the calcium looping rate was measured manually through an optical method analyzed below. The lower standpipe is constructed from a quartz glass standpipe segment, as shown in Fig. 4.2. When stopping the lower loop seal aeration (8), the rate of the solid bed height increment due to particle accumulation can be measured. The time required for the particle bed height in the lower standpipe to increase by 10 cm, 15 cm and 20 cm was noted. This procedure was repeated after a steady state twice. In this manner the calcium looping rate between the carbonator and regenerator was attained,

since the bulk density of a fixed bed of sorbent has been previously defined. All the data were documented in a diary in order to later evaluate the results from the log files.

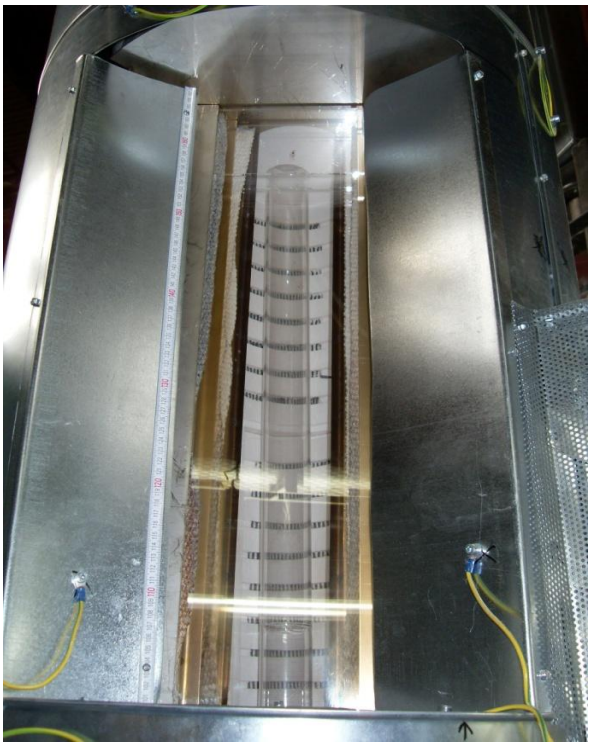

FIG 4.2: QUARTZ GLASS SEGMENT

4.4.3 Evaluation of the Results

During operation the LabView® software program saves all measurement data in an Excel file every three seconds for both the carbonator and the regenerator. After each experimental day the collected data are stored in a diagnostic table for further analysis. Before analyzing the data O_2 and CO_2 gas measurements are subjected to corrections due to calibration of ABB analyzers. Using a gas with specific concentration, the zero error and the deviation between them are defined in order to build the linear equation that corrects the gas measurements.
The analysis requires some data that cannot be measured directly but must be calculated using data from the initial log files which are the following:

- $F_{air,\ in}$: Air that enters from the loop seals in the carbonator
- F_{CO2}: Corrected CO_2 stream getting into the carbonator
- $F_{CO2,\ out}$: Corrected CO_2 stream getting off the carbonator
- E_{CO2}: CO_2 capture efficiency
- $M_{carbonator}$: Mass of the bed of carbonator
- τ: Space time of the carbonator

- $E_{CO2,eq}$: Chemical equilibrium-maximum CO_2 capture efficiency

4.5 Experimental Parameters

This campaign is designed in order to characterize the riser carbonator and regenerator operation. Two types of limestone were used, namely as Swabian Alb A and Swabian Alb B. Limestone Swabian Alb A stems from the region of Swabian Alb in Germany. For limestones Swabian Alb A and Swabian Alb B a coarse Particle Size Distribution (PSD) of (0.3-0.6 mm) was utilized. In addition, for limestone Swabian Alb A a fine PSD (0.1-0.3 mm) was also implemented. The carbonator was operated under realistic conditions. Carbonator temperature was set at approximately 650 °C. For the coarse and fine PSDs the carbonator velocity was close to 6 m/s and 4 m/s, respectively. Carbonator pressure drop was varied between 50-114 mbar. Therefore the space time (τ) was accordingly varied. The regenerator was operated at a constant temperature of 900 °C. Since the system was allowed to operate continuously for 5-10 h every experimental day and since no make-up flow was present the maximum carbonation conversion of the bed material during steady states varied in the range of 6-20 %. Moreover, the calcium looping ratio F_{Ca}/F_{CO2} has been varied between 3-23, thus varying the X_{carb} between steady states and the residence times that solids spent in each reactor. All experimental conditions of the carbonator are listed in Table 4.1:

TABLE 4.1: OPERATING CONDITIONS OF THE CARBONATOR

Parameter	Range
Temperature (°C)	645-656 °C
Superficial gas velocity (m/s)	4.1-6.1
Limestones used and PSDs	Swabian Alb A (0.1-0.3 mm)/(0.3-0.6 mm) Swabian Alb B (0.3-0.6 mm)
Fluidization regime	Fast Fluidization regime
Inlet CO_2 concentration (%)	10.4-15.7 % (mostly 11-12 %)
Bed solid inventory (kg/m^2)	480-1129
Bed pressure drop (mbar)	48-114
Space time (h)	0.3-0.6
Maximum average conversion	6.1-19.7
Fraction of active CaO	0.1-6.4
Active space time (h)	0.1-3.5

Capture efficiency	0.5-0.9
Carbonator Residence Time (min)	0.1-8.6
Regenerator Residence Time (min)	0.3-5.0

4.6 Experimental Simplifications

In order to perform this experimental campaign simplifications were made with respect to the real process. Firstly, the limestone was pre-calcined prior to experimentation. Secondly, there was no SO_2 in the flue gas fluidizing the carbonator. Thirdly, the regenerator was fluidized with air and the required energy for calcination was supplied by the electrical heaters using CH_4 combustion to maintain the temperature of the reactor. Moreover, no continuous make-up flow of limestone was implemented. However, material was added occasionally in order to maintain the DFB system inventory within acceptable limits in regard to system operation.

5. Results and Discussion

The following sections try to provide data in order to characterize regenerator and carbonator operation. The regenerator efficiency is linked with a suitable parameter, combining the carbonation conversion X_{carb} of the inlet solid stream and the residence time within the reactor. A similar analysis is conducted for the carbonator addressing also a number of issues such as sorbent decay, required calcium looping ratios and hydrodynamics.

5.1 Regenerator Operation

Previous work had defined the residence time needed in a stand alone fluidized bed calciner in order to achieve full conversion of $CaCO_3$ to CaO, based on residence time, particle size and temperature. In such units the carbonation conversion (X_{carb}) of the particles in the feed is 1. However, the X_{carb} of the particle flow entering the carbonator is typically below 15 %, which constitutes the greatest difference between a stand alone fluidized bed calciner and a regenerator within the CaL system. Therefore, it was considered appropriate to combine the carbonation conversion of the incoming particles and the residence time in the regenerator in order to find a suitable correlation for the regenerator efficiency. The factor $\frac{X_{carb}}{r_{reg}}$ represents such a suitable combination. The regenerator efficiency and (η_{reg}), defined in Eq. 3.7, and the carbonation conversion of the outlet sorbent flow from the regenerator (X_{calc}) are plotted in Fig. 5.1 and 5.2, respectively, for two different limestones and PSDs. All experimental points stem from steady states exhibiting constant temperature (900 °C) and partial pressures of $CO_2 < 0.3$ bar.

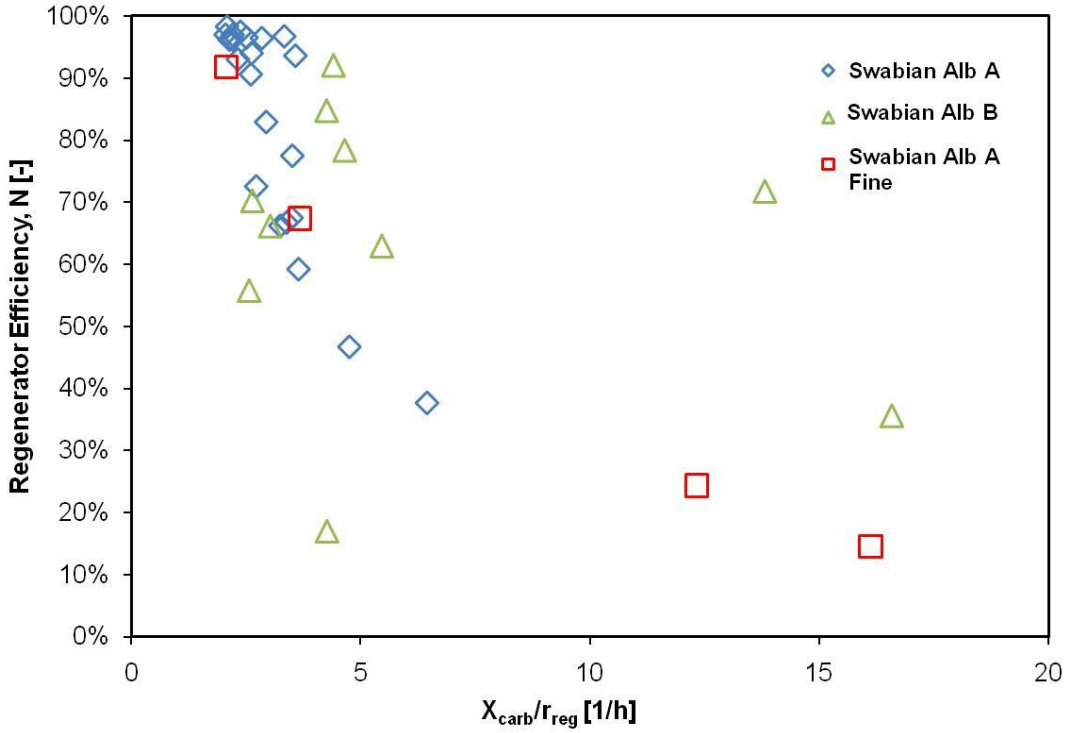

FIG 5.1: REGENERATOR REACTOR PERFORMANCE VS EFFICIENCY WITH T_{REG}=900 ˚C, P_{CO2}=0.3 bar, D_P=0.1-0.3 AND D_P=0.3-0.6

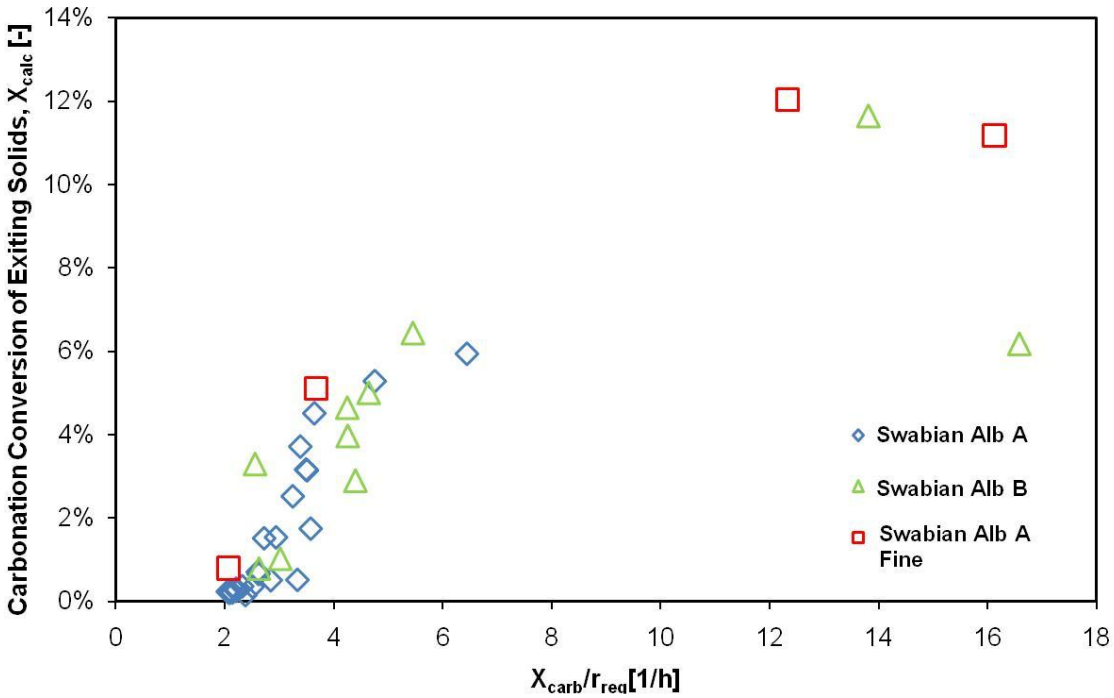

FIG 5.2: REGENERATOR REACTOR PERFORMANCE VS X_{CALC} WITH T_{REG}=900 ˚C, P_{CO2}=0.3 bar, D_P=0.1-0.3 AND D_P=0.3-0.6

Both η_{reg} and X_{calc} show a very good correlation with the proposed factor $\frac{X_{carb}}{r_{reg}}$. At $\frac{X_{carb}}{r_{reg}}$ values of around 2-3 1/h, the regenerator efficiency is generally above 90 % corresponding to carbonation conversion of the outgoing sorbent flow (X_{calc}) lower than 2 %. With increasing the factor $\frac{X_{carb}}{r_{reg}}$ the regenerator efficiency drops and the X_{calc} naturally increases. At values as higher than 6 1/h, the regenerator efficiency drops below 40 % while the X_{calc} value increases to above 6 %. The explanation of the above noted trends can be found when looking into the physical meaning of the parameter $\frac{X_{carb}}{r_{reg}}$. It represents the difficulty in regenerator's ability to calcine a carbonated particle entering the bed at given temperature and partial pressure of CO_2. At a given partial pressure of CO_2 and regenerator temperature, the average reaction rate in the regenerator should be constant. The particle size and carbonation conversion X_{carb} of the incoming particle define the $CaCO_3$ content within it to be calcined. Hence the higher the X_{carb}, the more duty is imposed to the regenerator and the difficulty for the reactor to perform increases. The difficulty for the regenerator increases when the residence time in the regenerator is limited, since then the exposure of the particle to calcination conditions is also limited, as is the case when operating with high values of F_{Ca}/F_{CO2}. Hence high values of $\frac{X_{carb}}{r_{reg}}$ correspond to low values of η_{reg} and vice versa. The results above may prove to be useful future tool for designing new facilities in order to have optimum regenerator operation under all circumstances.

5.2 Carbonator Operation

In regard to carbonator operation, examples of operational steady states are presented. Furthermore, the decay of the maximum conversion (X_{max}) with increasing sorbent specific CO_2 loading $L(t)_{CO2}$ is compared to what was expected in the TGA. Furthermore, the required Calcium Looping ratio F_{Ca}/F_{CO2} for a given CO_2 capture efficiency is investigated, while the role of X_{max} and η_{reg} in this relation is underlined. The parameter of active space time, which already has been indentified as a suitable parameter to characterize the carbonator, is tested for suitability. In addition, the physical explanation linking carbonator residence time and the CO_2 capture efficiency is given. However, it must be noted that carbonator residence time is not an independent parameter, but it is fully defined when the calcium looping ratio and car-

bonator space time are known. Finally, the flow structure of the riser carbonator is analyzed and offers an explanation in regard to the axial CO_2 profile measured.

5.2.1 Examples of Steady States

Examples of steady states leading to high CO_2 capture efficiencies are shown in Fig. 5.3, Fig. 5.4 and Fig. 5.5, conducted with different limestones, PSDs, values of maximum carbonation conversion (X_{max}) and calcination efficiencies. The steady states of Fig. 5.5 and Fig. 5.3 were conducted with use of the Swabian Alb A limestone exhibiting a PSD of 0.1-0.3 mm and 0.3-0.6 mm, respectively. The Fig. 5.4 corresponds to the Swabian Alb B limestone. The carbonator temperature and CO_2 inlet concentration are 650 °C and 11.3-11.6 vol-% respectively, while the CO_2 outlet concentration is 1-1.5 %, resulting in a CO_2 capture efficiency (E_{CO2}) of above 85 %. Differences in the noted calcium looping ratio (F_{Ca}/F_{CO2}) can be basically explained through the different X_{max} values, calcination efficiencies (η_{reg}) of the three steady states, rather than on chemical differences between the sorbents. In all cases operation is very straight forward. Achieving a steady state is met with relative ease and the only intervention after some hours of operation is the addition of small amounts of limestone to maintain a constant reactor inventory since some is lost in time due to attrition. In this experimental campaign 69 steady states were achieved.

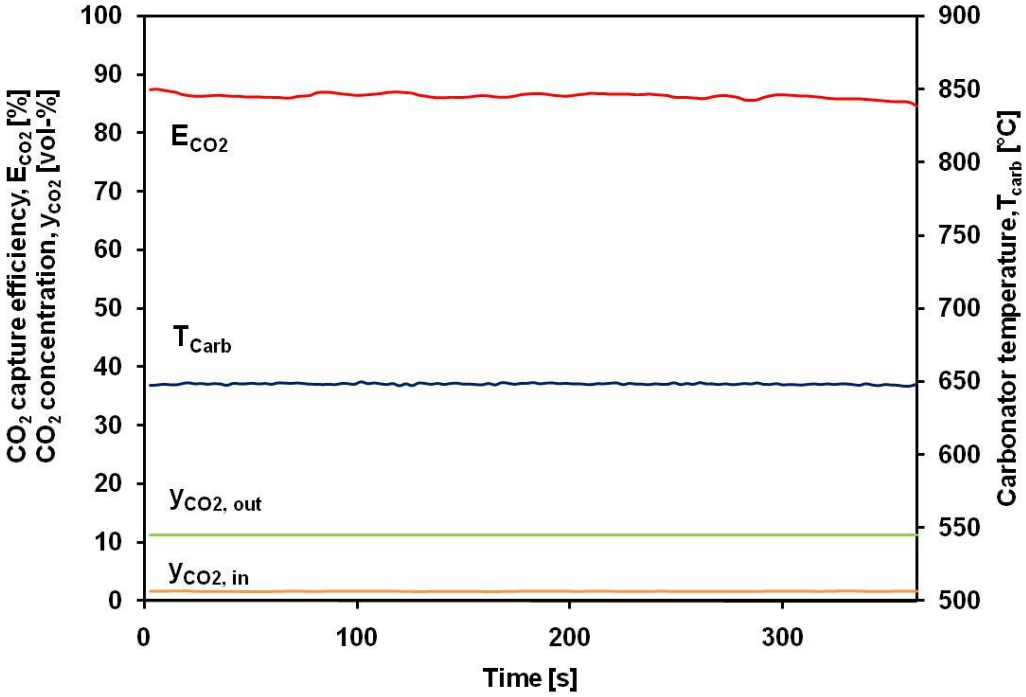

FIG 5.3: EXAMPLE OF A HIGH E_{CO2} STEADY STATE: INLET Y_{CO2}, T_{CARB}, OUTLET Y_{CO2} AND E_{CO2} ARE PLOTTED VS TIME AT τ = 0.33 h AND F_{Ca}/F_{CO2}= 5.7 X_{MAX}= 13, X_{CALC}= 0.5, PSD= 0.3-0.6 FOR SWABIAN ALB LIMESTONE A

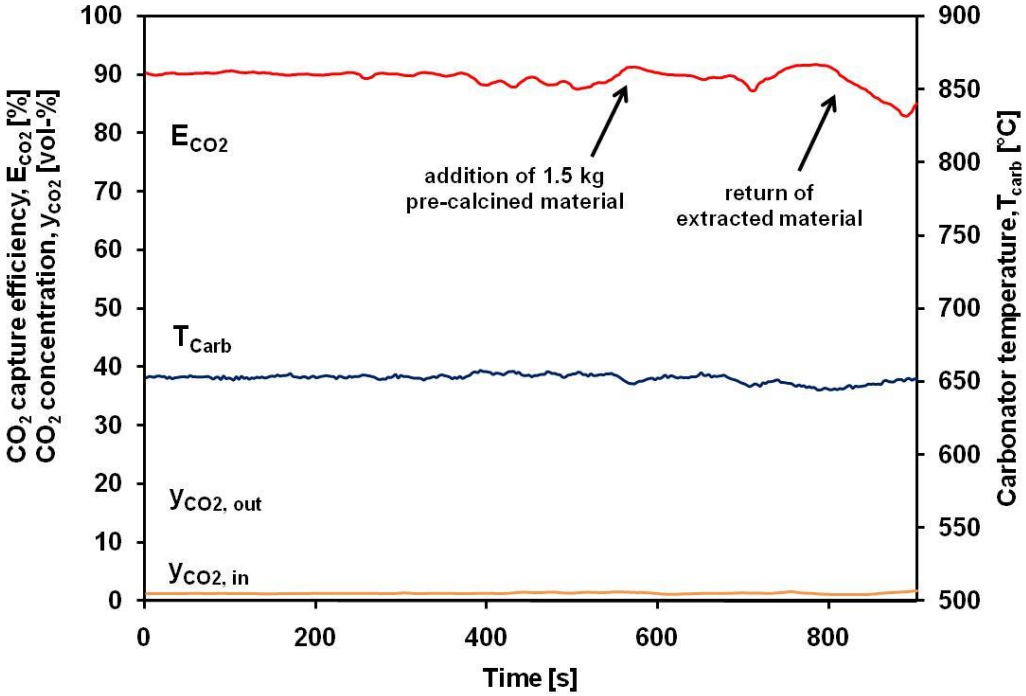

FIG 5.4: EXAMPLE OF A HIGH E_{CO2} STEADY STATE: INLET Y_{CO2}, T_{CARB}, OUTLET Y_{CO2} AND E_{CO2} ARE PLOTTED VS TIME AT τ = 0.30 h AND F_{Ca}/F_{CO2}= 14, X_{MAX}= 14.5, X_{CALC}= 12, PSD= 0.3-0.6 FOR SWABIAN ALB LIMESTONE B

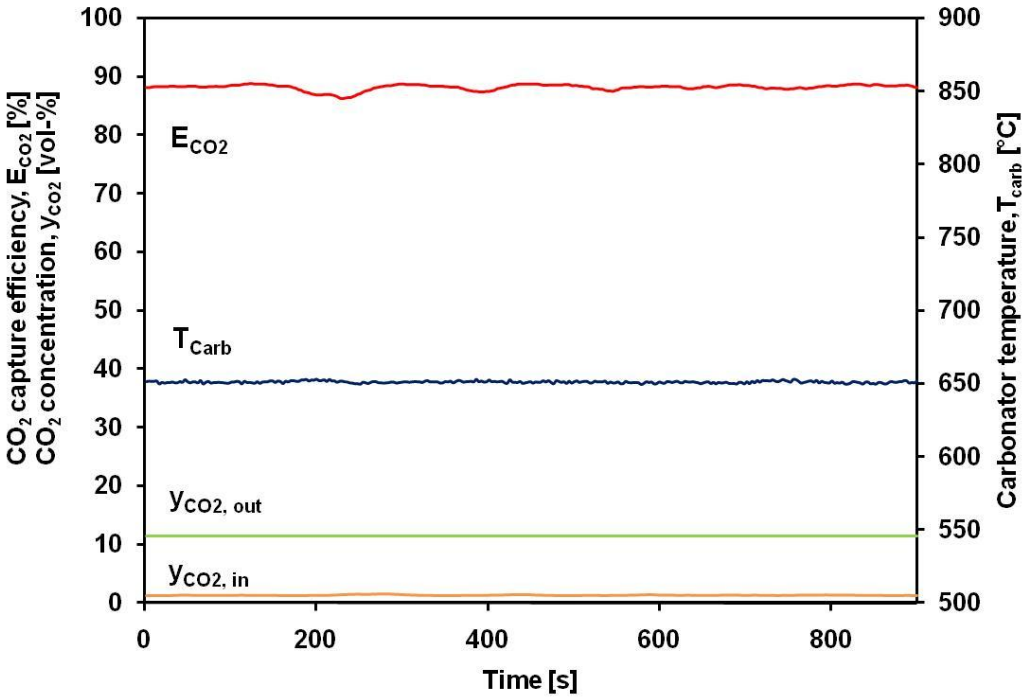

FIG 5.5: EXAMPLE OF A HIGH E_{CO2} STEADY STATE: INLET Y_{CO2}, T_{CARB}, OUTLET Y_{CO2} AND E_{CO2} ARE PLOTTED VS TIME AT τ = 0.46 h AND F_{Ca}/F_{CO2}= 23, X_{MAX}= 18, X_{CALC}= 12, PSD= 0.1-0.3 FOR SWABIAN ALB LIMESTONE A

5.2.2 Decay of Maximum Carbonation Conversion (X_{max})

In Fig. 5.6, the decay of the maximum carbonation conversion (X_{max}) is shown as a function of the cumulative sorbent specific CO_2 loading ($L(t)_{CO2}$) for both limestones and PSDs. Fig. 5.7 exhibits essentially the same graph as Fig. 5.6 but the scale of the y-axis, depicting the X_{max}, has been limited between (0-20 %) which is the range recorded during experimentation. The blue line in both Fig 5.6 and Fig. 5.7 represents the expected X_{max} decay of the Swabian Alb limestone as a function of $L(t)_{CO2}$, as derived from the corresponding X_N vs. N TGA curve of the form of Eq. 3.10 and from Eq. 3.11. Additionally, for calculation of the total calcium moles present in the DFB system ($n_{Ca,\ total}$), needed for calculation of the $L(t)_{CO2}$ as shown in Eq. 3.21, it has been assumed, that all sorbents after pre-calcination exhibited a carbonation conversion value of X_{carb} equal to 30 %.This is typical when pre-calcining $CaCO_3$ in our system. The arrows in Fig. 5.7 indicate the point at which fresh pre-calcined sorbent mass was added in the system, fact which explains the increase of the maximum carbonation conversion at that point. The mass of the added sorbent is noted beside the arrow.

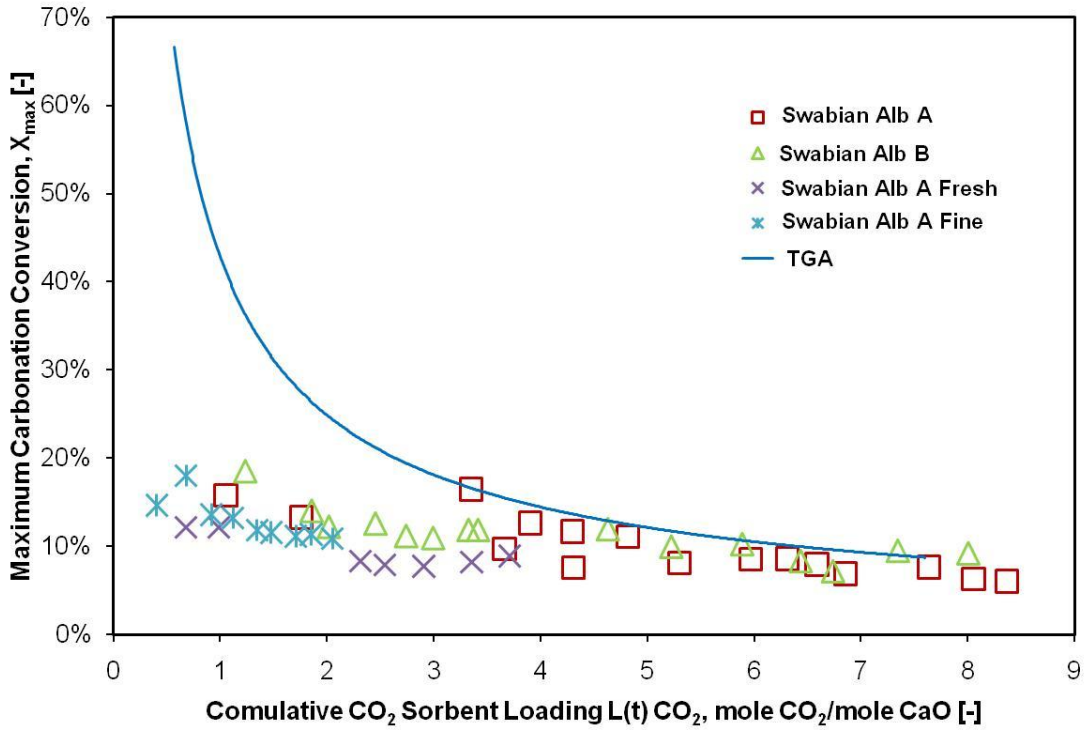

FIG 5.6: DECAY OF MAXIMUM CARBONATION CONVERSION Xmax WITH INCREASING CUMULATIVE SORBENT SPECIFIC CO_2 LOADING

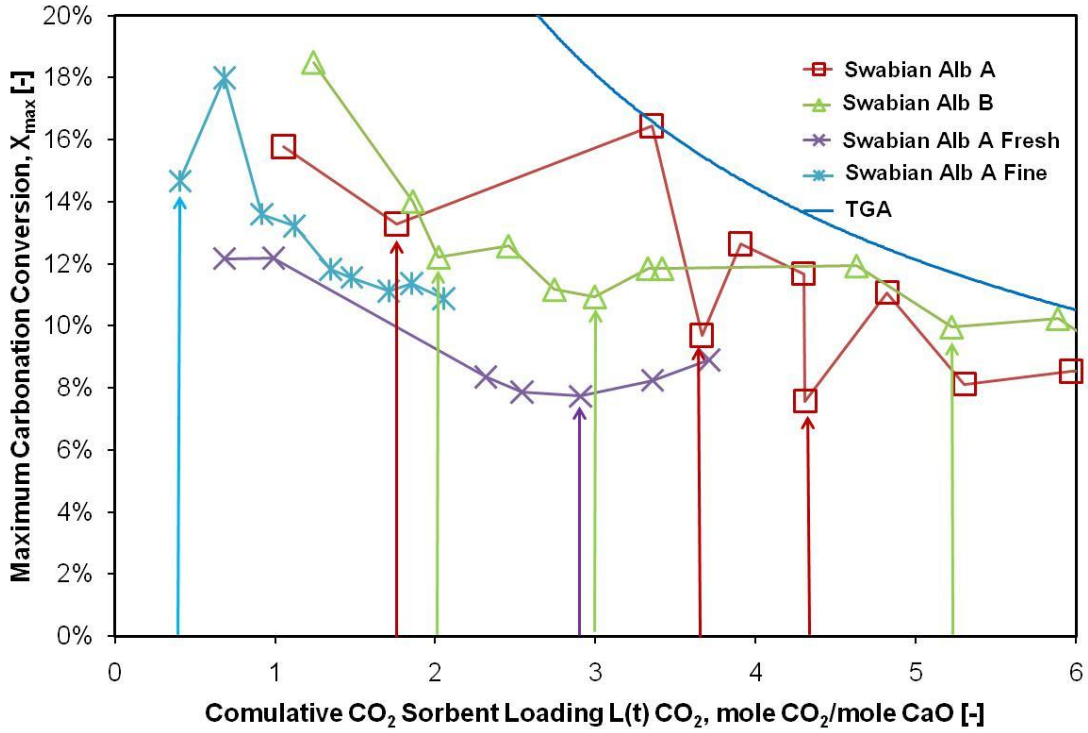

FIG 5.7: DECAY OF MAXIMUM CARBONATION CONVERSION WITH INCREASING CUMULATIVE SORBENT SPECIFIC CO_2 LOADING; (Xmax< 20 %)

As shown in Fig. 5.6 and Fig. 5.7, for low $L_{(t)CO2}$ values (< 3 mol CO_2/mol CaO), the X_{max} of the Swabian Alb limestone exhibits lower values than those extrapolated from TGA experimentation. For example at a CO_2 bed loading of 1 mol CO_2/ mol CaO the X_{max} would be expected to be slightly above 40 %. However, values measured for such a value of $L(t)_{CO2}$ were in the range of only 12-18 % only. The X_{max} continuously decays with increasing CO_2 capture and therefore $L(t)_{CO2}$. On the other hand, for $L(t)_{CO2}$ values greater than 3, the X_{max} values recorded during experimentation in the DFB system seem to exhibt similar values and decay trend with the extrapolated TGA values. Whenever an increase of X_{max} is noted, this can be attributed to the addition of fresh pre-calcined mass, as shown in Fig. 5.7, or to experimental error during solid analysis. Moreover, it is unclear if both the Swabian Alb limestone A & B exhibit a residual activity, similar to the behavior observed in the TGA. Experiments, with a CaL DFB facility, achieving much higher values of $L(t)_{CO2}$ will be needed in order to resolve the above issue. Differences noted in Fig. 5.6 and Fig. 5.7 between full carbonation-calcination TGA experiments and operation in a CaL DFB system can be explained based on that in a real DFB system partial carbonation and rapid particle heating-cooling rates exist which may lead to different sintering patterns than in the TGA. Based on Fig. 5.6 and Fig. 5.7 for the specific experiment, the comparison between the two different limestones and PSDs, in terms of Xmax decay, can not be achieved with ease. The comparison becomes more difficult when taking into account the fact that the addition of new mass, needed to maintain the hydrodynamic stability of the DFB system, increases the maximum carbonation conversion at a specific point. However, it seems that the Swabian Alb limestone B exhibits a slighty higher maximum carbonation conversion (X_{max}) in comparison to the Swabian Alb A limestone. Finally, it is also unclear why the Swabian Alb limestone A, with a fine PSD (0.1-0.3 mm), exhibits generally smaller values than the same limestone with a coarser PSD of (0.3-0.6 mm) for the same value of $L_{(t)CO2}$.

Future experiments studying the X_{max} decay in a DFB system may explore ways to minimize attrition in order to not have to add new mass in order to maintain hydrodynamic stability and to not vary the calcium looping rate between the beds in order to keep carbonator and regenerator residence times constant.

5.2.3 Calcium Looping Ratio (F_{Ca}/F_{CO2}) variation.

The calcium looping ratio is a key parameter to the process since it is linked greatly to O_2 consumption in the regenerator and therefore to process economics. The calculated values of F_{Ca}/F_{CO2} from Eq. 3.9 are plotted against the values measured visually (with use of the quartz standpipe segment, see Fig. 4.2) in Fig. 5.8. For lower F_{Ca}/F_{CO2} both methods produce similar results because visual measurement is easy. Deviation exists for higher F_{Ca}/F_{CO2} values resulting from the difficulty of visual measurements. Since calcium looping ratio values derived match for low F_{Ca}/F_{CO2} values, the use of Eq. 3.9 is considered accurate and is used for data analysis while visual measurement is considered to be a good indicator during experimentation.

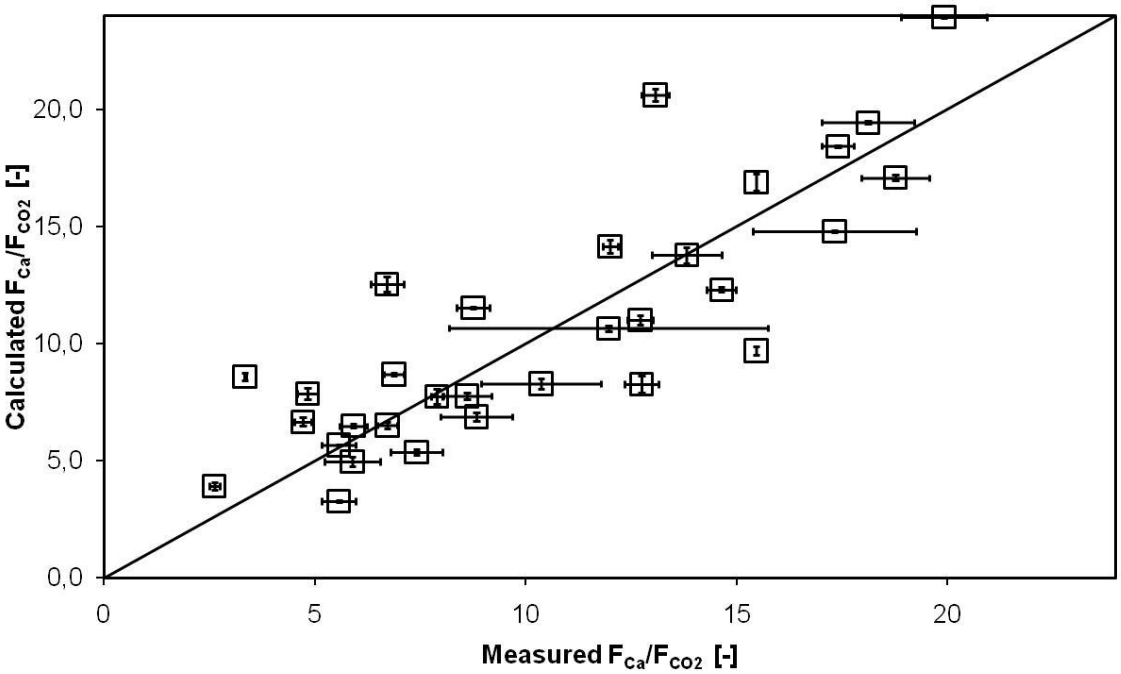

FIG 5.8: MEASURED F_{Ca}/F_{CO2} PLOTTED AGAINST CALCULATED F_{Ca}/F_{CO2}

Fig. 5.9 and Fig. 5.10 plots, for two different limestones and particle sizes, the E_{CO2}/E_{eq} against the calcium looping ratio (F_{Ca}/F_{CO2}) for several steady states. The equilibrium-normalized CO_2 capture efficiency (E_{CO2}/E_{eq}) quantifies the reactor performance in comparison to the optimum allowed by thermodynamics. Since the steady states where attained at different times they exhibit different values of cumulative sorbent specific CO_2 loading $L(t)_{CO2}$ and therefore different values of X_{max}. Moreover, the $\frac{X_{carb}}{r_{reg}}$ in the regenerator also varies, leading to different regeneration efficiencies (η_{reg}) and different values of carbonation conversions regarding the solid flow stream entering the carbonator (X_{calc}). Other conditions such temperature, space time were kept constant or varied within a narrow window.

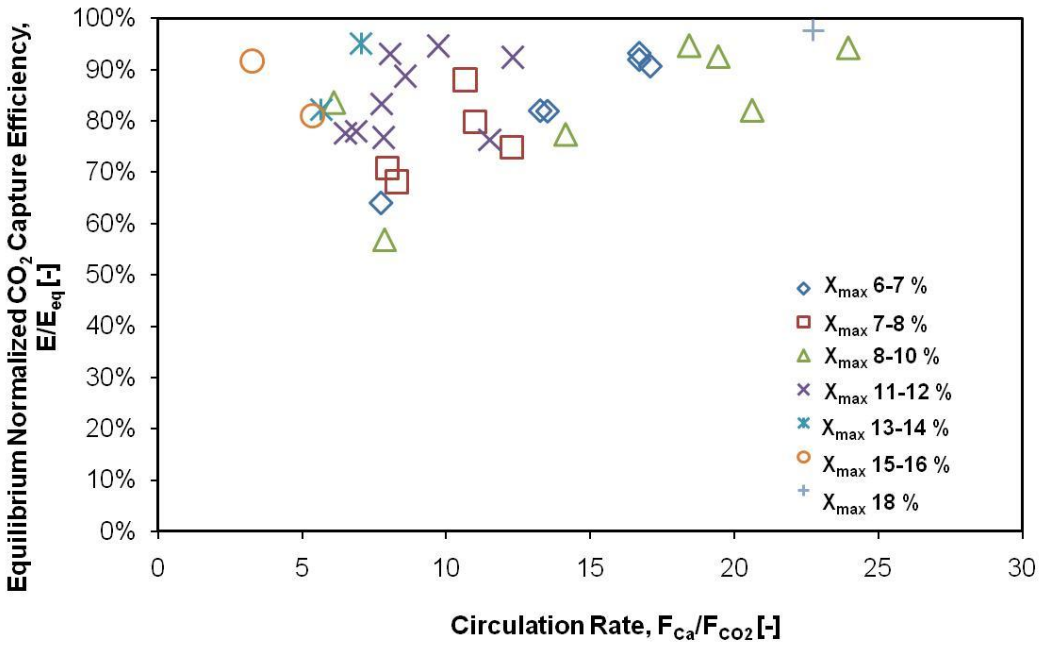

FIG 5.9: E_{CO2}/E_{EQ} PLOTTED VS F_{Ca}/F_{CO2} FOR STEADY STATES WITH INLET Y_{CO2} OF 11.3 %, T_{CARB} OF 650 °C , τ=0.27-0.6 h CLASSIFIED BY X_{MAX} FOR SWABIAN ALB A LIMESTONE

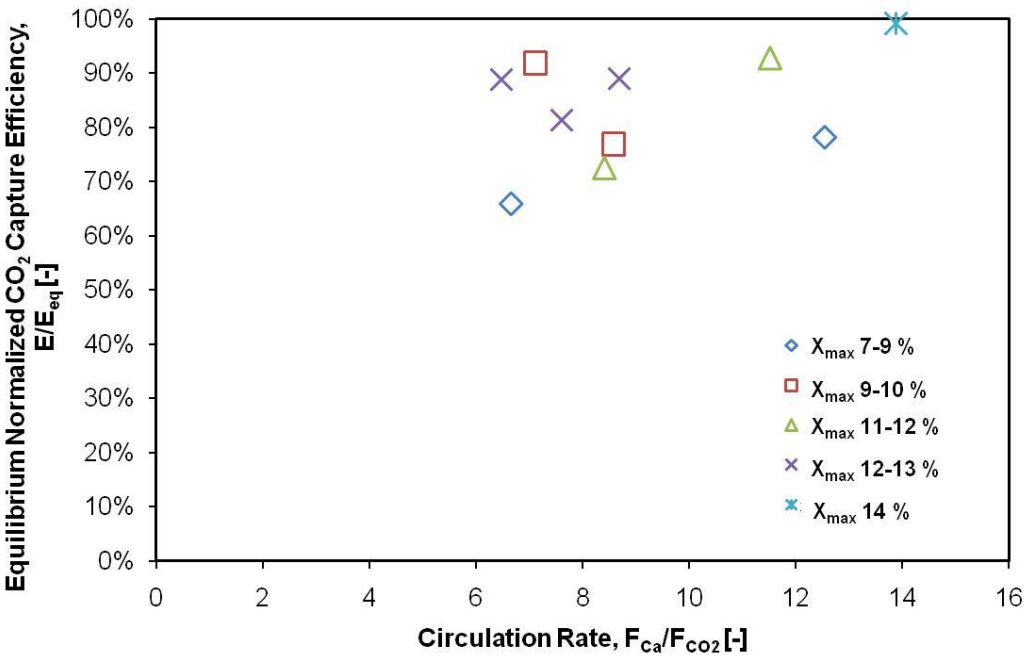

FIG 5.10: E_{CO2}/E_{EQ} PLOTTED VS F_{Ca}/F_{CO2} FOR STEADY STATES WITH INLET Y_{CO2} OF 11.3 %, T_{CARB} OF 650 °C, τ=0.29-0.49 h CLASSIFIED BY X_{MAX} FOR SWABIAN ALB B LIMESTONE

Some trends are evident from the above graph, like the fact that an increase in the calcium looping ratio (F_{Ca}/F_{CO2}) results in an increase in CO_2 capture efficiency, however two main issues are raised. The first is related to the impact of calcination efficiency (η_{reg}) on the values of F_{Ca}/F_{CO2} recorded. For example, some steady states of Fig. 5.9 required extremely high values of F_{Ca}/F_{CO2} (>15) in order to achieve high CO_2 capture efficiencies in the range of E_{CO2}/E_{eq} = 90 %. These steady states exhibited η_{reg} values in the range of 37-93 %. The second is related on the influence of the X_{max} on the required F_{Ca}/F_{CO2} value in order to achieve a given E_{CO2}/E_{eq} value. For example, it can be noted in Fig. 5.9 that for an F_{Ca}/F_{CO2} value of around 7.5 the E_{CO2}/E_{eq} is higher than 90 % when the X_{max} is in the range of 13-14 % while it is 55 % whne the X_{max} is in the range of 7-8 %. Although, the trend- that for the same F_{Ca}/F_{CO2} and with increasing X_{max} values E_{CO2}/E_{eq} -generally holds true, exeptions exist.Such an exception is noted in Fig. 5.9 where solids having an X_{max} of 6-7 % exhibit a better performance than thouse with an X_{max} of 7-8 %.

Since the product of the regeneration efficiency and calcium looping ratio ($F_{Ca}/F_{CO2}\cdot\eta_{reg}$) of every steady state expresses the calcium looping ratio that would have been required if the regenerator efficiency (η_{reg}) was equal to 1, as shown by Eq. 3.7 expressing the carbonator mass balance, this product is included in the x-axis. As a result, by eliminating the effect of

regeneration efficiency, in such a way, the plots of Fig. 5.9 and Fig. 5.10 are transformed into the graphs shown in Fig. 5.11 and Fig. 5.12, respectively.

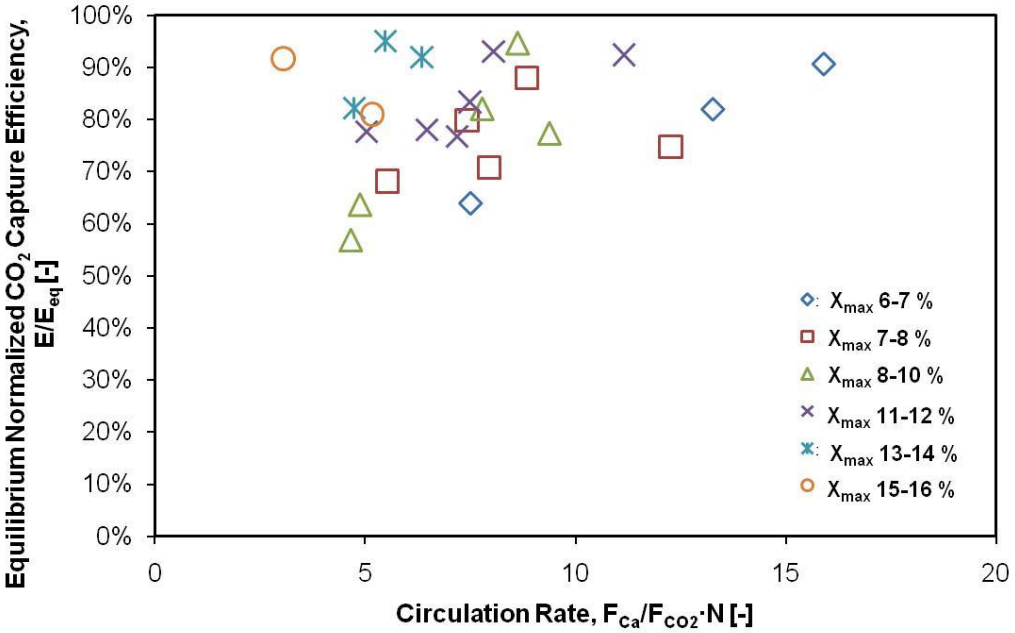

FIG 5.11: E_{CO2}/E_{EQ} PLOTTED VS F_{Ca}/F_{CO2}·N FOR STEADY STATES WITH INLET Y_{CO2} OF 11.3 %, T_{CARB} OF 650 °C , τ=0.27-0.6 h CLASSIFIED BY X_{MAX} FOR SWABIAN ALB A LIMESTONE

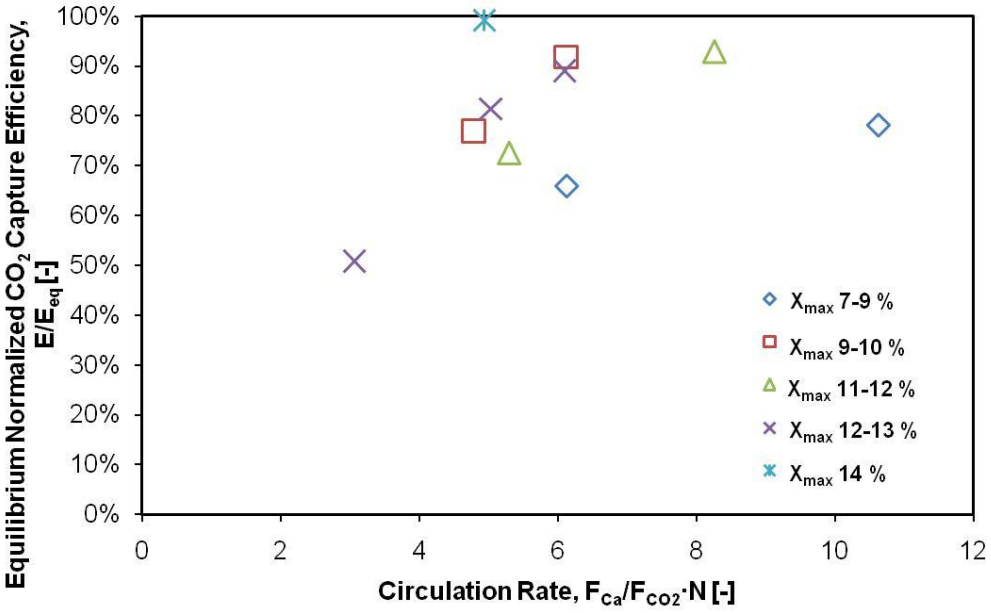

FIG 5.12: E_{CO2}/E_{EQ} PLOTTED VS F_{Ca}/F_{CO2}·N FOR STEADY STATES WITH INLET Y_{CO2} OF 11.3%, T_{CARB} OF 650 °C , τ=0.29-0.49 h CLASSIFIED BY X_{MAX} FOR SWABIAN ALB B LIMESTONE

From Fig. 5.11 and Fig. 5.12 it is shown that the bulk of the data correspond to $F_{Ca}/F_{CO2}\cdot\eta_{reg}$ values between 5 and 12. From Fig. 5.11 it is clear that the high F_{Ca}/F_{CO2} ratios noted in Fig. 5.9 are due to the low regeneration efficiencies in the regenerator caused by very limited residence times in the reactor. Moreover, for both limestones (Swabian Alb A & B, see Fig. 5.11 and Fig. 5.12) it is particularly clear that for a given $F_{Ca}/F_{CO2}\cdot\eta_{reg}$ higher E_{CO2}/E_{eq} values are achieved when the X_{max} is higher. As shown in Fig. 5.11 for higher maximum carbonation conversion values, which means that the material is more fresh, high efficiencies can be achieved with low calcium looping ratios. For example, as shown in Fig. 5.11, with a $F_{Ca}/F_{CO2}\cdot\eta_{reg}$ value of only 3 and an X_{max} value 15.8 the equilibrium normalized value of CO_2 capture efficiency is (E_{CO2}/E_{eq}) 92 %. On the other hand in order to achieve the same efficiencies at low maximum carbonation conversion values, higher circulation rates are necessary. This can be illustrated from Fig. 5.11 where a combination of only a very high $F_{Ca}/F_{CO2}\cdot\eta_{reg}$ value equal to16 lead to a CO_2 capture efficiency value 91 % when the X_{max} was as low as 6 %. It is of particular interest to examine which pairs of $F_{Ca}/F_{CO2}\cdot\eta_{reg}$ and X_{max} produce CO_2 capture efficiencies E_{CO2}/E_{eq} higher than 90 %. This pairs are plotted for Swabian Alb limestone A & B and both PSDs in Fig. 5. 11. From Fig. 5. 11 it is clear that a value E_{CO2}/E_{eq} of above 90 % can be maintained through different combinations of X_{max} and $F_{Ca}/F_{CO2}\cdot\eta_{reg}$ when other conditions, such as space time, temperature etc. remain constant or within a narrow window.

5.2.4 Active Space Time of the Carbonator, a Determining Factor?

The active space time (τ_a) is the product of τ and f_a, as shown in Eq. 3.16, and has shown to strongly coorelate to CO_2 capture efficiency either directly or through use of the equivelant concept of active inventory for a given flue gas flow [46]. A previous study [11], utilizing a BFB carbonator and Swabian Alb limestone A in continuous DFB mode, had shown that the equilibrium normalized CO_2 capture efficiency increases with active space time, while all experimental points fit a single line. The above statement holds true, in particular for runs conducted with the Swabian Alb limestone B, as shown in Fig. 5.14, with the exception of one outlier point which exhibits the lowest measured value of X_{max}, i.e 6.2 %. Therefore, increasing the active space time increases the ability of the bed to capture CO_2 and therefore higher values of equilibrium-normalized CO_2 capture efficiency are obtained. The Swabian limestone B exhibits critical τ_a in the vicinity of 0.15 %h which implies that beyond this active space time value, the CO_2 capture ability of the carbonator bed is enough for the CO_2 capture efficiency to start approaching equilibrium values (E_{CO2}/E_{eq}> 90 %).

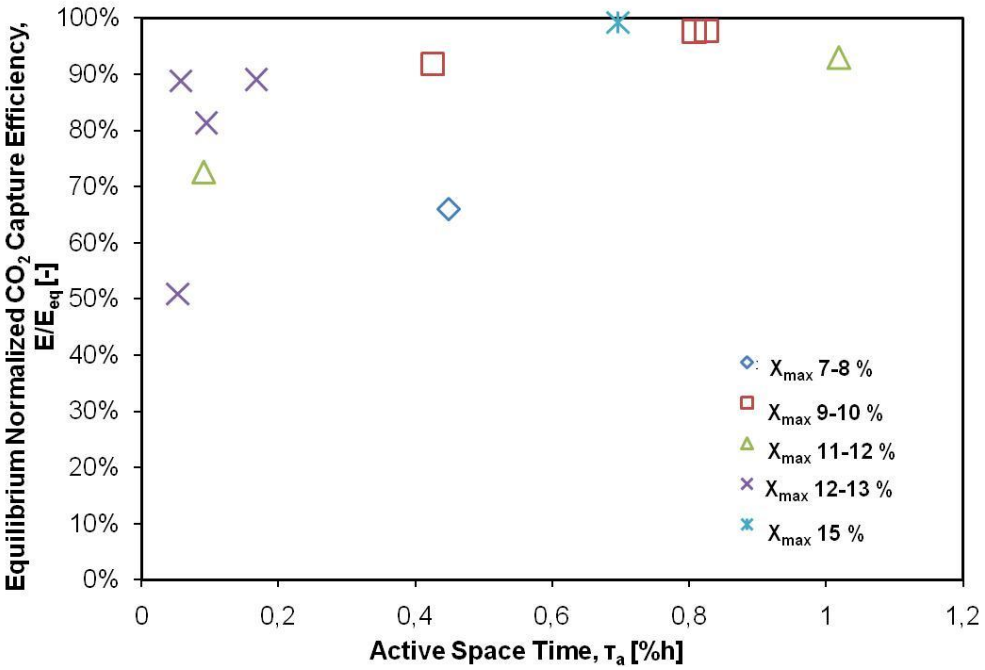

FIG 5.13: E_{CO2}/E_{EQ} PLOTTED VS ACTIVE SPACE TIME FOR STEADY STATES WITH INLET Y_{CO2} OF 11.3 %, T_{CARB} OF 650 °C, τ=0.29-0.49 h CLASSIFIED BY X_{MAX} FOR SWABIAN ALB B LIMESTONE

For Swabian Alb limestone A the equilibrium normalized CO_2 capture efficiency seems to increase with active space time for steady states conducted with the same value of $X_{max,}$ as shown in Fig. 5.13. Moreover, the value of X_{max} seems to influence the value of active space time needed to achieve a given CO_2 capture efficiency, i.e. for the same value of active space time, the CO_2 capture efficiency seems to increase when the X_{max} increases. This can be explained based on TGA results which show that sorbents exhibiting lower values of cycle number, and therefore higher values of X_{max}, exhibit a higher carbonation reaction rate. In addition, the existence of a number of steady states with X_{max} values greater than 12 % and E_{CO2}/E_{eq} values greater than 90 %) in combination with active space time values close to zero can be further attributed to a Swabian Alb limestone A characteristic. Swabian Alb limestone A exhibits an acceptable reaction rate within the transition regime between the fast reaction regime and diffusion controlled reaction regime. This means that even at f_a values approaching zero, i.e. at the end of the fast reacrion regime, the reaction rate would be far from becoming slow.

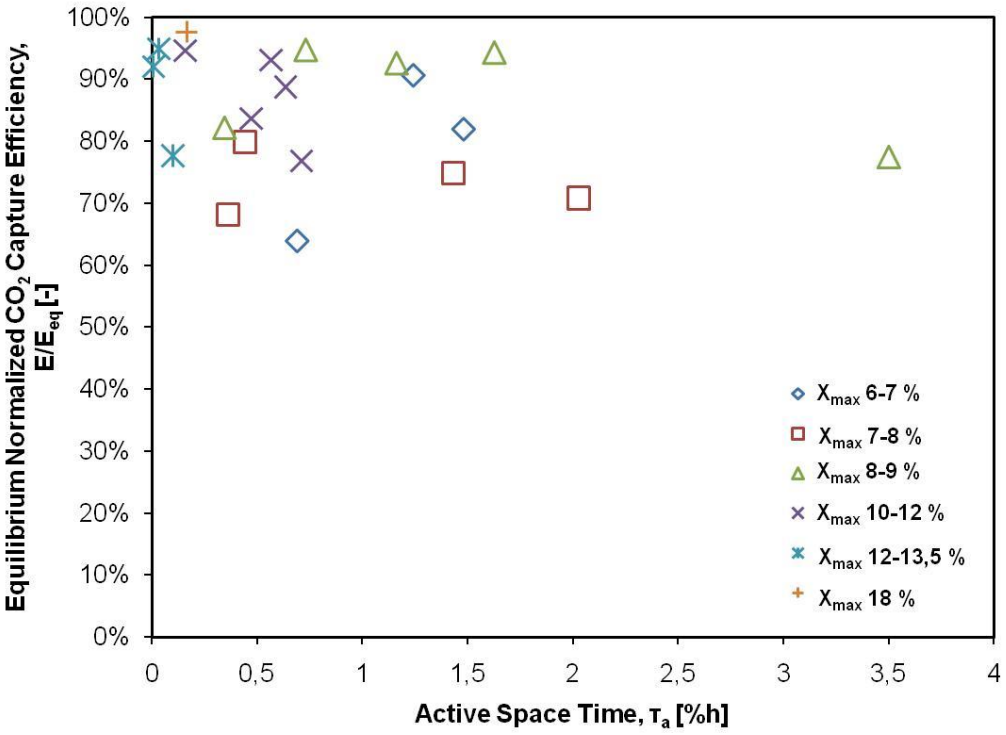

FIG 5.14: E_{CO2}/E_{EQ} PLOTTED VS ACTIVE SPACE TIME FOR STEADY STATES WITH INLET Y_{CO2} OF 11.3 %, T_{CARB} OF 650 °C, τ=0.27-0.6 h CLASSIFIED BY X_{MAX} FOR SWABIAN ALB A LIMESTONE

5.2.5 Physical Explanation of Residence Time

In Fig. 5.15 and Fig. 5.16 the equilibrium normalized CO_2 capture efficiency is plotted against the carbonator residence time, which is defined by Eq. 3.19, for limestones for the Swabian Alb limestones A & B, respectively and other given coditions.

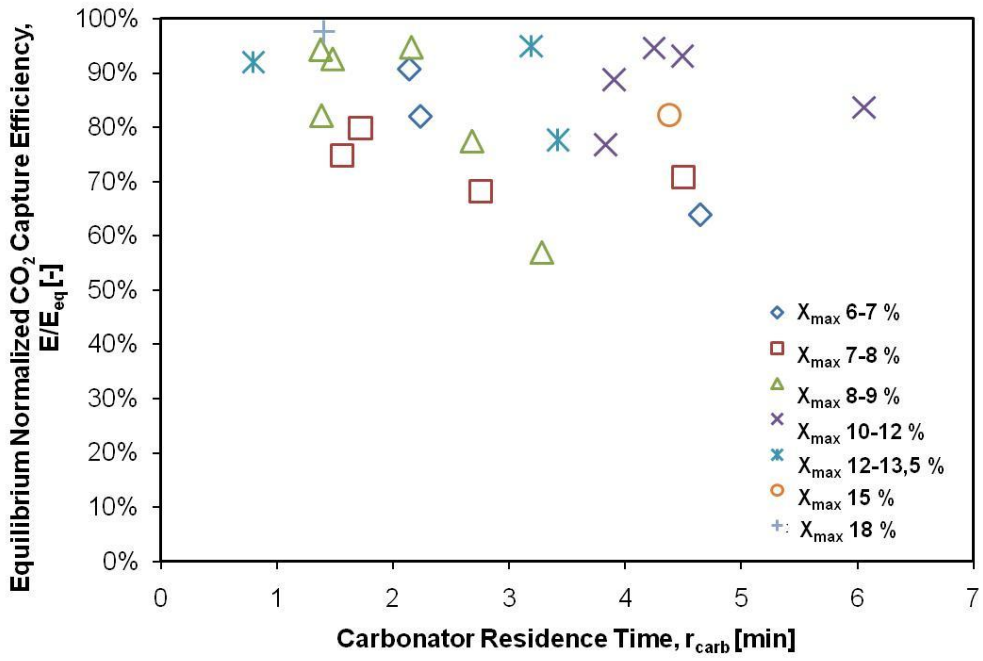

FIG 5.15: E_{CO2}/E_{EQ} PLOTTED VS CARBONATOR RESIDENCE TIME FOR STEADY STATES WITH INLET Y_{CO2} OF 11.3 %, T_{CARB} OF 650 °C, τ=0.27-0.6 h CLASSIFIED BY X_{MAX} FOR SWABIAN ALB A LIMESTONE

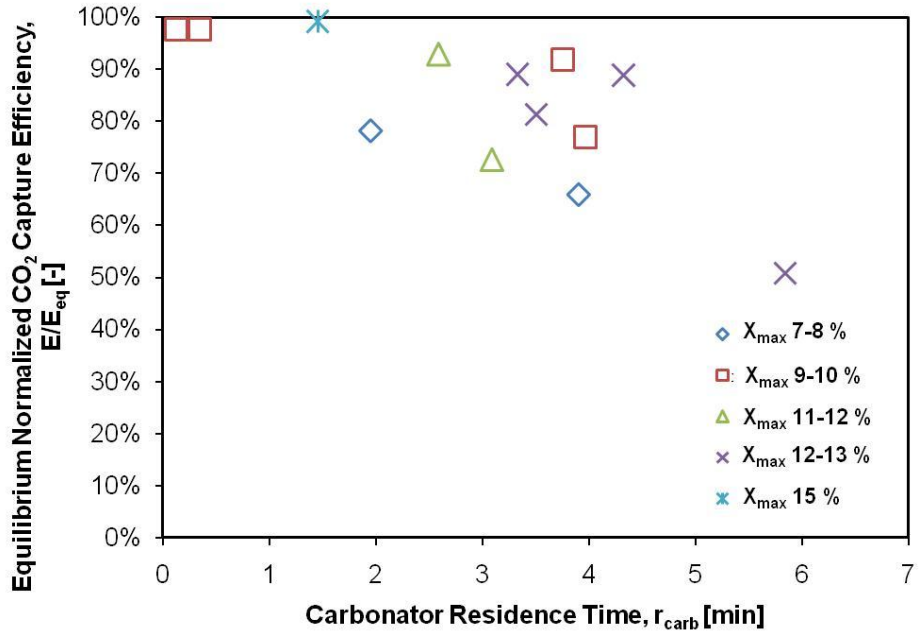

FIG 5.16: E_{CO2}/E_{EQ} PLOTTED VS CARBONATOR RESIDENCE TIME FOR STEADY STATES WITH INLET Y_{CO2} OF 11.3 %, T_{CARB} OF 650 °, τ=0.29-0.49 h CLASSIFIED BY X_{MAX} FOR SWABIAN ALB B LIMESTONE

Examining the behavior of Swabian Alb limestone A it is obvious that there a trend line of points, with high values of maximum carbonation conversion approaching equilibrium values even though residence time values are as high as 5 min, exists. For example, in Fig. 5.15, through carbonator residence time of 4.5 min and in combination with a maximum carbonation conversion value of 15 %, CO_2 capture efficiency close to the 82 % of the equilibrium value is achieved. The points with lower values of maximum carbonation conversion (below 10 %) also approach equilibrium values when residence times are small (below 2 min). The same behavior is also observed in Swabian Alb limestone B, as shown in Fig. 5.16. For example, an E_{CO2}/E_{eq} value of 90 % is achieved with an X_{max} value of 12-13 % and a residence time of above 4 min, while the same CO_2 with an X_{max} of 9-10 % and residence time below 1 min.

The explanation to the above observations can be summarized as follows: The average carbonation conversion rate during the experimental steady states is 1/min. This means that the X_{carb} increases in average by 1 % every minute it stays within the carbonator. Therefore when the X_{max} is as high as 15 % the sorbent can spent more than 4 min in the carbonator without all of the free active CaO (fa) being used up. This is of course not the case when the Xmax is as low as 6-7 %. To operate with such a degraded sorbent and achieve CO_2 capture efficiency values E_{CO2}/E_{eq} of above 90 % is possible only of the residence time in the carbonator is 2 min or less, as shown in Fig. 5.15 and Fig. 5.16. This is only possible at the highest values of $F_{Ca}/F_{CO2}\cdot\eta_{reg}$ (> 12) recorded during this experimentation.

5.2.6 Hydrodynamic Behavior of Riser carbonator

In this chapter is being studied the hydrodynamic behavior of the CFB carbonator according to specific parameters such as the riser velocity, the pressure drop profile, the total solid inventory and the limestone fluidization behavior.

5.2.6.1 Flow Structure of Riser Carbonator and Standpipes

In Fig. 5.17 the typical pressure drop and solid fraction (ε_s) profiles of the riser carbonator are presented.

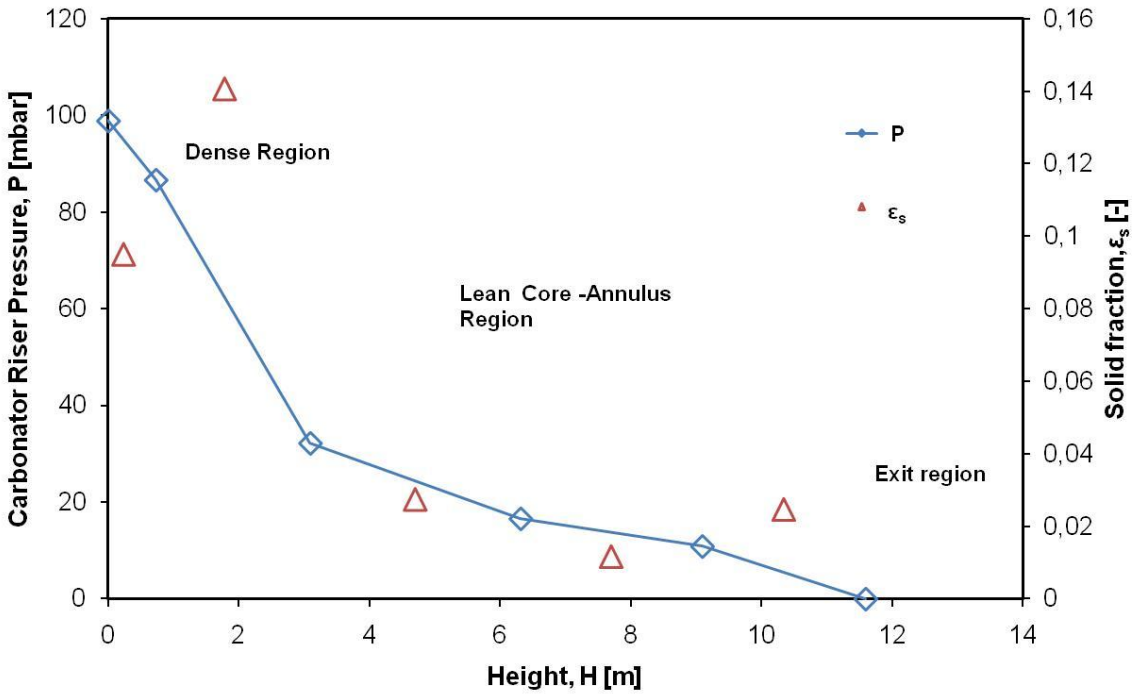

FIG 5.17: FLOW STRUCTURE AND SOLID FRACTION PROFILE ALONG THE RISER HEIGHT
(U_O=5.75 m/s, CARBONATOR INVENTORY= 3.88 kg, ΔP_{riser}= 98 mbar)

Three distinct regions are noted for the typical pressure drop profile and solid fraction (ε_s) of Fig. 5.17. In the middle of the riser a **'lean core-annulus region'** exists, exhibiting a solid fraction of 0.01-0.02. As is typical for this region the solid fraction is higher at the bottom than at its top. The solids move upwards from the center of the riser and downwards from the side. At the top of the riser and near the riser exit, the **'exit region'** is observed, having a solid fraction of above 0.02. A further region known as the **'dense region'** exists at the bottom of the riser, exhibiting high ε_s values. As illustrated in Fig. 5.17 the value of the solid fraction at 2.00 m height is about 0.14. The lower pressure drop and average ε_s value equal to 0.10 obtained in the first 0.48 m can be explained based on the influence of the distributor jets and due to that the return legs of the riser are placed approximately 1.20 m above the distributor. The determination of the height of the dense bed is not directly known from pressure transducer measurements since only 6 are used for the whole of the riser. However, the dense bed height can be calculated by approximation. The typical profile of Fig. 5.17 is taken into account to present an example. The solid average fraction in the region of the axial section 0.48-3.09 m is 0.14. It is certain from Fig. 5.17 that this section contains part of the lean core-annulus region the dense bed region and their border. It is assumed that the solid fraction of the dense bed region (ε_{sd}) and lean core-annulus region (ε_{slean}) within the section 0.48-3.09 m

is 0.2 [47] and 0.027 (same as the average ε_s value of the region (3.092-6.092 m), respectively. The following mass balance can be written for the axial riser section 0.48-3.092 m:

$$\varepsilon_{s2} \cdot a + \varepsilon_{s1} \cdot a = \varepsilon_{sm} \quad (5.1)$$

The symbol “a” represents the part of the axial region that is covered by the dense region. For the typical case of Fig. 5.17 and with the assumptions mentioned above the part of the axial region that is covered with the dense bed region is 65 %, since we have “a= 0.65”. This means that the border of the dense bed region is at approximately 2.20 m which is much more than predicted by the cold model [9]. The existence of the dense bed has a direct influence on the CO_2 axial profile in the carbonator. By measuring the CO_2 concentration in the first 730 mm above the riser carbonator distributor, the results indicate that the most of the CO_2 capture takes place in the axial section 0-730 mm above the distributor. The measurements indicate that during all experiments, for both limestones and particle sizes, the CO_2 capture efficiency taking place in the first 730 mm of the riser is above 80 % of the total CO_2 capture efficiency as derived at the carbonator exit. A typical axial carbonator profile is shown in Fig. 5.18.

The densification of the solid flow, after the lean core-annulus region leading to the formationn of the exit region, as shown in Fig. 5.17, is due to the geometry of the riser exit. The meachanism through which the densification is formed is showed in Fig. 5.19, depictining the upper part of the riser, the cyclone and the duct connecting them. Solids are move upwards from the center of the riser (red arrow). A part of them moves downwards from the sides (green arrows) while the rest (purple arrow) exit the riser and proceed to the cyclone through the duct. The downcoming solids collide with the upcoming ones and momentum exchange takes place, while they are further decelerated through the upcoming gas. Therefore, the downcoming particles at some point move to the center and start travelling upwards. Through this mechanism the exit region is formed, as a result of this internal solid recirculation pattern. In the carbonator riser the formation of the exit region is very evident due to that the riser exit is inclined and because it located below the riser top.

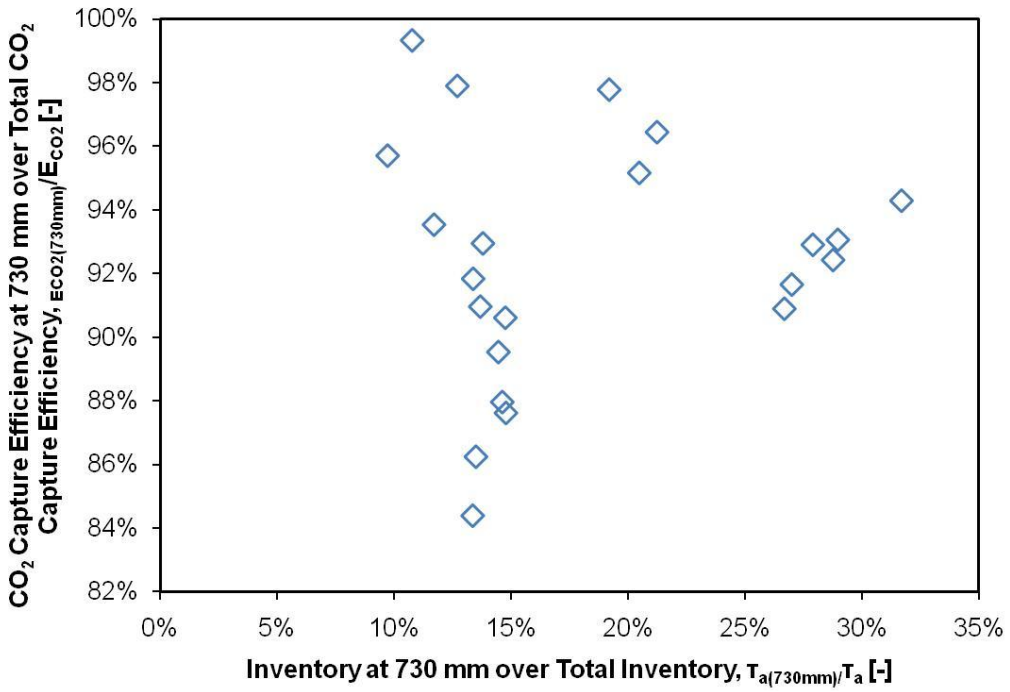

FIG 5.18: TYPICAL AXIAL CARBONATOR PROFILE (T_{CARB}= 650°C, F_{Ca}/F_{CO2}= 4-24, $\tau\alpha_{730mm}$= 0.05-0.2 h, τ_{α}= 0.33-0.53 h)

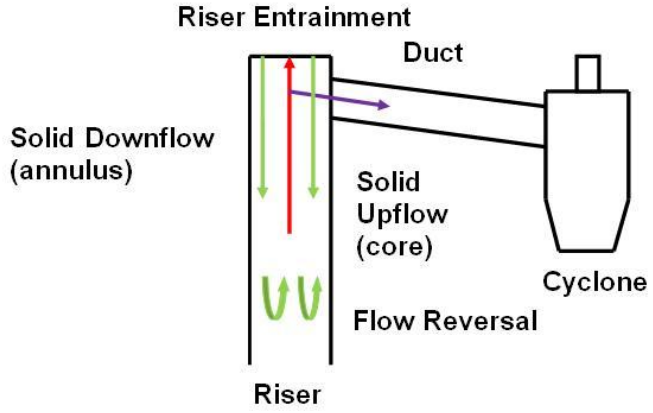

FIG 5.19: SCHEMATIC OF SOLIDS BEHAVIOR IN THE EXIT REGION OF THE RISER CARBONATOR

The standpipe of the double exit loop seal (see Fig. 4.1) operates generally in the slugging or slip-stick regime. On the contrary, the lower standpipe transferring solids from the regenerator to the carbonator operates in mildly bubbling regime. The critical reason that can explain this difference is that the upper standpipe has to cope with a higher solid flow and pressure drop through it. This is because the only a fraction of the riser entrainment equal to the calcium looping rate passes through the lower loop-seal and because the BFB is most of the times slightly pressurized (c.a. 30 mbar).

5.2.6.2 Effect of Carbonator Riser Pressure Drop ($\Delta P_{riser\text{-}carb}$)

Increment of carbonator riser pressure drop ($\Delta P_{riser\text{-}carb}$) is primarily caused due to higher mass availability in the carbonator. However, the increment of carbonator riser pressure drop does not result in a uniform change of the pressure drop and solid fraction profle in the carbonator. This is illustrated in Fig. 5.20 and Fig. 5.21, where experimental runs, with varying $\Delta P_{riser\text{-}carb}$ and other conditions same, are plotted.

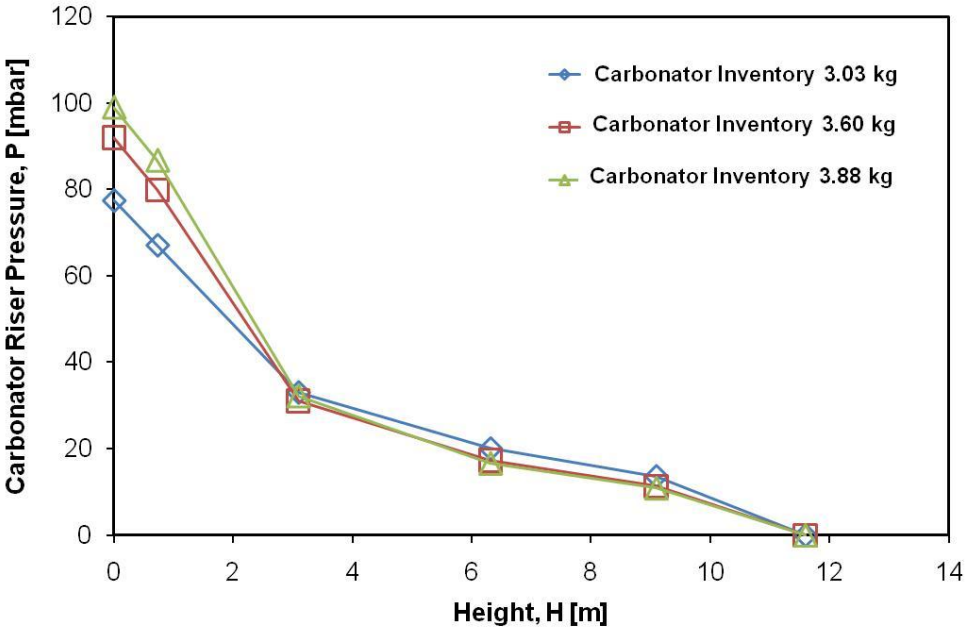

FIG 5.20: EFFECT OF TSI ON THE RISER PRESSURE DROP PROFILE FOR SWABIAN ALB A LIMES-TONE (U_O= 5.75 m/s, T_{CARB}= 650˚C, CARBONATOR INVENTORY= 3.03, 3.6, 3.88 kg , $\Delta P_{riser\text{-}carb}$= 77, 91, 98 mbar)

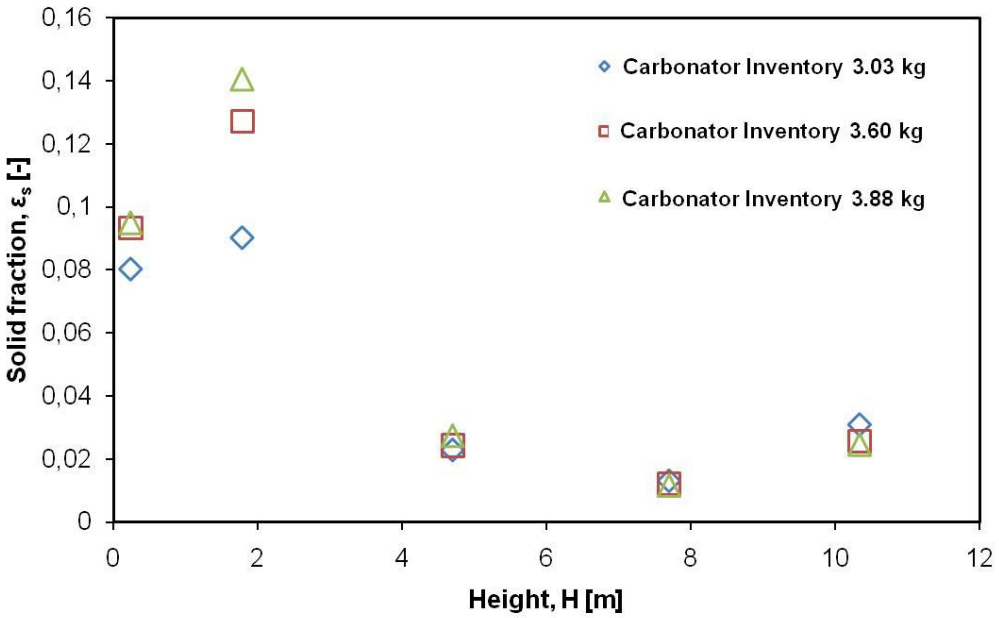

FIG 5.21: EFFECT OF TSI ON THE SOLID FRACTION PROFILE FOR SWABIAN ALB A LIMESTONE (U_O= 5.75 m/s, T_{CARB}= 650˚C, CARBONATOR INVENTORY= 3.03, 3.6, 3.88 kg , $\Delta P_{riser\text{-}carb}$= 77, 91, 98 mbar)

The pressure drop readings between the axial section 3.09-12.13 m, as shown in Fig. 5.20, remain practilcally unchaged. Therefore, it can be concluded that increasing the $\Delta P_{riser\text{-}carb}$ and hence the mass in the riser carbonator does not significantly affect the lean core-annulus and exit regions. However, the increment of $\Delta P_{riser\text{-}carb}$ causes an increase of the pressure drop within the axial section 0-3.09 m of the same amount, as can be seen in Fig 5.20. Therefore, the solid fraction profile of this region increases. The mechanism of mass accumuluation in the dense bed of the riser carbonator when increasing $\Delta P_{riser\text{-}carb}$ can be summarized in that the height of the dense bed is increased.The effect of $\Delta P_{riser\text{-}carb}$ increment on the riser pressure drop and solid fraction profile are similar to those predicted from the cold model experimentation [9].

5.2.6.3 Effect of Carbonator Riser Velocity

The effect of velocity on the riser pressure profile and solid fraction profile is presented in Fig. 5.22 for two runs conducted with the coarse PSD (0.3-0.6 mm) of the Swabian Alb A limestone and exhibiting the same carbonator riser pressure drop ($\Delta P_{riser\text{-}carb}$) and all other operational parameters.

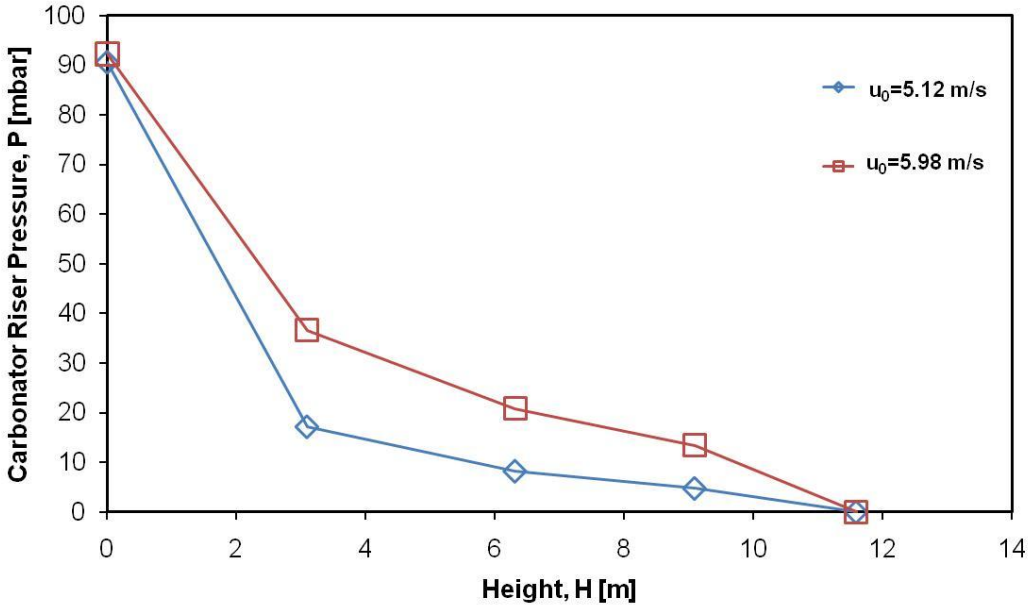

FIG 5.22: EFFECT OF VELOCITY IN THE RISER PRESSURE DROP PROFILE FOR SWABIAN ALB A LIMESTONE (U_O= 5.12, 5.98 m/s, CARBONATOR INVENTORY= 3.6 kg, $\Delta P_{riser\text{-}carb}$= 92 mbar, PSD= 0.3-0.6 mm, T_{CARB}= 650˚C)

As shown in Fig. 5.22 by increasing the velocity for the same $\Delta P_{riser\text{-}carb}$, higher pressure drop gradients and solid fraction values (ε_s) are obtained in the lean core-annulus and exit regions. The opposite is true for the axial section 0-3.09 mm above the distributor, which is the region that incorporates the dense bed. Such a trend has been predicted from the experimental campaigns of the cold model [48]. The increment of the pressure drop- solid fraction at the exit region of the bed is a clear indicator that the riser entrainment increases [9]. Due to this behavior, increasing the velocity beyond a maximum value leads to riser malfunction. This value has found to be approximately 6.0 m/s for the coarse PSDs of Swabian Alb limestones A & B, while it is approximately 4.3 m/s for the fine PSD. Mass accumulates in the upper standpipe (above from the quartz standpipe segment) while solid flow from the loop seal to the riser stops and the riser becomes leaner. After accumulation to a certain height in the upper standpipe, solids are discharged abruptly back to the riser making the riser dense again. This phenomenon is periodic, but may also lead the facility to trip and breakdown operation, since mass may gather up to the cyclone barrel. Standpipe size of larger diameter and loop seal, cyclones design with lower pressure drops may be a potential solution to the problem.

5.2.6.4 Limestone Fluidization Behavior

In Fig. 5.23 the pressure drop and solid fraction profile are plotted, while the carbonator riser superficial velocity, pressure drop and other parameters are constant.

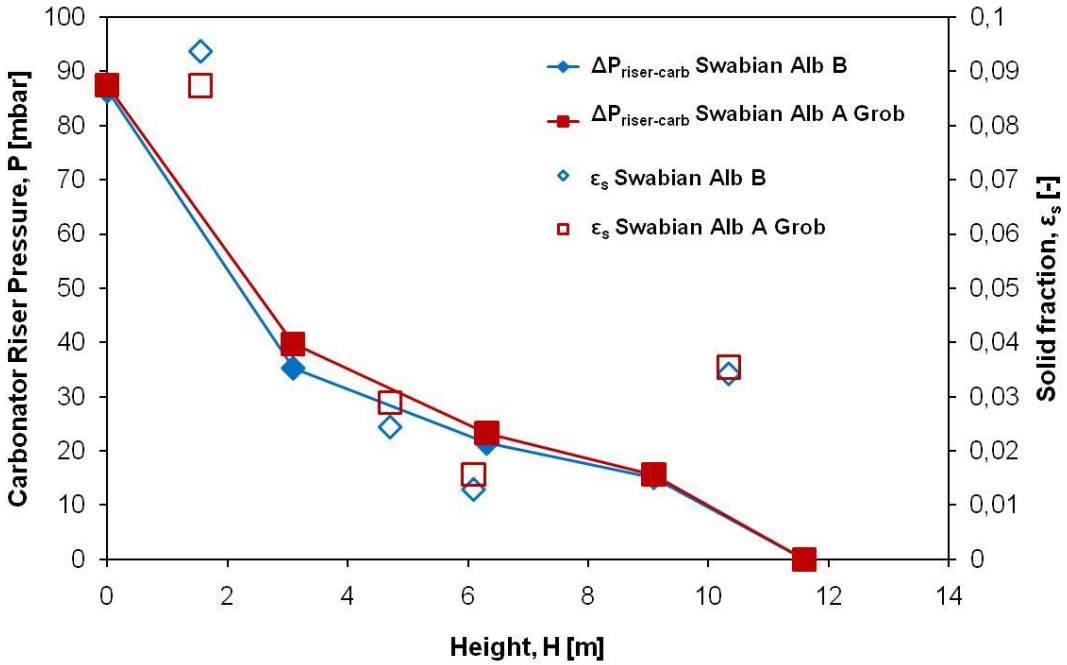

FIG 5.23: PRESSURE DROP AND SOLID FRACTION PROFILE ALONG THE RISER FOR DIFFERENT PARTICLE SIZES (U_O=5.8 m/s, $\Delta P_{riser-carb}$=86 mbar , PSD= 0.3-0.6 mm, T_{CARB}=650°C)

As far as the fine PSD (0.1-0.3 mm) of the Swabian Alb limestone A is concerned, it was not possible to directly compare it with the other two, as operation was impossible for velocities above 4.3 m/s, above which solid accumulation in the upper standpipe is obeseved. However, the classical flow structure (dense bed, lean core-annulus and exit region) presented in Fig. 5.20-Fig. 5.23 is evident also for the fine PSD.

5.2.6.5 Riser Entrainment and Cone Valve Discharge

Previous work with use of the scaled cold model has showed that there is an exponential equation connecting the riser superficial velocity and riser entrainment [9]. However, during this experimental campaign, entrainment measurements with use of the upper standpipe quartz segment (11 & 12, Fig. 4.1) were difficult. This can be attributed to the fact that circulation rate measurements were carried out under difficult conditions, as riser entrainment was too high to measure accurately. However, it can be stated, with relative certainty that the entrainment range was between 10-20 kg/m^{2}s, which is below what has been expected from the

cold model. This difference may be a result of the fact that cyclone dimensions and of the duct connecting the riser to the cyclone were constructed differently to the cold model.

Previous studies in the cold model showed that the cone valve discharge is mainly controlled by the product of the pressure drop through the valve and the opening of the valve [9]. Therefore cold model experiments suggested that the cone valve discharge can be controlled through closing or opening the cone valve and by increasing or decreasing the absolute pressure of the BFB. In our experimental campaign the flow has been controlled perfectly by varying the cone valve opening from 2-8 mm from the fully closed position in different operating conditions.

6. Conclusions

Through experimentation with use of the 10 kW_{th} Calcium Looping Dual Fluidized Bed facility significant progress has been in achieved in the effort to characterize regenerator and carbonator operation. Regarding the carbonator high CO_2 capture efficiencies (over 85 %) are possible, regardless of the limestones and PSD used, at the gas-solid contacting mode provided by the CFB. Moreover, almost complete calcination is possible in the regenerator.

The regeneration efficiency (η_{reg}) is characterized through the ratio of the carbonation conversion of the incoming solids (X_{carb}) and the residence time in the regenerator (r_{reg}) for a given particle size, partial pressure of CO_2 (<0.3 bar) and temperature (900 °C). For values of $\frac{X_{carb}}{r_{reg}}$ between 2-3 1/h the regenerator works perfectly with efficiencies over 90%. This means that an incoming particle with a high value of X_{carb} (e.g. 15 %) would need 3-4.5 min for almost complete regeneration. At $\frac{X_{carb}}{r_{reg}}$ values of 6 1/h the regeneration efficiency falls to as low as 40 %, while the carbonation conversion of the outgoing particles (X_{calc}) reaches an unacceptable 6 %.

Both limestones exhibited continuous decay of the maximum carbonation conversion (X_{max}) with increasing CO_2 capture. In the early hours of experimentation (values of cumulative sorbent specific CO_2 loading, $L(t)_{CO2}$, around 1), the material is still fresh and the measured values of X_{max} were approximately 12-18%), while within the last hours ($L(t)_{CO2}$> 6) the values measured were between 6-8%.

The calcium looping ratio F_{Ca}/F_{CO2} values where significantly higher than the product of $F_{Ca}/F_{CO2}\cdot\eta_{reg}$, especially for the higher values of F_{Ca}/F_{CO2}. The latter is explained due to limited residence time in the regenerator. However, it is the $F_{Ca}/F_{CO2}\cdot\eta_{reg}$ that is important for carbonator operation, as shown from the carbonator mass balance. Moreover it is the $F_{Ca}/F_{CO2}\cdot\eta_{reg}$ that is important for assessing the calcium looping ratio (F_{Ca}/F_{CO2}) for large scale facilities since those shall be equipped with a regenerator operating with an η_{reg} of above 90 %. For a constant X_{max} and with increasing $F_{Ca}/F_{CO2}\cdot\eta_{reg}$ values the CO2 capture efficiency increases due to the reduction of X_{carb}, the increment of f_a and therefore of the carbonation reaction rate and CO_2 capture efficiency. The required $F_{Ca}/F_{CO2}\cdot\eta_{reg}$ values in order to reach a CO_2 capture efficiency higher than 90 % of the equilibrium value depend heavily on the value of the maximum carbonation conversion, X_{max}. For example, in regard to the Swabian Alb A limestone, such an efficiency is achieved with an $F_{Ca}/F_{CO2}\cdot\eta_{reg}$ value of approximately 8 and

an X_{max} value of above 11 % or with an $F_{Ca}/F_{CO2}\cdot\eta_{reg}$ value of 6 and an X_{max} value of above 13 %, while results are similar for the Swabian Alb limestone B.

The active space time (τ_a) has shown to strongly correlate to the CO_2 capture efficiency. Increment of the active space time means essentially increment of the carbonator inventory for a given CO_2 flow or increment of the carbonation reaction rate of a given inventory or both and therefore leads to increasing CO_2 capture efficiency. The Swabian Alb limestone B exhibited a critical active space time value of 0.15 h, above which the CO_2 capture efficiency approaches equilibrium values (E_{CO2}/E_{eq}>90%). The X_{max} value seems to play a parametric role in the relationship of active space time and CO_2 capture efficiency and thus further experimental results must be generated in order to define possible modifications to the active space time (τ_a) value.

The carbonator residence time (r_{carb}) is fully defined when the space time (τ) and calcium looping ratio (F_{Ca}/F_{CO2}) values are set, has however an interesting physical meaning. For the space time window of operation, an increment of residence time for a given X_{max} leads to decreasing CO_2 capture efficiency (E_{CO2}). This can be explained, since increased residence times in the carbonator mean increasing levels of carbonation conversion X_{carb} and therefore decreasing levels of the free active CaO part of the bed (f_a), carbonation reaction rate and CO_2 capture efficiency. In regard to Swabian Alb limestone A limestone E_{CO2}/E_{eq} values higher than 90 % have not been recorded for X_{max} values below 9 % and r_{carb} values higher than 2.5 min. On the other hand such E_{CO2}/E_{eq} values, can be achieved with an X_{max} of above 15 % and a r_{carb} value of 4.5 min. This is possible since when the X_{max} values are high, e.g. 15 %, high residence times such as 4.5 min that lead to high carbonation conversion X_{carb} values, still allow sufficient f_a values and carbonation reaction rate to exist. Too high carbonator residence times ultimately lead to the X_{carb} becoming equal to the X_{max} and thus to low carbonation reaction rates and CO_2 capture efficiencies.

More than 80 % of the CO_2 capture efficiency realized in the carbonator takes place in the first 730 mm of the carbonator bed. This can be explained due to that this area is covered from the dense bed region and due to the fact the fresh calcined sorbents enter the carbonator at 1.2 m above the distributor. Regarding sorbent allocation within the carbonator pressure drop and solid fraction profiles were measured. The carbonator exhibits a dense, lean core annulus region. The dense bed accommodates 60% of the total mass. The solid fraction values of the different regions, their variation with carbonator inventory and velocity and the “C” shaped hydrodynamic profiles are in accordance with cold model predictions. In addition the

cone valve controlled the calcium looping ratio between the carbonator and the regenerator sufficiently, while the riser entrainment was between 15-20 kg/m^{2}s which was much lower than expected.

7.References

[1] Kennedy, C.; Steinberger, J.; Gasson, B.; Hansen, Y.; Hillman, T.; Phdungslip, A.; Mendez, G. V.: Greenhouse Gas Emissions from Global Cities, Environ. Sci. Technol. Vol. 43 (2009), p. 7297-7302

[2] World Energy Outlook 2009 Presentation at UNFCC meeting, Nobou Tanaka, 2009, Bangkok

[3] Curtright, A. E.; Morgan, M. G.; Keith, D. W.: Expert Assessments of Future Photovoltaic Technologies, Environ. Sci. Technol. Vol.42 No. 24 (2008), p. 9031-9038

[4] Braham, R. J.; Harris, A. T.: Review of Major and Scale-up Considerations for Solar Photocatalytic Reactors, Ind. Eng. Chem. Vol. 48 (2009), p. 8890-8905

[5] Erga, O.; Juliussen, O.; Lidal, H.: Carbon dioxide recovery by means of aqueous amines, Energy Convers. Manage. Vol.36 (1995), p. 387-392

[6] Feron, P.H.M.; Jansen, A.E.; Klaassen, R.: Membrane technology in carbon dioxide removal, Energy Convers. Manage. Vol.33 (1992), p. 421-428

[7] Yong, Z.; Mata, V.; Rodrigues, A.E.: Absorption of carbon dioxide at high temperature- a review, Sep. Purif. Technology Vol. 26 (2002), p. 195

[8] DuMotay, T.; Marechal: Great Britain Patent 2, 548 (1867)

[9] Charitos, A.; Hawthorne, C.; Bidwe, A.R.; Korovesis, L.; Schuster, A.; Scheffknecht, G.: Hydrodynamic analysis of a 10 kWth Calcium Looping Dual Fluidized Bed for post-combustion CO_2 capture, Powder Technology Vol. 200 (2010), p. 117-127

[10] Charitos, A.; Hawthorne, C.; Bidwe, A.R.; Holz, S.; Pfeifer, T.; Schulze, A.; Schlegel, D.; Schuster, A.; Scheffknecht, G.: Parametric study on the CO_2 capture efficiency of the Carbonate Looping Process in a 10 kWth Dual Fluidized Bed, 20th International Conference of fluidized bed combustion (Xian, P. R. China), p. 753-758

[11] Charitos, A.; Hawthorne, C.; Bidwe, A.R.; Holz, H.; Pfeifer, T.; Schulze, A.; Schlegel, D.; Schuster, A.; Scheffknecht, G.: Parametric investigation of the looping process for the CO_2 capture in a 10 kW Dual Fluidized Bed, Int. J. of Greenhouse Control, accepted for publication

[12] Alonso, M.; Rodriquez, N.; Grasa, G.; Abanades, J. C.: Modelling of a fluidized bed carbonator reactor to capture CO_2 from a combustion flue gas, Chemical Engineering Science Vol.64 (2009), p. 883-891

[13] Lu, D. Y.; Hughes, R. W.; Anthony, E. J.: Ca-based sorbent looping combustion for CO_2 capture in pilot-scale dual fluidized beds, Fuel Processing Technology Vol. 89 (2008), p. 1386-1395

[14] Fang, F.; Li, Z.; Cai, N.: Continuous CO_2 Capture from Flue Gases Using a Dual Fluidized Bed Reactor with Calcium-Based Sorbent, Ind. Eng. Chem. Res. Vol. 48 (2009), p. 11140-11147

[15] Bidwe, R.: Scaled Cold Model Investigation of a Dual Fluidised Bed System for the post-combustion removal of CO_2 using CaO. Master Thesis, University of Stuttgart 2007

[16] Korovesis, L.: Parametric analysis of the hydrodynamics of a Dual Fluidized Bed system for post-combustion capture of CO_2 through a scaled cold model. Master Thesis, University of Stuttgart 2008

[17] Schlegel, D.: Parametric study on the CO_2 capture efficiency of the Carbonate Looping process in a 10 kW Dual Fluidised Bed. Master Thesis, University of Stuttgart 2009

[18] Shimizu, T.; Hirama, T.; Hosoda, H.; Kitano, K.; Inagaki, M.; Tejima, K.: A twin fluid-bed reactor for removal of CO_2 from combustion processes, Trans IChemE Vol. 77 Part A (1999), p. 62 – 68

[19] Abanades, J.C.: The maximum Capture efficiency of CO2 capture using a carbonation / calcination cycle of CaO/CaCO3, Chemical Engineering Journal Vol. 90 (2002), p. 303-306.

[20] Abanades, J.C.: Anthony, E.J.; Lu, D.; Salvador, C.; Alvarez, D.: Capture of CO_2 from Combustion Gases in a Fluidized Bed of CaO, AiChE Journal Vol. 50 No. 7 (2004), p. 1614 – 1622

[21] Hawthorne, C.; Trossmann, M.; Cifre, P.; Schuster, A.; Scheffknecht, G.: Simulation of the carbonate looping power cycle, Energy Procedia (2008), p. 1388 – 1394

[22] Romeo, L. M.; Abanades, J. C.; Escosa, J. M.; Pano, J.; Gimenez, A.; Biezma, A. S.; Ballesteros, J. C.: Oxyfuel carbonation/calcination for low cost CO2 capture in existing power plants , Energy Conversion and Management Vol. 49 (2008), p. 2809-2814

[23] Poboß, N.; Schuster, A.; Scheffknecht, G.: Machbarkeitsstudie für das Carbonate Looping Verfahren zur CO_2 Abscheidung aus Kraftwerksabgasen, (2008), BMWi

[24] MacKenzie, A.; Granatstein, D. L.; Anthony, E. J.; Abanades, J. C: Economics of CO_2 capture Using the Calcium Cycle with a Pressurized Fluidized Bed Combustor, Energy & Fuels Vol. 21 (2007), p. 920-926

[25] Abanades, J. C.; Grasa, G.; Alonso, M.; Rodriguez, N.; Anthony, E. J.; Romeo, L. M.: Cost Structure of a Post Combustion CO_2 Capture System Using CaO, Environ. Sci. Technol. Vol. 41 (2007), p. 5523-5527

[26] Hendriks, C. A.; Worrell, E.; Price, L.; Martin, N.; Ozawa Meida, L.: The reduction of greenhouse gas emission from the cement industry, IEA Greenhouse Gas R&D Programme (1999)

[27] Metz, B.; Davidson, O.; Bosch, P.; Dave, R.; Meyer, L.: Intergovermental Panel on Climate Change-Fourth Assessment Report, Climate Change (2007)

[28] Worrell, E.; Price, L.; Martin, N.; Hendriks, C. A.; Ozawa Meida, L.: Carbon Dioxide Emis sions from the Global Cement Industry, Annual Review of Energy and the Environment Vol. 26 (2001), p. 303-329

[29] Weimer T., Berger R., Hawthorne C., Abanades J.C.: Lime enhanced gasification of solid fuels: Examination of a process from simultaneous hydrogrn production and CO_2 capture, Fuel Vol. 87 (2008), p.1678- 1686

[30] Alonso, M.; Rodriquez, N.; Gonzalez, B.; Grasa, R,; Murillo, R.; Abanades, J, C,: Cargggbon dioxide capture from combustion flue gases with a calcium oxide chemical loop. Experimental results and process development, Int. J. Greenhouse Gas Control (2009)

[31] Dieter, H.; Bidwe, A; Schuster, A: Design and Construction of a 200KW_{th} Calcium Looping Dual Fluidized Bed Facility for CO_2 Capture, I International Workshop in Spain in Oviedo on In-Situ CO_2 Removal of the Institute of Process Engineering and Power Plant Technology of Stuttgart University (2009)

[32] Sanchez, A.; Sacristan, B: Development of post-combustion CO_2 Capture with CaO in a Large Test facility:"CaOling", Available at: http://www.co2captureandstorage.info/networks/loopingpdf/16%20septiembre/C11.pdf

[33] Baker, E. H.: The calcium oxide-carbon dioxide system in the pressure range 1-300 atmospheres, J. Chem. Soc. Vol. 70 (1962), p. 464-470

[34] Abanades, J. C.; Anthony, E. J.; Alvarez, D.; Lu, D.: In-Situ Capture of CO_2 in a Fluidized Bed Combustor, In 17th International conference on Fluidized Bed Combustion, Florida (2003)

[35] Hawthorne, C.; Charitos, A.; Perez-Pulido, C.A.; Bing, Z.; Scheffknecht, G.: Design of a Dual Fluidized Bed System for the Post-Combustion Removal of CO_2 Using CaO. Part I: CFB Carbonator Reactor Model, Tagungsband: Proceedings of the CFB9 conference (2008), p. 759 – 764

[36] Lysikov, I.; Salanov, N.; Okunev, G.: Change of CO_2 carrying capacity in isothermal recarbonation-decomposition cycles, Ind. Eng. Chem. Res Vol.46 (2007), p. 4633-4638

[37] Grasa, G.; Abanades, J.C.: CO_2 Capture Capacity of CaO in Long Series of Carbonation/Calcination Cycles, Ind. Eng. Chem. Res. 45 (2006), p. 8846 – 8851

[38] Abanades, J.C.; Alvarez, D.: Conversion Limits in the Reaction of CO2 with Lime, Energy & Fuels Vol. 17 (2003), p. 308 -315

[39] Grasa, G.; Abanades, J.C.: CO_2 Capture Capacity of CaO in Long Series of Carbonation/Calcination Cycles, Ind. Eng. Chem. Res. 45 (2006), p. 8846 – 8851

[40] Manovic, V.; Anthony, E. J.; Grasa, G.; Abanades, J. C.: CO_2 Looping Cycle performance of a High-Purity Limestone after Thermal Activation/Doping, Energy & Fuels Vol. 22 (2008), p. 3258-3264

[41] Manovic, V.; Anthony, E. J.; Grasa, G.; Abanades, J. C.: CO_2 Looping Cycle performance of a High-Purity Limestone after Thermal Activation/Doping, Energy & Fuels Vol. 22 (2008), p. 3258-3264

[42] Fennell, P. S.; Davidson, J. F.; Dennis, J.S.; Hayhurst, A. N.: Regeneration of sintered limestone sorbents for the sequestration of CO_2 from combustion and other systems, Journal of the Energy Institute Vol. 80 (2007), p. 116-119

[43] Hughes, R. W.; Lu, D.; Anthony, E. J.; Wu, Y. H.: Improved long-term conversion of limestone- derived sorbents for in situ capture of CO_2 in a fluidized bed combustor, Industrial & Engineering Chemistry Research Vol. 43 (2004), p. 5529-5539

[44] Sun, P.; Grace, J.R.; Lim, C. J.; Anthony, E. J.: Investigation of attempts to improve cyclic CO_2 capture by sorbent hydration and modification, Industrial & Engineering Chemistry Research Vol. 47 (2008), p. 2024-2032

[45] Manovic, V.; Anthony, E. J.: Steam reactivation of spent CaO-based sorbent for multiple CO_2 capture cycles, Environmental Science & Technology Vol. 41 (2007), p. 1420-1425

[46] Rodriguez, N.; Alonso, M.; Abanades, J. C.: Average Activity of CaO particles in a Calcium Looping System, Chemical Engineering Journal Vol. 156 (2010), p. 388-394

[47] Werther, J; Fluid mechanics of large-scale CFB units, in: A.A. Avidan (Ed.), Proceedings of the 4th international conference on circulating fluidized beds, Pennsylvania, USA (1993), p. 1-14

[48] Charitos, A.; Hawthorne, C.; Bidwe, A.; He, L.; Scheffknecht, G.: Design of a Dual Fluidized Bed System for the Post-Combustion Removal of CO_2 Using CaO. Part II: CFB Carbonator Reactor Model

8. Annex

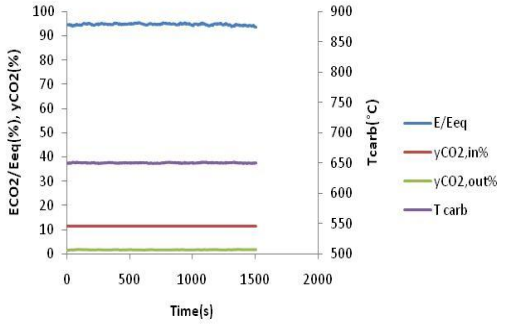

Fig. 8.1: Inlet yco_2, Tcarb, outlet yco_2 E co_2/Eeq are plotted vs time at τ of 0.57 h and $Fcao/Fco_2$ of 18.43

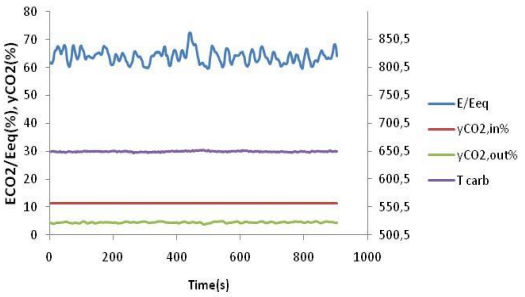

Fig. 8.2: Inlet yco_2, Tcarb, outlet yco_2 E co_2/Eeq are plotted vs time at τ of 0.52 h and $Fcao/Fco_2$ of 7.74

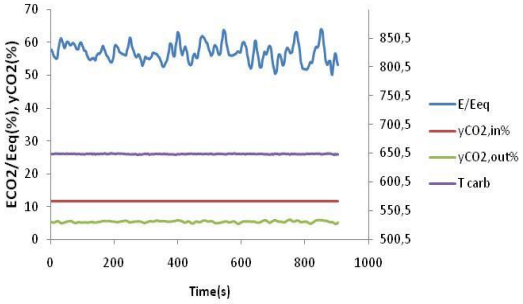

Fig. 8.3: Inlet yco_2, Tcarb, outlet yco_2 E co_2/Eeq are plotted vs time at τ of 0.37 h and $Fcao/Fco_2$ of 7.86

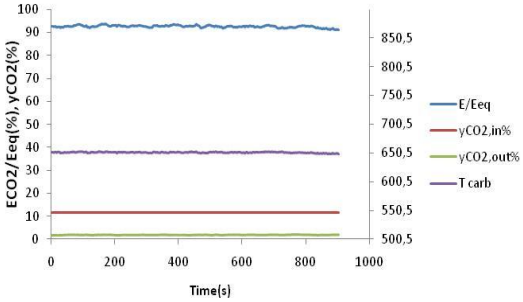

Fig. 8.4: Inlet yco_2, Tcarb, outlet yco_2 E co_2/Eeq are plotted vs time at τ of 0.42 h and $Fcao/Fco_2$ of 19.44

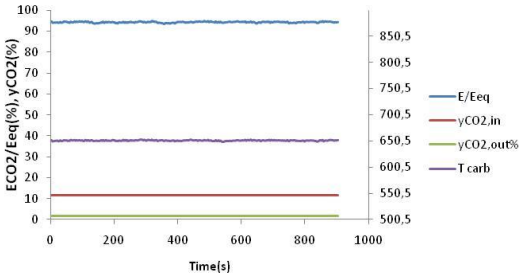

Fig. 8.5: Inlet yco_2, Tcarb, outlet yco_2 E co_2/Eeq are plotted vs time at τ of 0.48 h and $Fcao/Fco_2$ of 23.95

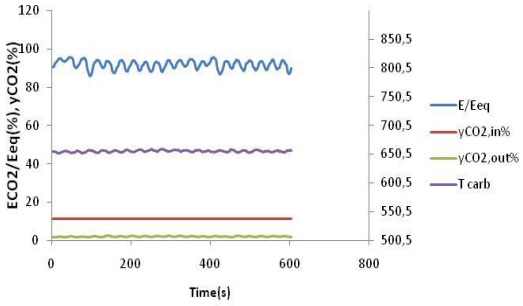

Fig. 8.6: Inlet yco_2, Tcarb, outlet yco_2 E co_2/Eeq are plotted vs time at τ of 0.38 h and $Fcao/Fco_2$ of 8.63

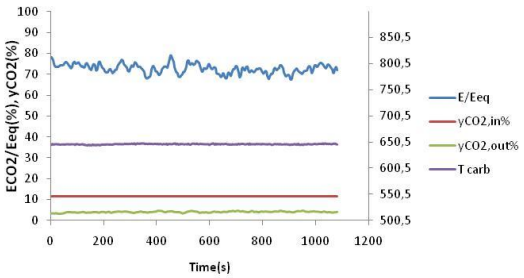

Fig. 8.7: Inlet yco_2, Tcarb, outlet yco_2 E co_2/Eeq are plotted vs time at τ of 0.37 h and Fcao/Fco_2 of 8.41

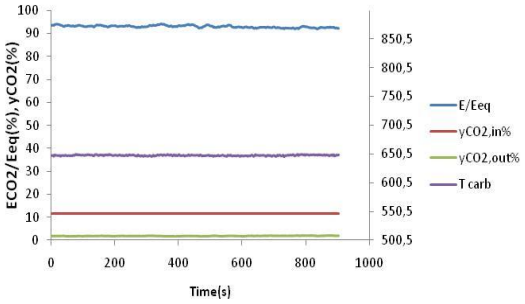

Fig. 8.8: Inlet yco_2, Tcarb, outlet yco_2 E co_2/Eeq are plotted vs time at τ of 0.43 h and Fcao/Fco_2 of 11.52

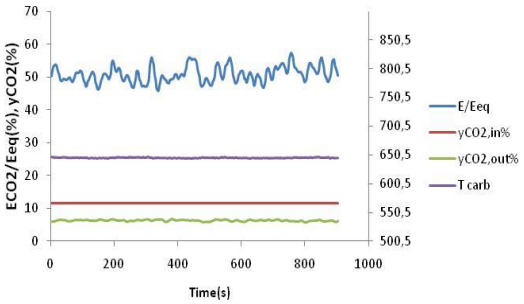

Fig. 8.9: Inlet yco_2, Tcarb, outlet yco_2 E co_2/Eeq are plotted vs time at τ of 0.33 h and Fcao/Fco_2 of 3.91

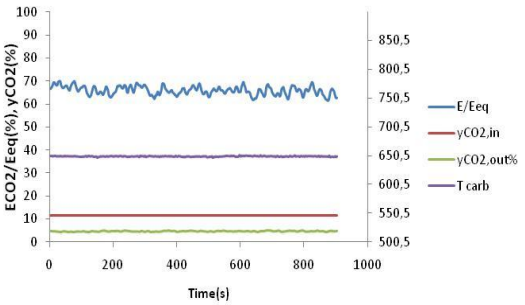

Fig. 8.10: Inlet yco_2, Tcarb, outlet yco_2 E co_2/Eeq are plotted vs time at τ of 0.37 h and Fcao/Fco_2 of 6.66

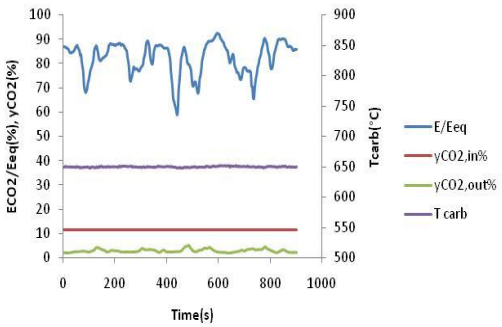

Fig. 8.11: Inlet yco_2, Tcarb, outlet yco_2 E co_2/Eeq are plotted vs time at τ of 0.44 h and Fcao/Fco_2 of 7.00

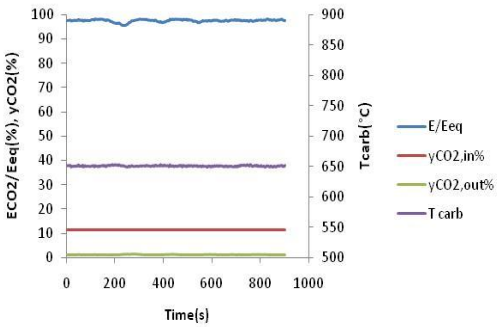

Fig. 8.12: Inlet yco_2, Tcarb, outlet yco_2 E co_2/Eeq are plotted vs time at τ of 0.46 h and Fcao/Fco_2 of 23.00

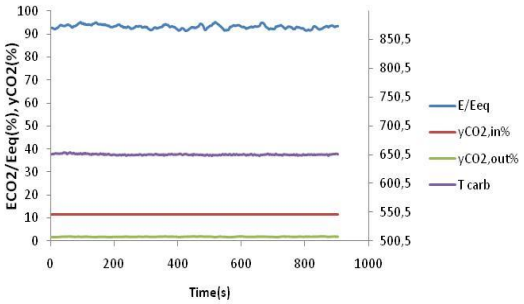

Fig. 8.13: Inlet yco_2, Tcarb, outlet yco_2 E co_2/Eeq are plotted vs time at τ of 0.52 h and $Fcao/Fco_2$ of 8.00

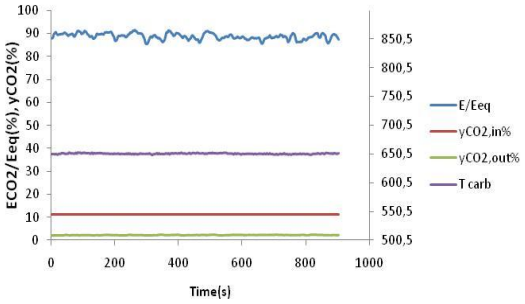

Fig. 8.14: Inlet yco_2, Tcarb, outlet yco_2 E co_2/Eeq are plotted vs time at τ of 0.48 h and $Fcao/Fco_2$ of 8.60

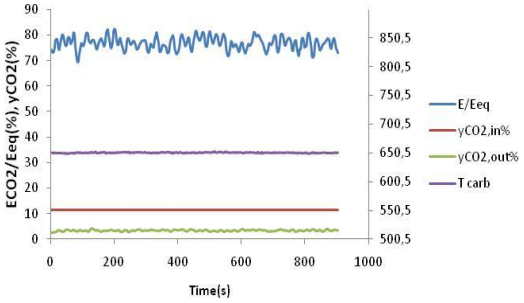

Fig. 8.15: Inlet yco_2, Tcarb, outlet yco_2 E co_2/Eeq are plotted vs time at τ of 0.43 h and $Fcao/Fco_2$ of 7.80

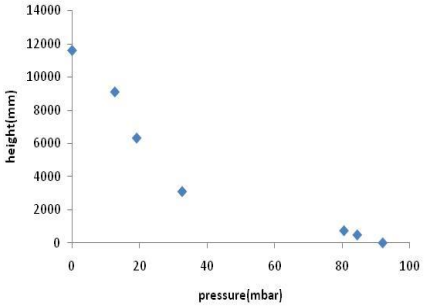

Fig. 8.16: Pressure drop profile along the riser, dp= 92mbar

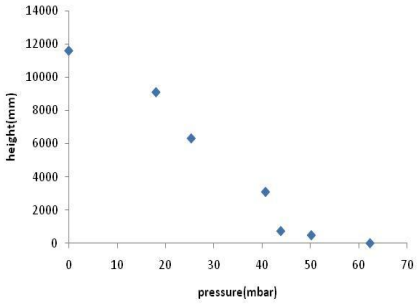

Fig. 8.17: Pressure drop profile along the riser, dp= 62mbar

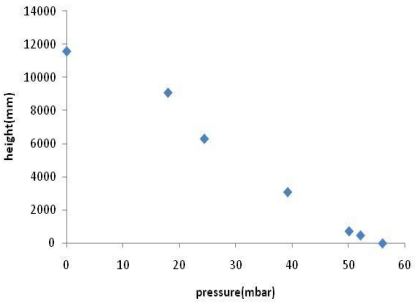

Fig. 8.18: Pressure drop profile along the riser, dp=56mbar

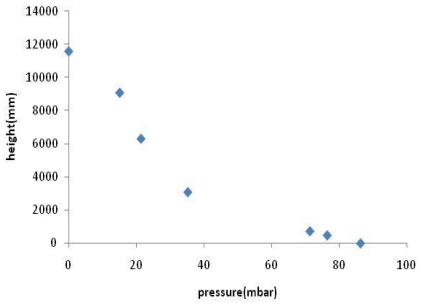

Fig. 8.19: Pressure drop profile along the riser, dp= 86mbar

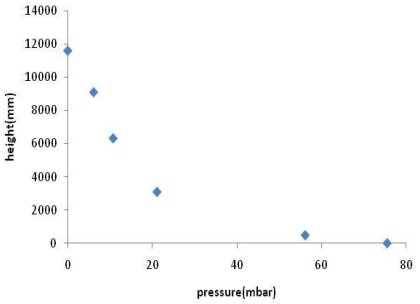

Fig. 8.20: Pressure drop profile along the riser, dp= 75mbar

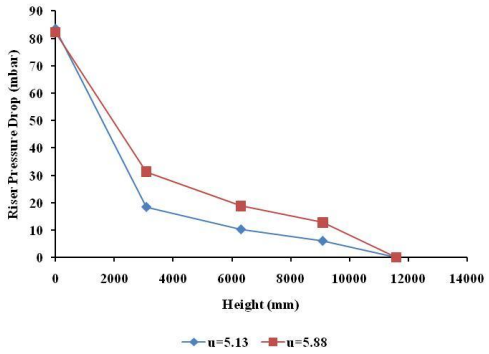

Fig. 8.21: Effect of velocity in the riser pressure drop profile drop profile (u=5.13m/s, u=5.88m/s), dp=82mbar

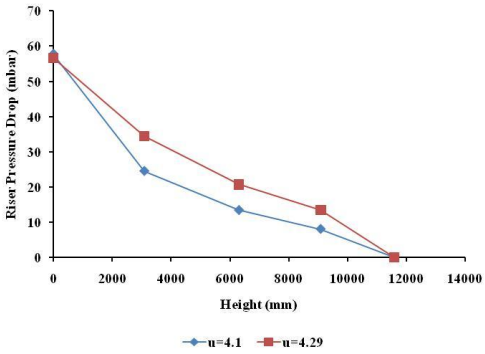

Fig. 8.22: Effect of velocity in the riser pressure drop profile drop profile (u=4.10m/s, u=4.29m/s), dp=57mbar

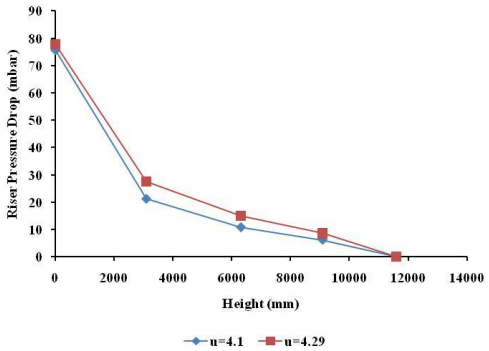

Fig. 8.22: Effect of velocity in the riser pressure drop profile drop profile (u=4.10m/s, u=4.29m/s), dp=75mbar